ROYAL SOCIETY OF CHEMISTRY

Check for updates

Electrocatalytic conversion of biomass-derived furan compounds: mechanisms, catalysts and perspectives

Peipei Zhu,* Mingzhu Shi, Zhipeng Shen, Xunfan Liao [ID] and Yiwang Chen [ID] *

Renewable biomass, with its abundant resources, provides a viable solution to address the energy crisis and mitigate environmental pollution. Furan compounds, including 5-hydroxymethylfurfural (**HMF**) and furfural (**FF**), serve as versatile platform molecules derived from the degradation of lignocellulosic cellulose, offering a crucial pathway for the conversion of renewable biomass. The electrocatalytic conversion of furan compounds using renewable electricity represents an enticing approach for transforming them into value-added chemicals. However, the complex chemistry of furan compounds leads to low selectivity of the target product, and the lower current density and Faraday efficiency make it difficult to achieve molded applications. Therefore, it is crucial to gain a better understanding of the mechanism and conditions of the reaction, enhance reaction activity and selectivity, and indicate the direction for industrial applications. Herein, we provide a comprehensive review of the recent advancements in the electrocatalytic of **HMF** and **FF**, focusing on mechanisms and pathways, catalysts, and factors affecting like electrolyte pH, potential, and substrate concentration. Furthermore, challenges and future application prospects are discussed. This review aims to equip researchers with a fundamental understanding of the electrochemical dehydrogenation, hydrogenation, and hydrolysis reactions involving furan compounds. Such insights are expected to accelerate the development of cost-effective electrochemical conversion processes for biomass derivatives and their scalability in large-scale applications.

Key Laboratory of Fluorine and Silicon for Energy Materials and Chemistry of Ministry of Education, College of Chemistry and Chemical Engineering, Jiangxi Normal University, 99 Ziyang Avenue, Nanchang 330022, China. E-mail: ppzhu@jxnu.edu.cn; ywchen@ncu.edu.cn

1 Introduction

Excessive reliance on non-renewable fossil fuels has led to economic, social, and environmental issues, necessitating a shift to renewable energy sources.[1] Among these, biomass

Peipei Zhu received her M.S. degree in 2016 and her PhD degree in 2019 from Nanchang University, China. She studied as a visiting (Joint-Supervision) PhD student at Nanyang Technological University, Singapore. Currently, she is a lecturer of the College of Chemistry and Chemical Engineering, Jiangxi Normal University. Her research interest focuses on water-involved electrocatalysis and synthesis.

Peipei Zhu

Xunfan Liao is a professor of chemistry at Jiangxi Normal University. He received his PhD degree from Nanchang University under the supervision of Prof. Yiwang Chen and Prof. Alex K.-Y. Jen in 2018 and worked as a visiting researcher at University of Washington in 2017–2018. From 2018–2020, he has been working at the College of Materials Science and Engineering at Donghua University as an associate professor. His current research interests focus on organic photo-electronic materials and devices.

Xunfan Liao

energy, particularly lignocellulosic biomass, is promising for sustainable chemical and fuel production.[1–3] Lignocellulose, comprising cellulose, hemicellulose, and lignin, is an abundant and renewable feedstock.[4–11] In 2004, the U.S. Department of Energy released a list of the most promising bio-derived platform molecules, which was later updated and revisited by Bozell and Petersen in 2010.[12] Among these, furfural (**FF**, $C_5H_4O_2$) and 5-hydroxymethylfurfural (**HMF**, $C_6H_6O_3$) stand out as representative furan compounds generated by the acid-catalysed dehydration of pentose (C5) and hexose (C6) sugars, respectively. These compounds have the potential to serve as alternative commodity chemicals to fossil-fuel-based platform chemicals through oxidation, dehydration, and hydrogenation processes targeting functionalities (–C=O on furfural, –OH and –C=O on **HMF**) attached to their furan ring.[13] The use of furfural and 5-hydroxymethylfurfural as bio-based platform molecules for the production of biorefinery building blocks and value-added chemicals is widely recognized. Through oxidation and reduction reactions, **HMF** and **FF** can be transformed into a diverse range of products with added value.

The primary method for biomass conversion is thermochemical catalysis, requiring high temperature and pressure.[14] With the costs of renewable energy, electrochemical processes are emerging as viable routes.[15,16] Electrocatalytic conversion can be conducted at room temperature and pressure using simple equipment, allowing precise control of selectivity and conversion rates by adjusting applied potential, electrode materials, and electrolytes. The transformation of the C–O/C=O functional groups in furan compounds produces high-value chemicals and biofuels, offering promising applications for the reuse of biomass derivatives and the green production of fine chemicals. Current research efforts are heavily focused on exploring catalysts, analyzing active sites, and dissecting reaction mechanisms.[17,18] Therefore, there is an urgent need for a systematic review and summary of the progress in electrochemical conversion reactions of furan compounds. Additionally, the latest reviews on this topic are crucial for a thorough understanding of the fundamental principles of electrocatalysis

and the proper design of catalysts, ultimately facilitating the scaled-up application of electrocatalysis in the production of biomass-derived products.

Herein, based on the importance of electrocatalytic furan compound conversion mentioned above, in order to deepen the understanding of the reaction mechanism and catalyst design, and to provide references for enhancing the selectivity and activity of electrochemical conversion, we summarize the recent progress of electrocatalytic conversion of biomass derived furan compounds (**FF** and **HMF**). **FF** and **HMF** exhibit versatility in electrocatalysis to various valuable products, such as biofuels, bioplastics, medicine and chemicals, as shown in Fig. 1. This paper focuses on the electrochemical hydrogenation, hydrolysis, and oxidative dehydrogenation mechanisms of furan compounds, as well as the corresponding catalysts and factors affecting the reaction performance. In addition, the review discusses the latest advancements in the paired electrolysis of furan compounds, providing insights into innovative approaches for their electrochemical conversion. Finally, the practical challenges and application prospects associated with the electrochemical conversion of biomass-derived furan compounds are discussed. This discussion not only serves as a theoretical foundation for the efficient electrochemical conversion of biomass derivatives but also provides valuable insights for the transition to industrial-scale production.

2 Advances in electrocatalytic production of furan compounds

HMF has evolved into a multifunctional molecule capable of being oxidized and reduced to yield chemicals with higher added value.[19,20] As illustrated in Fig. 2a, the primary products resulting from the oxidation process include 2,5-diformyl furan (**DFF**), 5-hydroxymethyl-2-furancarboxylic acid (**HMFCA**), 5-formyl-2-furancarboxylic acid (**FFCA**), and 2,5-furandicarboxylic acid (**FDCA**), each holding promising applications. For instance, **HMFCA** serves as a valuable monomer in polyester synthesis, while **FFCA** demonstrates broad prospects in fuel, chemical intermediates, pharmaceuticals, and other industries.[21,22] Through hydrogenolysis or hydrogenation, **HMF** can be transformed into 5-methylfurfural (**5-MF**) and 2,5-bishydroxymethylfuran (**BHMF**). **5-MF** can then be converted to 2,5-dimethylfuran (**DMF**) through direct hydrolysis of aldehydes or through the **5-MF** → **MFA** → **DMF** process (Fig. 2b).[23,24] However, the conversion of **MFA** to **DMF** is very difficult, because once the alcohol group on **HMF** is hydrolysed first, it will be difficult for the alcohol group to hydrolysis. Notably, **BHMF** stands out as a crucial precursor in the production of functionalized polyethers, polyurethanes, and polyamides.[25] An essential hydrogenolysis product stemming from **HMF** is 5-methylfurfuryl alcohol (**MFA**), and **DMF** represents an ideal liquid biofuel component for transportation due to its advantageous characteristics, including a high-octane number, a reasonable boiling point, and low solubility in water.[4,26,27]

Furfural (**FF**) stands out as a platform chemical, boasting a commercial production of 250 000 tons per year derived from

Yiwang Chen is a full professor of Chemistry at Nanchang University and Jiangxi Normal University. He received his PhD from Peking University in 1999 and conducted his postdoctoral work at Johannes Gutenberg-Universität Mainz and Philipps-Universität Marburg in Germany. He has been honored by the National Science Fund for Distinguished Young Scholars in 2014. Currently he is serving as a president of Gannan Normal University since 2022. His research interests include polymer/perovskite solar cells, hybrid supercapacitors, sodium ion batteries, intelligent elastomers, zinc–air batteries and electrocatalysis.
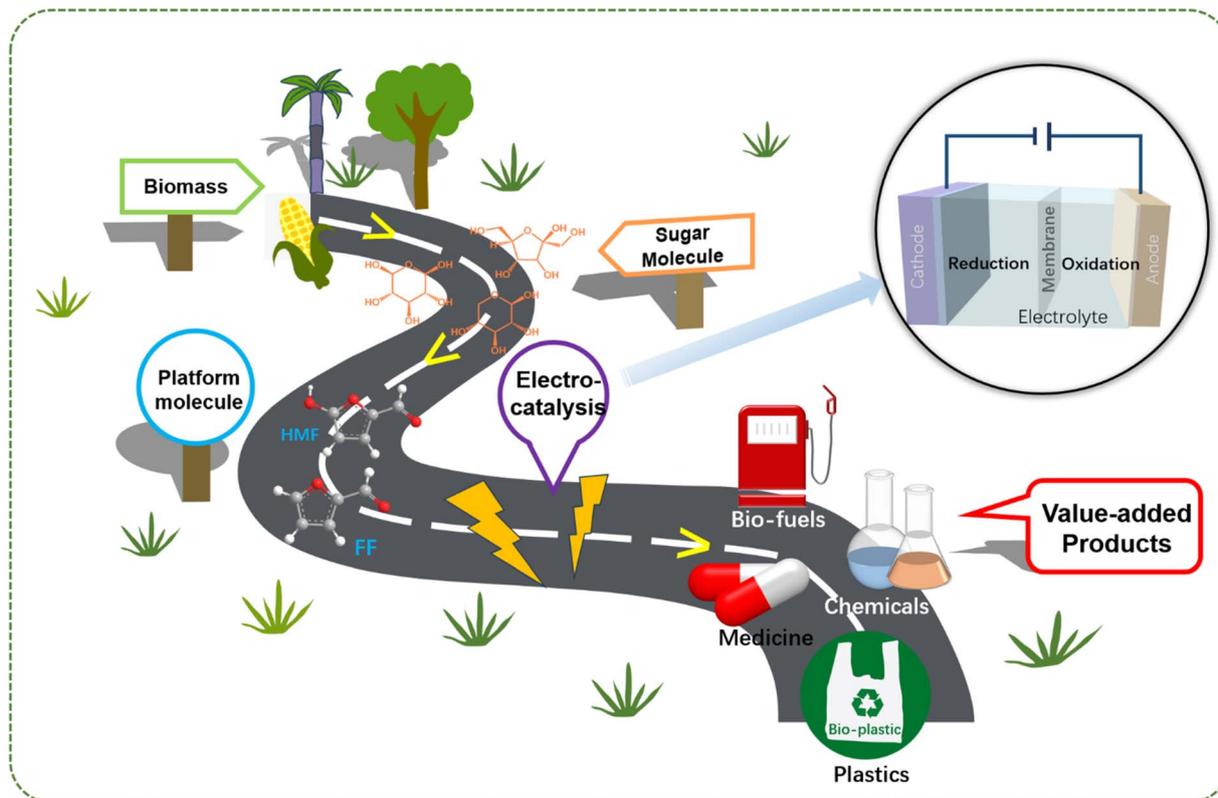
Yiwang Chen

Fig. 1 Schematic diagram of biomass sources of **HMF** and **FF** platform molecules and their electrochemical conversion to high value-added chemicals and fuels.
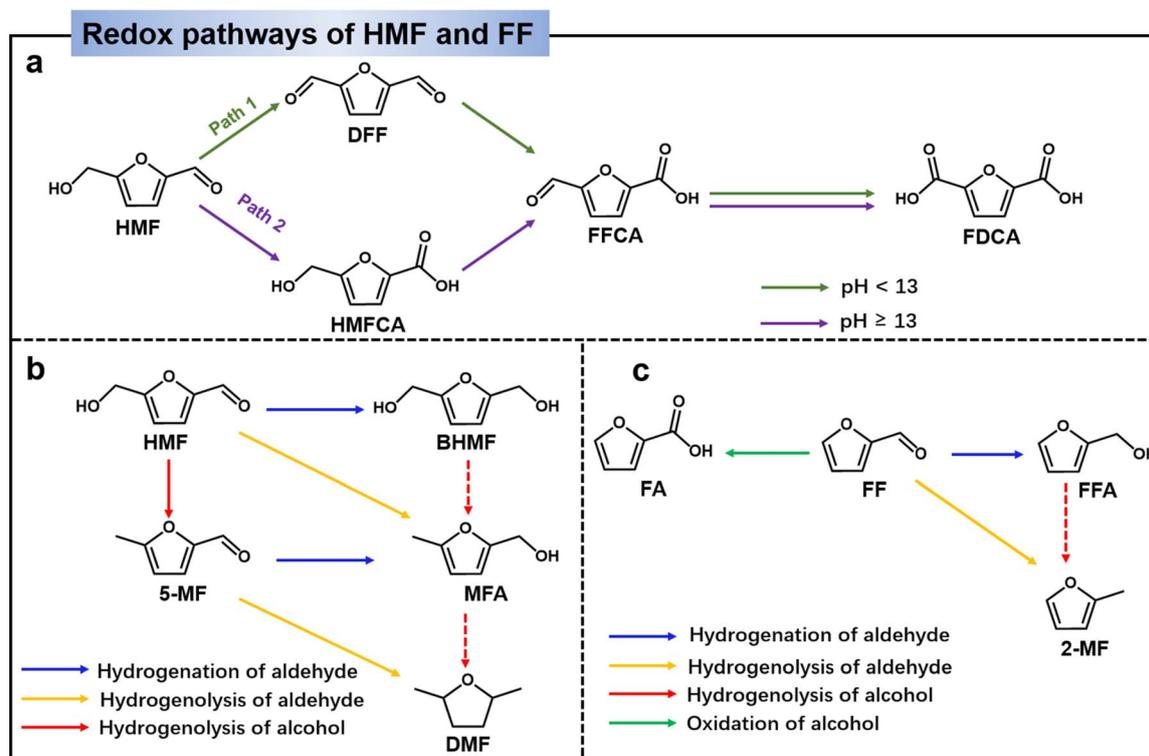

Fig. 2 The main electro-oxidation pathways (a) and electro-reduction pathways (b) of **HMF**, and (c) electrochemical conversion pathways of **FF**. The dashed arrows indicate steps experimentally found to be difficult to occur.

the treatment of agricultural waste.[28] Due to its chemical and structural complexity, **FF** offers the potential for direct or indirect conversion into over 80 valuable compounds, primarily through reduction and oxidation processes.[29] The pathways for **FF** transformation into major platform molecules are depicted in Fig. 2c. Among the significant products resulting from **FF** reduction, furfuryl alcohol (**FFA**) emerges as an intermediate crucial to pharmaceutical and polymer industries.[30,31] Further hydrogenolysis of the side C–O bond of **FFA** leads to the production of 2-methylfuran (**MF**), which holds substantial promise as a liquid biofuel with high energy density. Additionally, **MF** serves as a green solvent and feedstock for the production of pharmaceuticals, pesticides, and perfume intermediates.[4,32] On the other hand, **FF** can undergo transformation to produce furoic acid (**FA**) *via* an oxidation process. **FF** is a versatile chemical for the production of a variety of pharmaceutical drugs, agriculture, fragrances, flavors, biofuels.[33]

3   Selective electrochemical oxidation of furan compounds

3.1   Pathway and mechanism for electrochemical oxidation of furan compounds

The electrochemical oxidation of biomass-derived compounds has garnered substantial attention, primarily due to the kinetically unfavorable nature of water oxidation and the relatively low value of its resulting product (O_2).[34–36] In this section, we will provide an overview and outlook on the electrochemical oxidation of furan compounds. This coverage encompasses the reaction pathways and mechanisms involved, as well as the design principles for electrocatalysts in this context. The determination of electrochemical reaction pathways and mechanisms is crucial for selecting appropriate reaction conditions, improvement of product selectivity and rational design of highly active and selective electrocatalysts. In this section, we will elucidate the electrooxidation pathways and mechanisms, exploring them from the perspective of **HMF** and **FF** as substrates, respectively.

3.1.1   Direct reaction mechanism (OH* mechanism).
Direct oxidation typically exhibits a distinct potential-dependent oxidation (PD oxidation) character, driven by the applied voltage rather than being dominated by chemical redox mediator pairs. This mechanism, also known as the OH* mechanism, is characterized by a more positive onset potential compared to indirect oxidation.[37] In the OH* mechanism, the valence state transition of the catalyst is not involved, and the applied voltage primarily promotes the adsorption and electron transfer of OH⁻, followed by substrate dehydrogenation.[38,39] The direct oxidation process involves the adsorption of organic molecules and OH⁻ on the electrode, followed by the production and desorption of the products.[40] In this direct oxidation mechanism, hydroxide ions (OH⁻) are adsorbed on the electrode surface under a certain potential, losing electrons to form adsorbed hydroxyl groups (OH*). OH* then activates the adsorbed substrate molecule, causing oxidative dehydrogenation.[41–43] The oxidation pathways and

corresponding mechanisms are illustrated in Scheme 1. For **HMF**, under a non-strong alkaline media (pH < 13), the hydroxymethyl group of **HMF** absorbed on the electrode surface triggers the deprotonation of the C–H bond and the O–H bond through the activation of OH⁻, resulting in the production of **DFF** intermediate.[40] Subsequent reactions lead to the formation of **FFCA** and **FDCA** (Scheme 1a).[3,41]

In a strong alkaline environment (pH ≥ 13), the aldehyde group will preferentially adsorb on the catalyst surface, *via* addition with H_2O, **HMF** will be converted into diol, which then interacts with OH⁻ to activate C–H/O–H and deprotonate to generate carboxyl (*i.e.*, **HMFCA**). Later on, **FFCA** is gained through the same OH⁻ activation and deprotonation process on the other alcohol chain. Following, the nucleophilic addition and dehydrogenation steps are repeated to form **FDCA** (Scheme 1b).[44,45] Indeed, the energy of the C–H/O–H bond dissociation of the **HMF** can be used to assess the oxidative activity of its direct oxidation process. It is important to note that the substrate molecule (**HMF**) itself needs to be adsorbed on the catalyst surface for the reaction. Therefore, the balance of substrate molecule and OH⁻ adsorption on the electrode surface is identified as an important factor determining the efficiency of direct oxidation.[45]

3.1.2   Indirect oxidation mechanism (electrochemical–chemical (E–C) mechanism).
Unlike direct oxidation, the applied potential of indirect oxidation does not directly drive the oxidation of the substrate. The valence of the catalyst changes during the oxidation process. The catalyst actually acts as a redox medium to drive the oxidation of the substrate, which is a chemical process that does not require an applied potential. As shown in Fig. 3a, indirect oxidation involves a two-step sequential process of single electron transfer. In a first step, the pristine catalyst is reconstituted under an applied voltage to electrochemically oxidize from the low valent/reduction state to the high valent/oxidation state ($M^{n+} \rightarrow M^{n+1}$(MOOH/(MOH)O)), and subsequently, the high-valent/oxidation state intermediate is chemically oxidized by hydride transfer of organic functional groups (activation and cleavage of C–H/O–H bonds) (Scheme 1c (3) or hydrogen atom transfer (Scheme 1d (3)),[41] this process (Fig. 3a process ②) is spontaneous and non-electrochemical, while the high-valent catalyst is reduced back to the low-valent state ($M^{n+1} \rightarrow M^{n+}$) (Fig. 3a process ①).[39,46,47] In summary, Scheme 1c is a potential-dependent (PD) indirect oxidation pathway *via* hydride transfer. Scheme 1d refers to the potential-independent (PID) indirect oxidation pathway *via* hydride atom transfer.[48]

As an example, Wang's group[46] demonstrated that the indirect oxidation of nucleophilic reagents *via* a proton-coupled electron transfer (PCET) process on β-Ni(OH)₂. β-Ni(OH)₂ is first oxidized to $Ni^{2+\delta}O(OH)$ on electrode surface, and then $Ni^{2+\delta}O(OH)$ acquires protons and electrons from the nucleophilic reagent. Consequently, the nucleophilic reagent is oxidized while $Ni^{2+\delta}O(OH)$ is re-reduced to β-Ni(OH)₂, while the oxidation potential of the nucleophilic reagent is highly consistent with that of Ni^{2+} (Fig. 3b).[46,49] According to reports, a strong alkaline environment (pH ≥ 13) is more conducive to the preferential adsorption of **HMF**'s aldehyde group onto the
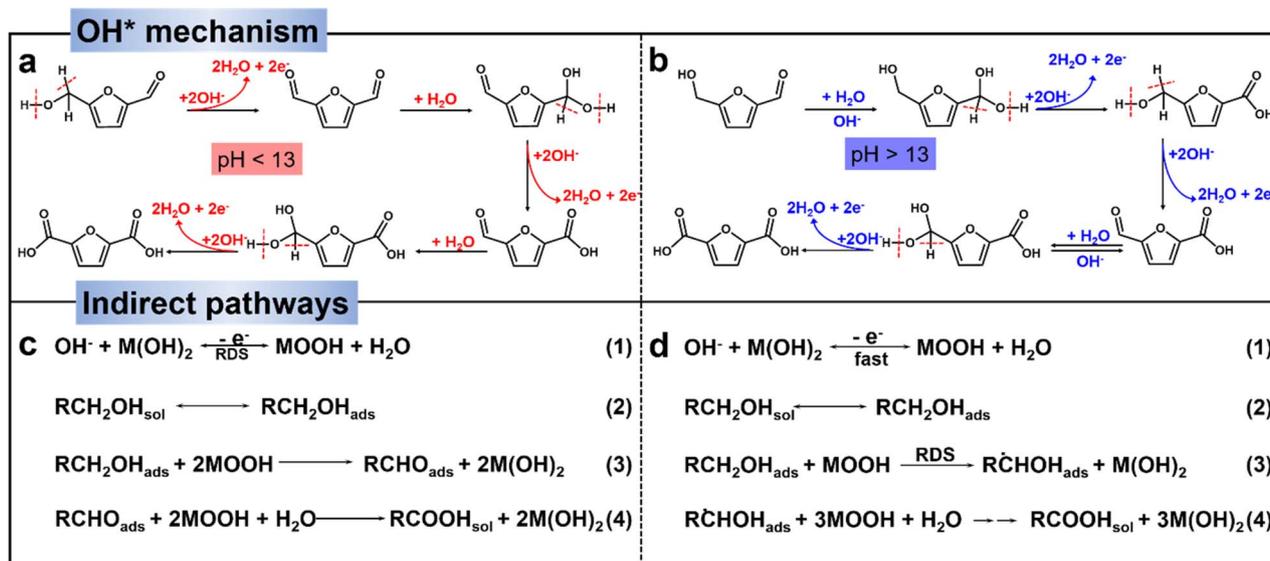
Scheme 1 (a) and (b) OH* mechanisms for electro-oxidation of **HMF**.[37] Copyright 2023, Wiley-VCH. (c) and (d) Schematic dehydrogenation for two indirect oxidation pathways in alkaline aqueous media (RCH$_2$OH represents the organic molecule containing aldehyde/alcohol, M(OH)$_2$ represents low-valence state of the mediator and MOOH represents high-valence state of the mediator).[41] Copyright 2021, Royal Society of Chemistry.

catalyst surface, leading to its oxidation to form **HMFCA**. At this point, the high concentration of OH$^-$ in the electrolyte is advantageous for the electrochemical oxidation of **HMF** under low potential, indicating that the elevated OH$^-$ concentration in the electrolyte favors the potential-dependent indirect oxidation of **HMF**. In contrast, under non-strong alkaline electrolyte conditions (pH < 13), due to the much stronger bonding of **HMF** on the catalyst surface compared to OH$^-$, the medium is difficult to oxidize. Therefore, under non-strong alkaline conditions, the hydroxyl group of **HMF** is preferentially adsorbed onto the catalyst surface. Through **DFF** as an intermediate, direct oxidation occurs at the electrode surface. This process

usually requires a high potential and does not involve the oxidation–reduction of intermediates.[38,50]

3.1.3 Mixing mechanism. It is worth noting that the two mechanisms mentioned above are likely to co-exist. Combined with the experimental results in the literature, Zou *et al.* proposed a hybrid mechanism described as follows (Fig. 4a).[3] For path 1, **HMF** is oxidized to **DFF** in the first step, a reaction that typically occurs in a non-strong base electrolyte. Due to its competitive relationship, the low OH$^-$ concentration is conducive to the adsorption of **HMF** and hinders the high valence conversion of the catalyst molecules at the original potential. Furthermore, it was demonstrated that the
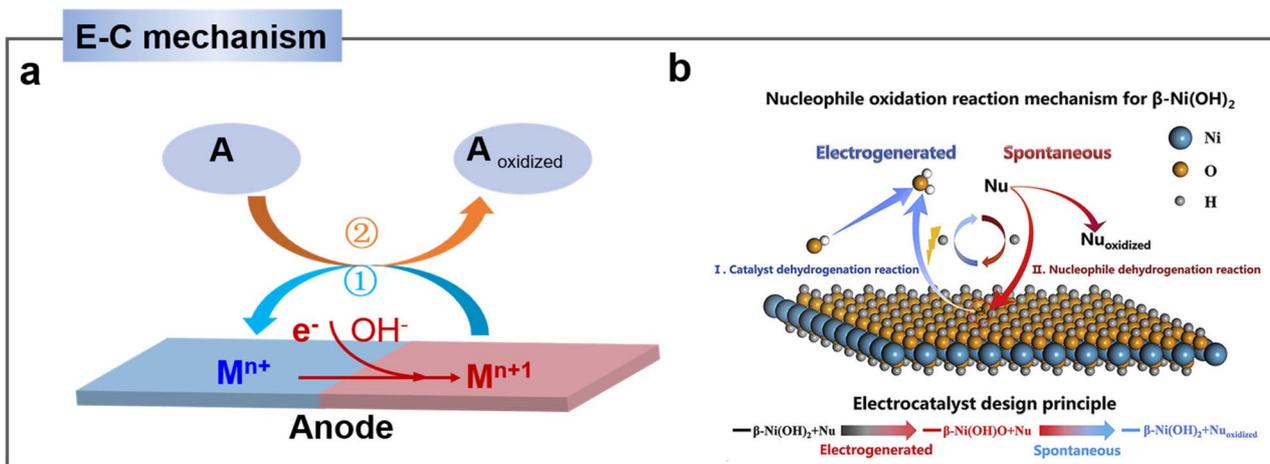

Fig. 3 (a) Schematic E–C mechanism of indirect oxidation mediated by heterogeneous redox mediator (M^{n+} represents low valence state and M^{n+1} represents high valence state of the mediator, A represents substrate). (b) Schematic illustration of **HMF** oxidation reaction (HMFOR) mechanism on Ni(OH)$_2$ electrode.[46] Copyright 2020, Elsevier.
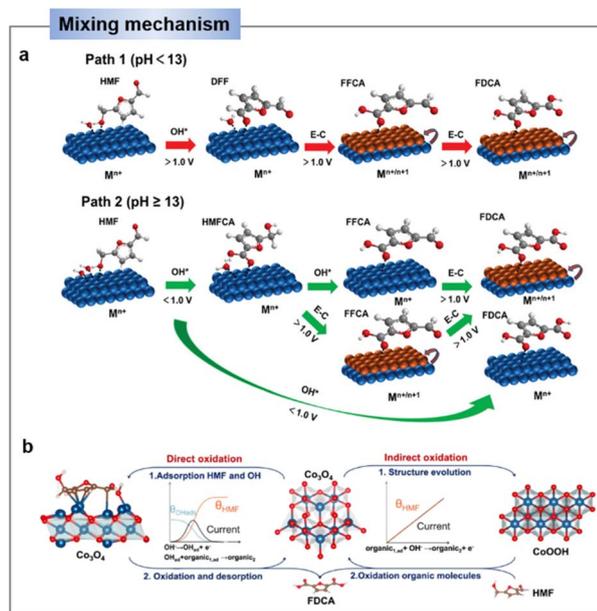
Fig. 4 (a) The mixing mechanisms of the electrooxidation of HMF.[3] Copyright 2023, Wiley-VCH. (b) Schematic representation of the direct and indirect oxidation of HMF on Co_3O_4 catalyst.[38] Copyright 2022, American Chemical Society.

generation potential of **DFF** is lower than the oxidation potential of the catalyst.[50,51] The reason for applying a high potential is to promote OH^- adsorption at the electrode, which further activates the **HMF**.[41] It is therefore reasonable to assume that this step follows the OH* mechanism. The subsequent oxidation of **DFF** to **FFCA** and further oxidation to **FDCA** is largely dependent on the charge.[52] Essentially, metal oxide (M^{n+}) catalysts are oxidized to hydroxyl oxides (M^{n+1}) at correspondingly high pressures, which are thought to be the active sites for **FDCA** formation.[53] In addition, high potential promotes the process of deprotonation of the **DFF**, this step follows the E–C oxidation mechanism.[54] It is worth noting that the voltage required to produce **FDCA** from this step is higher in a non-alkaline (low pH) than that in alkaline electrolyte, when the **DFF** is generally used as the final product. For path 2, this process usually takes place in a strong alkali solution. The reaction from **HMF** oxidation to **HMFCA** occur at a low potential with high selectivity. It demonstrated that the strongly alkaline (pH ≥ 13) are more favorable for preferential adsorption and oxidation.[38,55] Zou's group reviewed that the deprotonation of **HMF** at low potential only requires the activated OH^- adsorption, which follows the OH* mechanism.[3] The second step of **FFCA** generation from **HMFCA** is more complicated because its generation potential overlaps with the potential of **HMFCA** to **FDCA** with low selectivity.[51] Therefore, this step is considered to be a hybrid mechanism of E–C and OH*, which is different from path 1 mentioned above. With the generation of high-valent catalytic species, **FDCA** becomes the main product, so it can be judged that the generation of **FDCA** mainly follows an E–C mechanism.[47] Since **FFCA** and **FDCA** have similar active sites and oxidation potentials, there is selective competition between

them. However, due to the narrow range of oxidation voltages of **FFCA**, the selectivity of **FDCA** is significantly increased when larger voltages are applied.[56] The direct and indirect oxidation of **HMF** over Co_3O_4 catalysts was investigated by Lu et al.[38] It is demonstrated that the direct oxidation of **HMF** occurred at low potentials, which is beyond the potential for the oxidation of Co^{3+} to Co^{4+} (1.3–1.42 V vs. RHE), following the OH* mechanism. In contrast, the co-oxidation zone at high potential is included in the oxidation of Co^{3+} to Co^{4+}, meaning that there is both an OH* mechanism and an E–C mechanism, and implying that the direct activity of **HMF** oxidation reaction (HMFOR) is highly dependent on the activity of the hydroxyl groups and aldehydes on the catalyst. It has been demonstrated that Co_3O_4 has a higher aldehyde oxidation activity and NiO has a higher hydroxyl oxidation activity (Fig. 4b).[38]

3.1.4 Furfural (FF) oxidation mechanism. Holewinski et al. proposed that oxidation selectivity of the furan compounds is governed by a balance between several properties of the catalyst via attenuated total reflectance surface-enhanced infrared absorption spectroscopy (ATR-SEIRAS) with modulation excitation spectroscopy (MES) as well as density functional theory (DFT) calculations.[57] There are two kinds of mechanism of furfural oxidation to furoic acid, including two-electron pathway and one-electron pathway. As shown in Fig. 5a, one molecule of furfural releases two electrons to form furoic acid (**FA**) (defined as the "two-electron pathway"). This reaction is a typical reaction mechanism for the oxidation of furfural under alkaline conditions. However, several recent reports have demonstrated the formation of hydrogen on the anode surface during experiments. For example, hydrogen indeed be formed during the electrochemical oxidation of furfural over heterogeneous catalysts such as ruthenium pincer catalysts[58] or Cu-based catalysts.[59,60] Thus, the following reactions (Fig. 5b) might be occurred. This reaction mechanism, in which one molecule of furfural releases an electron and a hydrogen atom to produce hydrogen, is defined here as "single electron pathway". Recently, Wang et al.[59] constructed a Cu-anodic
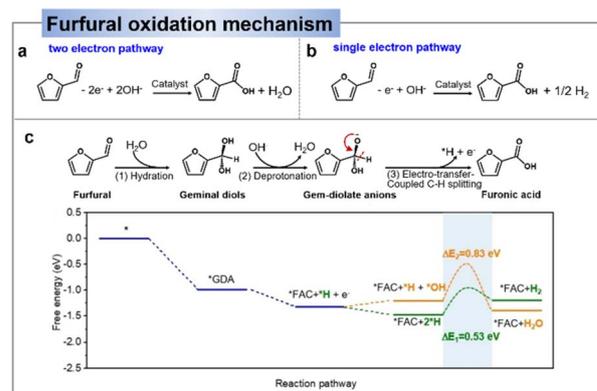

Fig. 5 Mechanisms of electrocatalytic oxidation of furfural to furoic acid: two-electron pathway (a) and one-electron pathway (b). (c) Proposed reaction pathway and corresponding free-energy diagram for the low-potential furfural oxidation on a Cu (111) surface.[59] Copyright 2021, Wiley-VCH.

electrocatalytic system grown on Cu foam to achieve low-potential oxidation of furfural and release hydrogen atoms from the aldehyde group to generate hydrogen gas. They suggested that furfural is rapidly and reversibly hydrated in alkaline aqueous solution to form geminal diols. The hydroxyl group of geminal diols can subsequently be deprotonated by hydroxyl ions to form the gem-diolate anions (**GDA**) as in Fig. 5c. Therefore, a low-potential furfural oxidation reaction pathway based on an intermediate **GDA** was proposed. The **GDA** is first adsorbed on the surface of Cu (111), and then undergoes an electron-transfer-coupled C–H splitting to generate a furfuryl acid (***FAC**) and an adsorbed hydrogen atom (***H**). Notably, due to the lower energy barrier, at low potentials, preferential binding to H_2 (*H + *H = H_2, ΔE_1 = 0.53 eV) rather than oxidation to H_2O (*H + OH$^-$ = H_2O+ e$^-$, ΔE_2 = 0.83 eV) is achieved by C–H splitting.[59] Meanwhile, Zhao et al.[33] found that Cu/CuO anodes catalyze furfural oxidation well under liquid flow fuel cells, but it do not release hydrogen efficiently, and Ag_2O proved to be the best anode catalyst to facilitate electron transfer for furfural oxidation and produced H_2 in this system. The results indicate that the anode catalyst plays a crucial role in both the oxidation of furfural and the production of hydrogen.

3.2 Electrocatalysts design for oxidation of 5-hydroxymethylfurfural (HMF)

In the past few years, research efforts have been dedicated to exploring electrocatalysts and processes to improve the selectivity toward a target product and increase its energy efficiency, extensive efforts have been devoted to designing electrocatalyst/electrode structures that optimize the chemisorption of key intermediates toward fast kinetics.[36,51,61,62] In recent publications which related to the electrochemical oxidation of furans, most of the reaction substrates have focused on **HMF**. Therefore, in this section, we will review the electrocatalytic oxidation of **HMF**. The recent literature on the electrocatalytic oxidation of furans has been studied and the electrocatalytic properties of these catalysts as well as reaction condition have been discussed.

3.2.1 2,5-Diformyl furan (DFF) as product. Currently, alkaline electrolytes are the most used media for the oxidation of furan compounds, as non-precious metal-based catalysts are usually active and durable in such electrolytes.[52,63] However, alkaline conditions hinder the selective oxidation of biomass-based alcohols to aldehydes due to the fact that aldehydes undergo alkali-catalyzed dimerization or aldol condensation reactions at high pH values.[51] In contrast, alkalis promote the conversion of aldehyde to reactive geminal diol, which in turn dehydrogenates to carboxylates.[64] It is thought that these problems can be avoided in neutral/near-neutral electrolytes, enhancing the selective of biomass alcohols to aldehydes. As reported by Duan et al., neutral media are more favorable for **DFF** generation than alkaline media.[51] However, the electrooxidation reaction of **HMF** is several orders of magnitude less active in neutral/near-neutral media than in alkaline media,[40] which is a major obstacle to the generation of **DFF**. Therefore,

the electrosynthesis of **DFF** usually requires the participation of noble metals with unique electron and better antioxidant properties.[65] The detailed catalysts are shown in Table 1. The main product of Pt and Ru in acidic and/or alkaline media is **DFF** has been demonstrated with poor conversion and yield/selectivity.[66–69] But electrooxidation of **HMF**s by monometallic Pt or Ru electrodes is not industrially feasible due to high capital expenditure. Therefore, there is a need to develop some composite or alloying strategies to convert **HMF**s efficiently.[44] Duan et al. used a single-atom ruthenium-doped nickel oxide (Ru$_1$-NiO) catalyst for the selective preparation of aldehydes in a neutral medium. At a current density of 10 mA cm^{-2}, Ru$_1$-NiO possessed a low potential of 1.283 V vs. RHE and an optimal selectivity of up to 90% for **DFF**. This is the best catalyst to date for the selective synthesis of **DFF** via electrooxidation of **HMF**.[51] It was shown by CV, Raman spectroscopy and operando EIS measurements that the reaction for the conversion of **HMF** to **DFF** under neutral electrolyte in the present study follows the OH* mechanism, in which the monoatomic Ru facilitates the oxidation of **HMF** in neutral medium by promoting hydrolytic dissociation to generate OH*. The results showed that neutral medium was more favorable for aldehyde production than alkaline medium (Fig. 6a and b). Considering the high cost of precious metals and the poor catalytic activity of **HMF** electrooxidation, the development of high-efficiency nonnoble metal catalysts is still in the mainstream due to the advantages of their convenient source, low price and high catalytic activity. MnO$_x$ was used for the electrooxidation of **HMF** under acidic media (pH = 1) considering the stability of MnO$_x$ in acidic solutions, with a **DFF** yield of 41.9% and a **HMF** conversion of 95.8%. However, the system requires high voltage (2.0 V vs. RHE), which leads to unavoidable by-product formation and low efficiency.[70] Co$_8$Ce$_2$O$_x$ showed good catalytic activity for **HMF** oxidation under neutral conditions, with 92% **DFF** selectivity at 1.5 V vs. RHE but lower FE selectivity (48.7%).[52] The doping of Ce modulated the electronic structure of Co and hindered the formation of CoOOH, the active site for **FDCA** generation.

In summary, noble metals promote the conversion of **HMF** to **DFF** but the efficiency is not satisfactory, which may be due to the theoretical weak adsorption of OH* and strong adsorption H*,[71] it is not favorable to the oxidation reaction. Ru has a strong adsorption for both OH* and H*, which is theoretically more suitable for neutral environments and favors water dissociation.[72] Therefore, the design of the catalyst, especially the nonnoble metal catalysts, and the highly active and stable hydroxyl oxidation catalysts can be obtained by adjusting the electronic structure and surface adsorption properties. It should be noted that water adsorption and dissociation steps need to be considered to provide active OH*. In addition, the formation of high-valent oxidatively active substances should be avoided to prevent further oxidation of **DFF**.

3.2.2 5-Hydroxymethyl-2-furancarboxylic acid (HMFCA) as product. **HMFCA** is suitable for obtaining in alkaline environments. Li et al.[73] showed that gold (Au) could oxidize aldehydes in **HMF** efficiently to form **HMFCA**, with 100% conversion at 0.6 and 0.9 V vs. RHE, and 98% selectivity for **HMFCA**. When they further increased the potential to 1.2 V vs. RHE, the selectivity

Table 1 Electrocatalytic oxidation of furan compounds

Substrate	Catalysts	Electrolyte	Concentration (mM)	Potential (V vs. RHE)	Conversion (%)	Product/sel. (%)	FE (%)	Ref.
HMF	Pt foil	0.1 M NaOH	—	0.44	70	DFF, ~26	—	70
HMF	Pt	NaHCO$_3$	—	—	—	DFF, —	—	66
HMF	Pt	1.0 M H$_2$SO$_4$	—	2.0	88.3	DFF, 13.1	—	67
HMF	Pt	0.3 M NaClO$_4$	—	0.73	9.0	DFF, 4.0	9.0	68
HMF	PtRu	0.1 M H$_2$SO$_4$	100	—	25	DFF, 89	—	44
HMF	Ru$_1$-NiO	1.0 M PBS	50	1.5	72.4	DFF, 90	70	51
HMF	MnO$_x$	H$_2$SO$_4$ (pH = 1)	20	2	95.8	DFF, —	—	71
HMF	Co$_8$Ce$_2$O$_x$	0.1 M Na$_2$B$_4$O$_7$	5	1.5	—	DFF, 92	48.7	72
HMF	Cu NPs	0.1 M KOH	10	1.23	—	FFCA, 67		113
HMF	Au/C	0.1 M KOH	20	0.9	100	HMFCA, —	—	73
HMF	Cu	1 M KOH	50	0.4	~70	HMFCA, 100	100	43
HMF	Ru$_1$-NiO	1 M KOH	50	1.3	—	HMFCA, 74	—	51
HMF	Co(OH)$_2$-CeO$_2$	0.1 M PBS (pH = 7)	10	1.4	~96	HMFCA, 89.4	—	76
HMF	CoO$_x$	0.1 M KOH	5	1.6	—	HMFCA, 48	—	52
HMF	Pd$_1$Au$_2$/C	0.1 M KOH	20	0.9	100	FDCA, 83	—	73
HMF	Pd$_7$/Au$_7$	1.0 M KOH	5	0.82	~42.4	FDCA, 38.7	85.8	74
HMF	Co$_1$Cu$_1$-CH	1.0 M KOH	10	1.42	99.57	FDCA, 99.91	98.88	114
HMF	Ni NPs	0.1 M KOH	10	1.5	—	—	—	115
HMF	Ni/CP	0.1 M KOH	5	1.36	99.7	FDCA, 99.4	99.4	61
HMF	hp-Ni	1.0 M KOH	10	1.423	—	FDCA, —	98	116
HMF	NiCu NTs	1.0 M KOH	20	1.424	~100	FDCA, 99	96.4	78
HMF	Ni-Cu/NF	1.0 M KOH	50	1.45	—	FDCA, 100	99.7	79
HMF	Rh-O$_5$/Ni(Fe)	1.0 M KOH	50	1.48	98	FDCA, 99.8	98.5	117
HMF	Ir-Co$_3$O$_4$	1.0 M KOH	50	1.42	—	FDCA, —	98	62
HMF	V$_O$-Co$_3$O$_4$	1.0 M KOH	10	1.47	—	FDCA, —	88.1	40
HMF	NiO-Co$_3$O$_4$	1.0 M KOH	10	1.35	—	FDCA, —	96.0	82
HMF	NiCo$_2$O$_4$	1.0 M KOH	10	1.45	—	FDCA, 99.4	99	87
HMF	Ni$_{0.5}$Co$_{2.5}$O$_4$	1.0 M KOH	50	1.5	—	FDCA, —	90.3	38
HMF	NiO-CMK-1	0.2 M KOH	20	1.85	65	FDCA, 79	70	56
HMF	Pt/Ni(OH)$_2$	1.0 M KOH	50	—	—	FDCA, —	98.7	89
HMF	CoO$_x$H$_y$	1.0 M KOH	10	1.5	—	FDCA, —	70	90
HMF	CF-Cu(OH)$_2$	1.0 M KOH	100	1.823	—	FDCA, —	100	53
HMF	E-CoAl-LDH-NSA	0.1 M KOH	10	1.52	—	FDCA, —	99.4	42
HMF	NiFe LDH	1.0 M KOH	10	1.23	98.6	FDCA, 99	99.4	118
HMF	d-NiFe LDH	1.0 M KOH	10	1.48	97.4	FDCA, 99.4	84.5	92
HMF	CoFe-LDH@NiFe-LDH	1.0 M KOH	10	1.4	—	FDCA,100%	99.8	93
HMF	Ru$_{0.3}$/NiFe-LDH	1.0 M KOH	5	1.48	99.4	FDCA, 99.2	—	94
HMF	NiCoFe LDH	1.0 M NaOH	10	1.52	—	FDCA, 88.9	~90	54
HMF	NiCoMn LDH	1.0 M NaOH	1	1.50	100	FDCA, 91.7	~65	91
HMF	CoOOH	1.0 M KOH	10	1.423	100	FDCA, 100	99	86
HMF	NiOOH	0.1 M KOH	5	1.47	—	FDCA, 96.2	96	47
HMF	MnO$_x$	0.1 M H$_2$SO$_4$	20	1.6	99.9	FDCA, —	34	67
HMF	Ni$_3$S$_2$/NF	1.0 M KOH	10	1.423	—	FDCA, 98.0	98.0	103
HMF	Co$_{0.4}$NiS@NF	1.0 M KOH	10	1.45	100	FDCA, 99	99.1	107
HMF	N-MoO$_2$-Ni$_3$S$_2$	1.0 M KOH	10	1.623	90	FDCA,100	—	119
HMF	Co$_9$S$_8$-Ni$_3$S$_2$@NSOC/NF	1.0 M KOH	10	1.4	100	FDCA, 98.8	98.6	120
HMF	NiS$_x$/Ni$_2$P	1.0 M KOH	10	1.46	—	FDCA, 98.8	95.1	109
HMF	NiCo-S	1.0 M KOH	10	1.45	99.1	FDCA, 98.0	96.4	121
HMF	Co-P/CF	1.0 M KOH	50	1.423	100	FDCA, 90.0	—	102
HMF	Ni$_2$P NPA/NF	1.0 M KOH	10	—	—	FDCA, 100	98	104
HMF	NiFeP	1.0 M KOH	10	1.435	—	FDCA, 100	94.6	108
HMF	CoNiP-NIE	1.0 M KOH	10	1.5	—	FDCA, —	87.2	122
HMF	MoO$_2$-FeP	1.0 M KOH	10	1.42	100	FDCA, 98.6	97.8	112
HMF	NiP-Al$_2$O$_3$/NF	1.0 M KOH	0.3	1.45	98.2	FDCA, 99.6	96	123
HMF	NiB$_x$	1.0 M KOH	10	0.6 vs. NER	99.8	FDCA, 99.0	99.5	105
HMF	Ni$_x$B (flow cell)	1.0 M KOH	10	1.45	100	FDCA, 98.5	100	84
HMF	Ni$_3$N@C	1.0 M KOH	10	1.45	—	FDCA, 98.0	99	55
HMF	Ni$_3$N	1.0 M KOH	50	1.47	—	FDCA, ~92.0	—	106
HMF	Ni$_3$N-V$_2$O$_3$	1.0 M KOH	10	—	—	FDCA, 98.7	—	124
HMF	VN	1.0 M KOH	10	20 mA	98.0	FDCA, 96.0	84	98
HMF	NF@Mo-Ni$_{0.85}$Se	1.0 M KOH	10	1.40	100	FDCA, 95.0	95.0	111
HMF	NiSe@NiOx	1.0 M KOH	10	1.423	—	FDCA, 99.0	99.0	100

Table 1 (*Contd.*)

Substrate	Catalysts	Electrolyte	Concentration (mM)	Potential (V *vs.* RHE)	Conversion (%)	Product/sel. (%)	FE (%)	Ref.
HMF	CoO–CoSe	1.0 M KOH	10	1.43	—	**FDCA**, 99.0	97.9	110
HMF	F–NiCo$_2$O$_4$/CC	1.0 M KOH	10	1.45	98.47	**FDCA**, 99.51	98.1	125
HMF	NiVW$_v$-LMH	1.0 M KOH	10	1.39	~100	**FDCA**, 99.2	—	126
FF	PbO$_2$	0.05 M H$_2$SO$_4$	10	2.0	100	**MA**, 65.1	33.4	127
FF	CuS	[Et$_3$NH]NO$_3$ (1.8 wt%)	1	1.6	70.2	**HFN**, 3.6	77.1	128
FF	Au/C	0.25 M HClO$_4$	50	0.8	—	**FA**, 99	100	129
FF	Cu/Cu foam	1.0 M KOH	50	0.3 V (H-cell)	—	**FA + H$_2$**, —	100	59
FF	PbO$_2$	0.1 M KOH	10	1.3 (Ag/AgCl)	—	**FA**, 99.3	85	130
FF	H–PdCu	0.1 M KOH	200	0.88 (OCV, H cell)	—	**FA**, —	93.3	131
FF	Ag$_2$O@Ni	2.0 M KOH	100	1.95 V (OCV)	—	**FA**, —	—	132
FF	Pt–Co$_3$O$_4$	1.0 M KOH	50	1.55 V	44.2	**FA**, 55	66.1	133

decreased to 81% due to further oxidation of **HMFCA** to **FFCA** and **FDCA**. This result suggests that Au is simultaneously capable of oxidizing **HMFCA**, but this requires a larger overpotential compared to oxidizing **HMF**.[74] It is worth noting that oxidation of **HMF** by the Au catalyst was pH sensitive, with a sharp decrease in current density and a slight decrease in alkalinity. Koper[75] attributed this to the deprotonation of the alcohol by the base in solution to form alcohol oxides, which increased the oxidation reactivity at the Au electrode. This metallic catalyst following OH* mechanism at low potential.

For non-precious metal, Zhao *et al.*[76] prepared Co(OH)$_2$–CeO$_2$ as the catalysts for **HMF** electrooxidation under the neutral condition of pH 7, and achieved **HMFCA** (89.4% selectivity) at 1.4 V (RHE). XPS and *in situ* Raman revealed that the evolution of active species between CoOOH and CoO$_2$ is the key factor for the selective electrooxidation of **HMF** (Fig. 6c and d).

The results showed that an increase in pH had a greater oxidizing effect on the oxidation of the alcohol hydroxyl group and that the alcohol hydroxyl group was better oxidized than the aldehyde group. To sum up, pH and potential have a large effect on the oxidation of the alcohol hydroxyl group. At low pH and potential conditions, the oxidation of alcohol hydroxyl groups was significantly inhibited and the products were mainly **HMFCA**, whereas at high pH conditions theoretically tended to produce **FFCA** and **FDCA**. Secondly, the addition of CeO$_2$ and electron transfer from Co(OH)$_2$ to CeO$_2$ led to the formation of more Co^{3+} substances, which were the key substances catalyzing the oxidation of **HMF** to generate **HMFCA**. In addition, as the potential increased, the Co active substance underwent a change from Co(OH)$_2$ → CoOOH → CoO$_2$, with CoOOH being the active substance at low potentials and CoO$_2$ being the active substance at high potentials. At high pH, Co^{3+} and Co^{4+} are
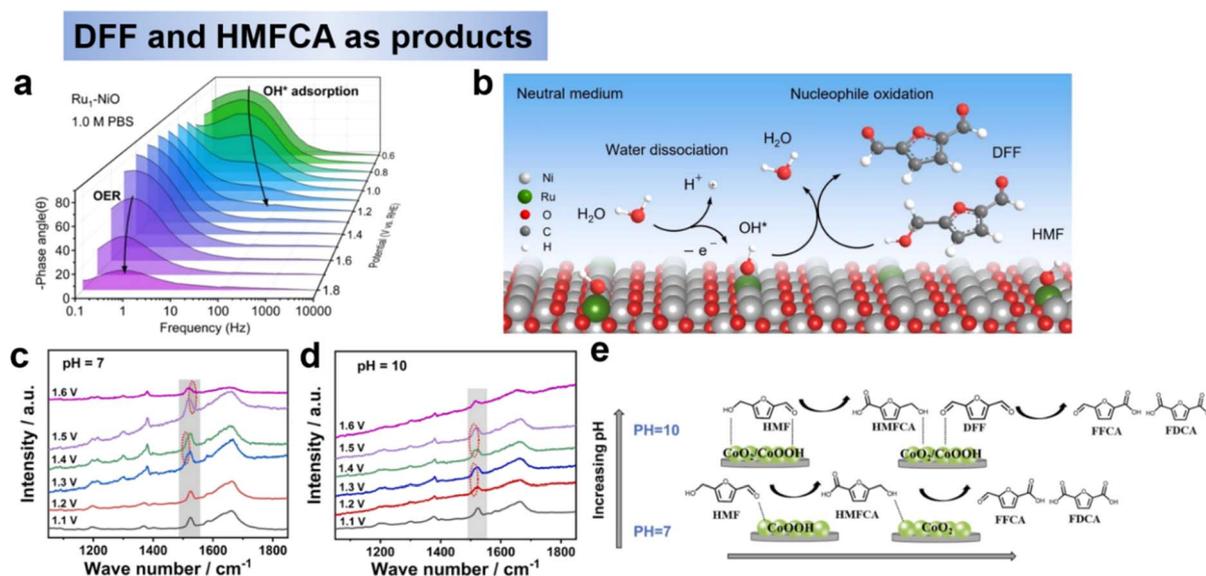

Fig. 6 (a) *Operando* EIS analysis of Bode plots of Ru$_1$-NiO under different potentials and (b) proposed HMFOR mechanism over Ru$_1$-NiO in the neutral medium.[51] Copyright 2022, Wiley-VCH. *In situ* Raman spectra of electrolyte change under different potential at pH 7 (c) and pH 10 (d), and (e) Schematic diagram of **HMF** conversion path on Co(OH)$_2$–CeO$_2$ catalyst at different pH and potentials.[76] Copyright 2023, Elsevier.

generated at low potentials, thus oxidizing the hydroxyl and aldehyde groups of **HMF**, which is the key difference between CoOOH selectively oxidizing aldehyde groups to generate **HMFCA** at low pH and low potential conditions (Fig. 6e).[76] Although not explicitly stated in the text, the reactions involved in this study follow the E–C. For the catalyst design of **HMFCA**, on the one hand, oxidation-resistant metals or metals with high redox potentials should be selected to avoid the generation of high-valent oxides in alkaline environments, which would be favorable for the further oxidation of **HMFCA** to **FFCA** and **FDCA**. On the other hand, the varied electronic configurations within the same valence state result in distinct selectivity, necessitating further investigation.

3.2.3 2,5-Furandicarboxylic acid (FDCA) as product.

Among those products of **HMF** electrooxidation reaction, **FDCA** is considered to be one of the most valuable oxidation products because it is commonly used as a precursor for the production of the biopolymer material polyethylene furanoate. Moreover, the theoretical oxidation potential of **HMF** oxidated to **FDCA** (0.3 V $vs.$ NHE) is much lower than that of OER (1.23 V $vs.$ NHE).[41] Therefore, **HMF** electrooxidation has drawn growing attention recent years. In this section, we will discuss some representative results of noble metal electrodes and non-precious metals and their composite electrodes for **HMF** electrooxidation, respectively, along with a description of the electrolysis conditions and electrochemical performance.

Noble metal catalysts. Single metals are difficult for **HMF** to be completely oxidized to **FDCA**, while noble metal alloy electrodes can effectively solve this problem. Chadderdon et al.[73] synthesized and optimized palladium–gold alloy (Pd_1Au_2/C) nanoparticles to selectively oxidize both hydroxyl and aldehyde groups of **HMF**, achieving 83% **FDCA** selectivity and 100% **HMF** conversion at an anodic potential of 0.9 V $vs.$ RHE, this excellent performance is due to the presence of the Au phase improves the activity of the isolated Pd, and the activation of aldehydes and hydroxyls by Au and Pd, respectively. A similar study was done by Park et al.[74] They further designed a three-dimensional palladium–gold alloy electrode (Pd_7/Au_7) for **HMF** oxidation reaction, and finally obtained a 38.7% **FDCA** selectivity using gold nanoparticles wrapped around palladium nanoparticles in 1.0 mol L^{-1} KOH and at an anodic potential of 0.82 V $vs.$ RHE. Interestingly, although the alloying elements were the same in the two studies mentioned above, the reaction paths for the formation of **FDCA** were different. Chadderdon[73] believes that the Pd site preferentially undergoes dehydrogenation of **HMF** to **DFF**, which is further oxidized to obtain **FFCA**, and then Au catalyzes the conversion of **FFCA** to **FDCA**, while park believes that Au on top preferentially converts the **HMF** oxidized to **HMFCA**, while **HMFCA** → **FFCA** → **FDCA** occurs on the Pd site. This may be due to the different morphologies and electronic structures produced by the different preparation methods, resulting in the surfaces being exposed to different crystalline planes, and the different crystalline planes will lead to different adsorption energies of the intermediates, which is the main reason for the difference in selectivity. In addition, one is a flow reactor and the other is a half-cell, and the difference in the reaction vessel will also have an effect, and we encourage the

use of uniform criteria for judgement. Although the noble metals showed considerable activity, their post-reaction characterization was insufficient for further active site identification, the material is expensive and the synthesis process is complicated.

Nonnoble metal catalysts. Considering the cost of noble metals and the poor catalytic activity of **HMF** electrooxidation, although the start-up potentials of nonnoble metal electrocatalysts are slightly higher, the development of highly efficient nonnoble metal catalysts (including nonnoble metal compounds) is still a general trend due to their convenient sources and low prices, and a large number of research results have been produced. Among the various nonnoble metal catalysts, nickel-based and cobalt-based metals are the most active class. Various nickel-based compounds exhibit different compositions and properties, making them adaptable to different applications. Qi et al.[61] prepared a nickel nanosheet catalyst vertically anchored on a carbon paper substrate by electrodeposition, which exhibited enhanced catalytic activity in the **HMF** electrooxidation reaction, with 99.7% **HMF** conversion and 99.4% **FDCA** yield at a low potential of 1.36 V $vs.$ RHE. The high catalytic activity was attributed to the unique electronic structure of the Ni/CP electrode. Compared with Ni catalysts with nanoparticle morphology, nanosheet Ni with small grain size can transfer electrons to the semiconducting carbon carriers, and the electron-deficient Ni is easily oxidized to high-valent $Ni^{\delta+}$ (δ = 2–3, Fig. 7a and b), especially in the form of NiO or NiOOH at the edge position, which is the key active phase for efficient **HMF** electrooxidation.[77] The reaction of **HMF** electrooxidation to **FDCA** may follow both pathways 1 and 2 as mentioned in Section 2.1. In addition to single-metal Ni catalysts, alloy catalysts have also been used to promote the oxidation of **HMF** to **FDCA**. To further promote the activity of the **HMF** oxidation reaction, the design of bimetallic catalysts is a strategy. Zheng et al.[78] reported a bimetallic catalyst, Cu-doped Ni nanotubes (NiCu NTs, Fig. 7c), for the oxidation of **HMF** to **FDCA** with simultaneous precipitation of H_2 at the cathode. When being employed as an anodic catalyst for the oxidation of **HMF** to **FDCA**, NiCu NTs showed 100% **HMF** conversion and 99% **FDCA** yield in 1.0 M KOH. To gain more insight into the working mechanism over the NiCu NTs catalyst, HPLC (Fig. 7d) and *in situ* Raman spectra (Fig. 7e) were examined, the results demonstrated that the conversion of **HMF** to **FDCA** follows the pathway of **HMF–HMFCA–FFCA–FDCA**, where the aldehyde groups are first oxidized to form a **HMFCA** intermediate, and the hydroxymethyl groups are consecutively oxidized to yield **FFCA** and then **FDCA**, which is consistent with aerobic **HMF** oxidation reactions. It is widely accepted that the formation of NiOOH on the surface is the first step in the aqueous oxidation of Ni-based catalysts in alkaline media. From this, it can be reasonably deduced that during the oxidation of **HMF**, the catalyst surface is also first oxidized to $Ni^{3+}OOH$, which as the active site then rapidly oxidizes the **HMF**, while Ni^{3+} is reduced to have Ni^{2+}. Although the electrooxidation reaction of **HMF** shows increasing potential, the OER is the main competing reaction at high current densities, which leads to low Faraday efficiency (FE) of the product and catalyst detachment from the
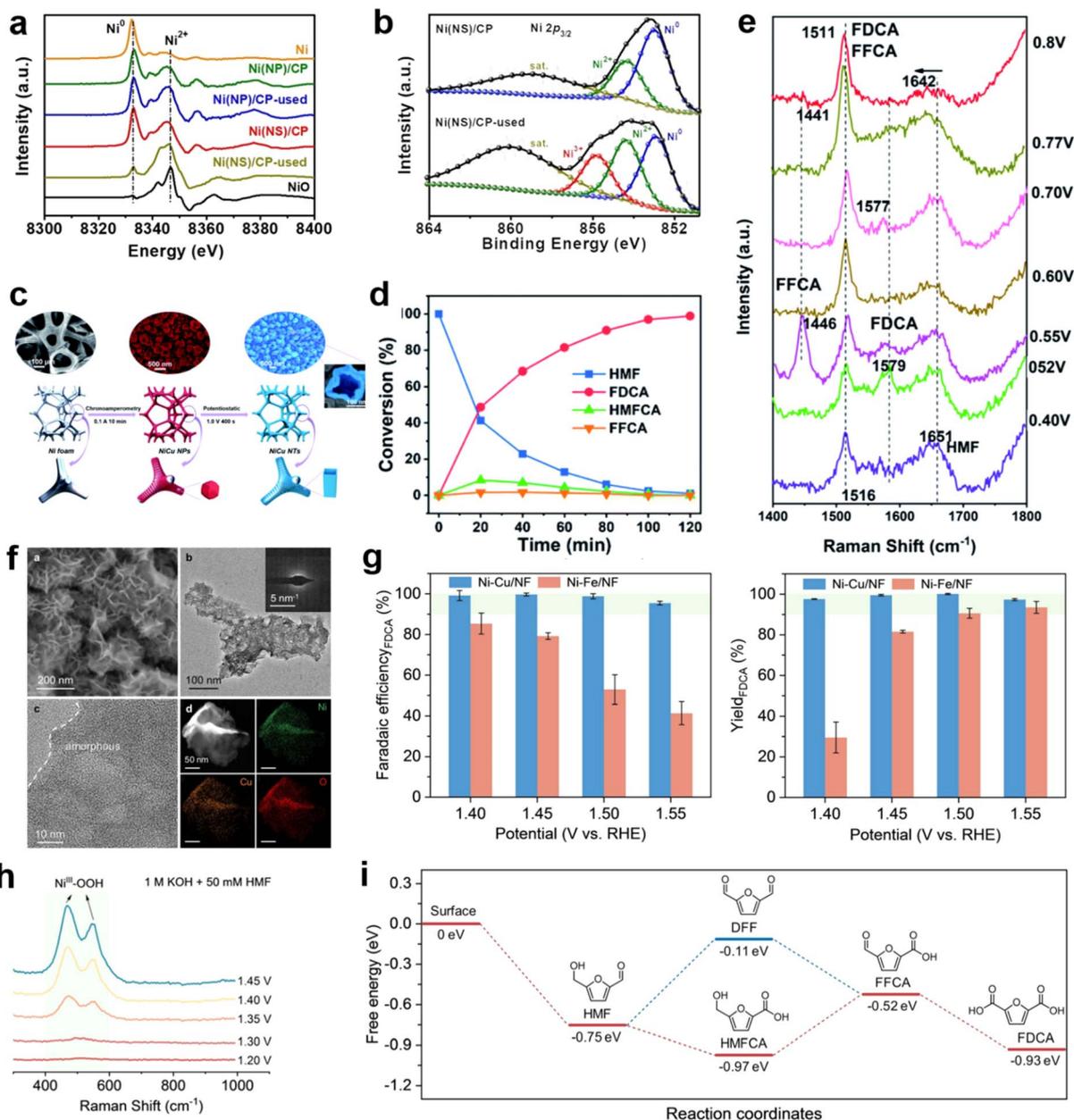
Fig. 7 Chemical states of Ni/CP hybrid electrodes: (a) first derivative normalized XANES spectra at the Ni K-edge for samples and (b) Ni 2p$_{3/2}$ XPS spectra of Ni(NS)/CP and Ni(NS)/CP-used.[77] Copyright 2021, Wiley-VCH. (c) Schematic illustration of the preparation route for the porous NiCu NTs electrode, and SEM images and (d) relative change (%) of **HMF** conversion and product yield during the electrooxidation process and (e) Raman spectra in **HMF** solution.[78] Copyright 2022, American Chemical Society. (f) FE-SEM and TEM image of Ni–Cu/NF and (g) FE and yields of **FDCA**, (h) *in situ* Raman spectroscopy of Ni–Cu/NF and (i) Gibbs free energy diagrams of HMFOR on *m*-Ni-Cu/NF.[79] Copyright 2023, Wiley-VCH.

electrode. In order to inhibit the OER, Sun *et al.*[79] reported a bimetallic Ni–Cu electrocatalyst (Ni–Cu/NF) loaded on Ni foam to enhance the oxidation reaction of **HMF** (Fig. 7f). A current density of 1000 mA cm^{-2} could be achieved at the reversible hydrogen electrode, and both FE and yield remained close to 100% over a wide range of potentials (1.4–1.55 V *vs.* RHE) (Fig. 7g). *In situ* Raman and theoretical calculations show that Cu doping hinders the deprotonation of OH* to O*, thus

greatly inhibiting the OER process. Meanwhile, from the EIS and Raman results, NiOOH acts as the active site for **HMF** oxidation, following the reaction path with **HMFCA** as the intermediate (Fig. 7h and i). From the above results, it can be inferred that metal catalysts usually consist of *in situ* derived hydroxides or hydroxyl oxides as the active substances for the generation of **FDCA**, and therefore need to be driven by high potentials. The mechanism (OH* or E–C mechanism) is

followed by both active species and pH *versus* oxidation potential, and some multisite catalysts may incorporate both of the above mechanisms, which requires further testing and calculations.

Metal oxides, –hydroxides, –oxyhydroxides. Metal oxides have a great advantage in oxidation reactions due to their flexibility in chemical composition and electronic states.[80] The most studied oxides are nickel- and cobalt-based oxides because of their excellent adsorption properties.[81] Further studies have found that $NiO(OH)_{ads}$ or $NiOOH$ to be the active centre of **HMF** oxidation.[56,81,82] Nickel-based materials have relatively high onset potentials for **HMF** electrooxidation, usually around 1.30 V *vs.* RHE.[82–85] In contrast, cobalt-based electrocatalysts typically possess a lower onset potential for the electrocatalytic oxidation of **HMF**.[86] Co_3O_4 were selected as catalysts to investigate the and optimized the **HMF** adsorption behavior by Wang's group.[40,62] First, the adsorption behavior of **HMF** on Co_3O_4 was optimized by introducing Ir single-atom sites, as shown in Fig. 8a. Compared with Co_3O_4, the Ir–Co_3O_4 electrocatalyst showed a stronger adsorption of **HMF** through the C=C group (Fig. 8b), resulting in Ir–Co_3O_4 showed a higher yield (98%) and faradaic efficiency (98%).[62] Since the HMFOR process includes the oxidation of hydroxyl and aldehyde groups, the different adsorption energies and positions of OH on the catalyst have an important effect on the activity of HMFOR, and there is also competition for the adsorption of OH by OER. Therefore, Wang *et al.* developed an oxygen vacancy on Co_3O_4 catalyst (V_O-Co_3O_4) to solve the competition for the adsorption of OH. As show in Fig. 8c, due to the introduction of oxygen vacancies (V_O) in Co_3O_4, OH^- can fill into V_O in the V_O-Co_3O_4 lattice. The involvement of lattice OH^- not only breaks the competitive adsorption between OH^- and **HMF**, but preferentially couples with organic molecules through lattice oxygen oxidation reaction rather than competing with **HMF** for adsorption on metal sites, which is the mechanism on Co_3O_4 electrode (Fig. 8d), thus accelerating the rate-determining step of **HMFCA** hydrogenation.[40]

Spinel oxides (AB_2O_4) have received much attention due to their abundant active sites, tunable coordination structures and high electrocatalytic stability, and their octahedral and tetrahedral sites play different roles in HMFOR.[87] In previous work, **HMF** was taken as a whole, thus, the reaction activity of the aldehyde (–CHO) and hydroxyl (–OH) groups has not yet been distinguished.[50] In order to deeper understanding of the reaction mechanism for HMFOR, Wang *et al.*[38] designed $Ni_{0.5}Co_{2.5}O_4$ catalysts for the reactivity of aldehydes (–CHO) and hydroxyls (–OH) to gain insight into the reaction mechanism. It was found that the direct oxidation activity of **HMF** was highly dependent on the activity of hydroxyl groups and aldehydes on the catalyst. The results showed that NiO has high hydroxyl oxidation activity and Co_3O_4 has high aldehyde oxidation activity (Fig. 8e). By introducing Ni into the tetrahedral sites of Co_3O_4, the best HMFOR performance was obtained at the $Ni_{0.5}Co_{2.5}O_4$ electrode (Fig. 8f), resulting in 92.4% **FDCA** yield and 90.4% Faraday efficiency. It is worth noting that Ni doping also changes the reaction mechanism to direct oxidation, with the aldehyde group still oxidized preferentially in 1 M KOH to

produce **HMFCA**, while hydroxyl oxidation was preferred at pH = 13.[38] Overall, metal oxide catalysts need to be further enriched due to their flexible and tunable structures. In addition, there is a need to develop methods to improve the performance of oxides, such as performing elemental doping and constructing heterojunctions in order to improve the adsorption and electron transfer to the reactants during the reaction process.

In addition, nickel hydroxide electrodes are more suitable for prolonged alkaline electrocatalysis due to the abundance of hydroxyl groups, which provide active sites and strong adsorption of substrates.[88] However, the surface HMFOR of nickel-based catalysts is still limited by the lower rate of Ni(OH)O generation from the active intermediate. Thus, Wang *et al.*[89] adjusted the adsorption energy of $Ni(OH)_2$ with **HMF** through the introduction of Pt, and explored the transformation of active species $Ni^{\delta+}$ in the process of HMFOR. In particular, *operando* Raman spectroscopy confirmed that $Ni(OH)_2$ was electrooxidized to Ni(OH)O, which further oxidized **HMF** to **FDCA** without the formation of $NiO_x(OH)_y$ (Fig. 9a, the peak at 473 and 553 cm^{-1}), that is considered to be the active substance of OER (Fig. 9b). It can be seen that the HMFOR on the $Ni(OH)_2$ catalyst surface follows the E–C mechanism.[89] Since the mechanism of CoO_xH_y is different from that of Co_3O_4, Luo *et al.*[90] combined experimental and a theoretical study to explain that electrogenerated Co^{3+} and Co^{4+} species act as chemical oxidants but with distinct roles in selective **HMF** oxidation. It was found that Co^{3+} generated at a low potential acted as the only oxidant to oxidize the aldehyde group, and as the potential increased, the selectivity of **FDCA** increased with concentration of Co^{4+} increased, which indicated that Co^{4+} was essential for the initial oxidation of the hydroxyl group in the molecule. It was found that the reaction was "E–C" mechanism (Fig. 9c).[90]

Furthermore, the layered double hydroxide (LDH) has been reported to have superior catalytic performance over single metal hydroxide since the second metal atoms could tune the electronic structure and introduce optimal surface chemical properties.[42,54,91] Subsequent studies on LDHs have focused on modulating the electronic structure to inhibit the OER competition response. Wang *et al.*[92] reports the electrooxidation of **HMF** to **FDCA** catalyzed by carbon paper supported cationic defect-rich nickel–iron alloy LDH (d-NiFe LDH/CP) under alkaline conditions. The d-NiFe LDH/CP exhibits excellent catalytic performance due to the electronic structure change induced by vacancy implantation. At a voltage of 1.48 V *vs.* RHE, the conversion of **HMF** was 97.35%, and the yield of **FDCA** reached 96.8% with a Faraday efficiency of 84.47% (Fig. 9d).[92] Zhao *et al.*[93] have prepared CoFe-LDH@NiFe-LDH as the catalysis for HMFOR, it was shown that the synergistic action of multiple active species could promote the electrooxidation of **HMF**, and the reactive species of the reaction was M^{3+} (M = Ni, Co, Fe). The **HMF** reaction on CoFe-LDH@NiFe-LDH electrodes contained two pathways, namely the **HMFCA** pathway at low potentials and the **DFF** pathway at high potentials (Fig. 9e and f). Additionally, Li's group[94] loaded single atom Ru on NiFe-LDH to enhance the catalytic ability of NiFe-LDH (Fig. 9g). As shown in Fig. 9h, the electron cloud around Ru^{3+} was transferred to Fe^{3+}, Ru^{3+} attracted the electron cloud of Ni^{2+}, and the loaded Ru
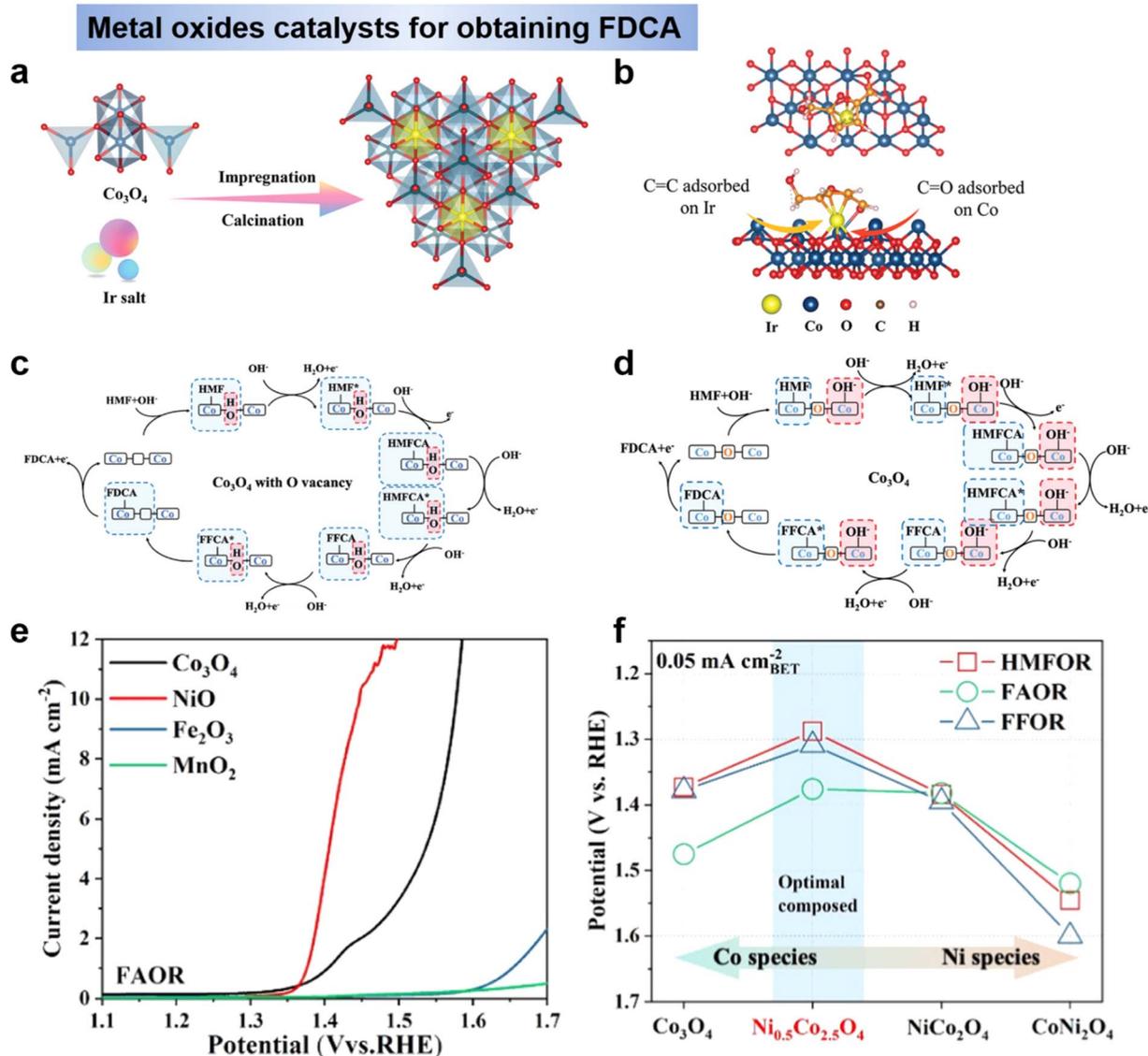
Fig. 8 (a) Scheme of the fabrication of Ir–Co_3O_4 and (b) the adsorption model of **HMF** molecules on Ir–Co_3O_4.[62] Copyright 2021, Wiley-VCH. (c) The reaction mechanism of HMFOR on V_O-Co_3O_4 and (d) on Co_3O_4.[40] Copyright 2022, Wiley-VCH. (e) Electrochemical behavior of FAOR on Co_3O_4, NiO, Fe_2O_3, and MnO_2 electrodes.[38] Copyright 2022, American Chemical Society. (f) Activity comparison for HMFOR, FAOR, and FFOR.[38] Copyright 2022, American Chemical Society.

atoms optimized the adsorption energy of the catalyst for **HMF** through electronic structure adjustment. The introduction of Ru in HMFOR not only promotes the oxidation of the hydroxyl group in **HMF**, but also the oxidation of the aldehyde group in **FFCA**, and in optimal conditions $Ru_{0.3}$/NiFe exhibits excellent **HMF** conversion (99.43%), **FDCA** selectivity (99.24%) and yield (98.68%) in HMFOR (Fig. 9i) and maintained excellent cycling performance (Fig. 9j). Although LDH has good HMFOR activity, especially when it is exfoliated into multilayer or monolayer structures, which can maximally expose its active sites and thus optimize its electrocatalytic performance. However, LDH nanosheets are easily detached and reaggregated in practical applications, so the preparation of monolayer LDH is a challenge that might be improved by the construction of self-supporting structures. Secondly, LDH catalysts require clearer

identification of active sites due to their complex composition and structure. Outside of this occasion, LDHs lack stability when exposed to highly alkaline electrolyte solutions for long periods of time. Therefore, methods to further improve the catalytic performance of LDHs for **HMF** electrooxidation (*e.g.*, design defects) should be developed.

By summarizing the metal hydroxides in the above research, we learn that most of the active species of that are oxy-hydroxides (MOOH). In order to gain a deeper understanding of the reaction mechanism of oxyhydroxides and to develop strategies to improve its performance, two of its mechanisms were explored using $Ni(OH)_2$/NiOOH as a model. Impressively, the indirect mechanism we mentioned above, the $Ni(OH)_2$ is first oxidized to NiOOH under applied bias. Then NiOOH acts as a chemical oxidant with the alcohol by non-electrochemical
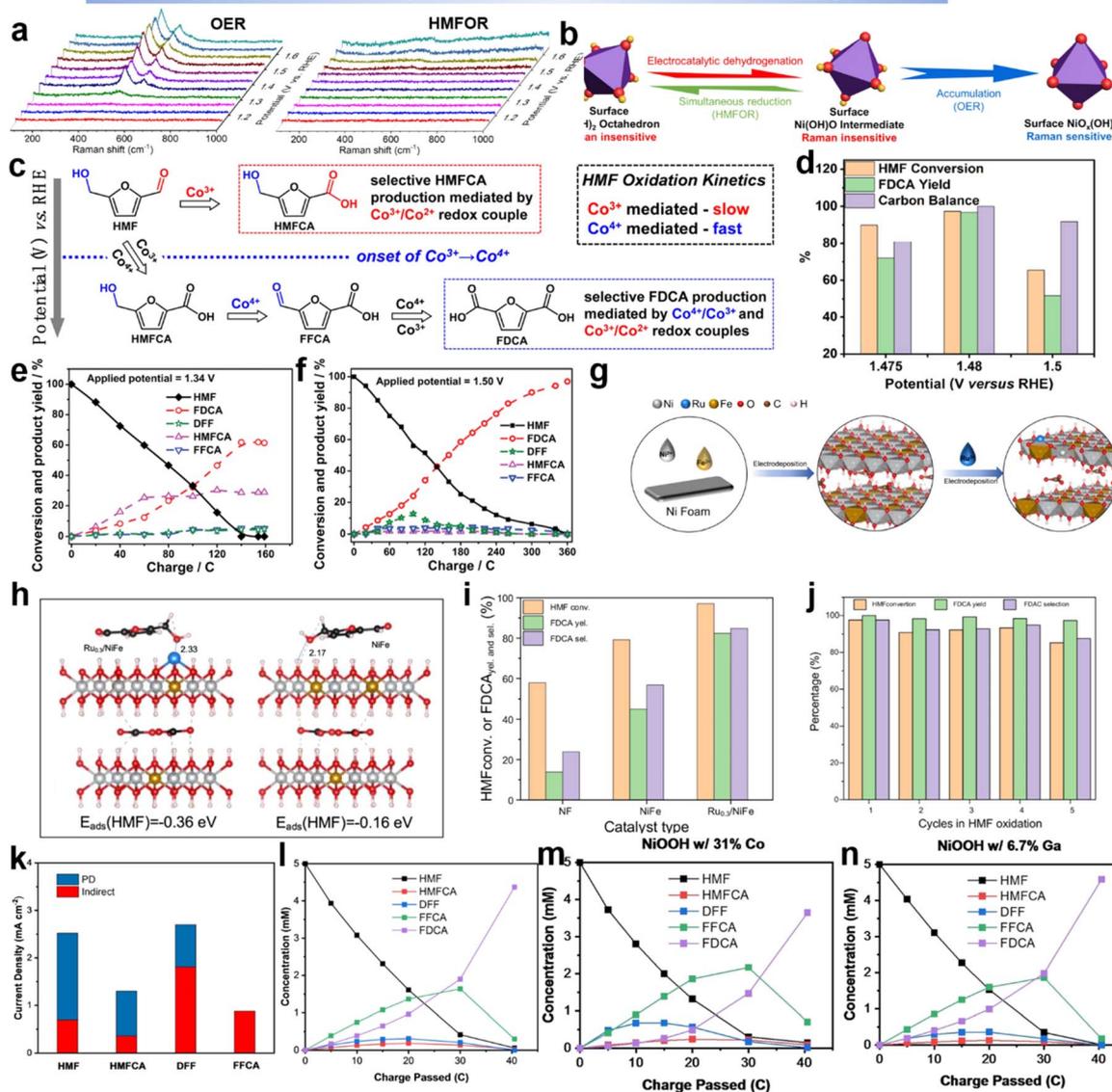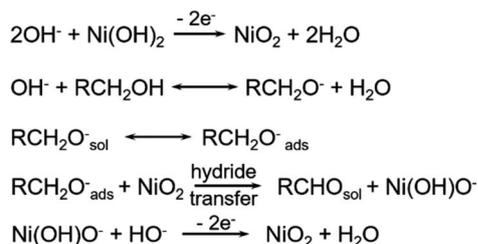
Fig. 9 (a) *Operando* Raman spectroscopy during OER and HMFOR and (b) schematic representation of crystal structure transformation.[89] Copyright 2021, Wiley-VCH. (c) Mechanistic illustration of the PD oxidation of **HMF**.[90] Copyright 2021, Wiley-VCH. (d) **HMF** conversion, **FDCA** yield, and carbon balance under different applied voltages catalyzed by d-NiFe LDH.[92] Copyright 2021, American Chemical Society. Variation of conversion ratios of **HMF**, **DFF**, **HMFCA**, **FFCA** and **FDCA** with consumed charges at the potentials of 1.34 V *vs.* RHE (e) and 1.50 V *vs.* RHE (f).[93] Copyright 2021, Wiley-VCH. (g) Schematic of the preparation process of Ru$_{0.3}$/NiFe and (h) side view of **HMF** adsorption configuration and corresponding adsorption energy in both models.[94] Copyright 2023, Elsevier. (i) The effects of different catalysts on **HMF** conversion, **FDCA** selectivity and yield and (j) **HMF** selectivity, **FDCA** conversion and selectivity obtained by Ru$_{0.3}$/NiFe in **HMF** oxidation.[94] Copyright 2023, Elsevier. (k) Component of the current due to indirect (red) and PD (blue) oxidation in a pH 13 solution.[95] Copyright 2022 Wiley-VCH. (l)–(n) Change in concentration of **HMF** and its oxidation products using pristine, Co-containing, and Ga-containing NiOOH.[95] Copyright 2022, Wiley-VCH.

transfer of hydrogen atoms to react with the alcohol by transferring the carbon from the α-position of the alcohol to the Ni^{3+} site in NiOOH, thus reducing NiOOH back to Ni(OH)$_2$ (Scheme 1d).[47] In this case, the applied voltage does not directly drive the oxidation of the **HMF**, but is only related to the regeneration of NiOOH. In addition to the well-known indirect mechanism, there is a second potential-dependent oxidation mechanism (direct mechanism), whereby oxidation reactions can also occur at potentials more positive than those required for the Ni(OH)$_2$/

NiOOH transition. It was thought in the early days that the NiOOH remains in the NiOOH state throughout the oxidation process,[47] however, Choi *et al.*[39,95] showed that the second pathway is only active when Ni^{4+} is present and that it involves hydride transfer from the carbon at the α-position of the alcohol to those Ni^{4+} sites (Scheme 2). For the second pathway, the application of the potential is required not only to generate active Ni^{4+} sites but also to drive the hydrogenation reaction. Therefore, the oxidation rate *via* this pathway is potential-

$$2OH^- + Ni(OH)_2 \xrightarrow{-2e^-} NiO_2 + 2H_2O$$

$$OH^- + RCH_2OH \rightleftharpoons RCH_2O^- + H_2O$$

$$RCH_2O^-_{sol} \rightleftharpoons RCH_2O^-_{ads}$$

$$RCH_2O^-_{ads} + NiO_2 \xrightleftharpoons[\text{transfer}]{\text{hydride}} RCHO_{sol} + Ni(OH)O^-$$

$$Ni(OH)O^- + HO^- \xrightarrow{-2e^-} NiO_2 + H_2O$$

Scheme 2 Proposed PD oxidation mechanism of alcohols to aldehydes *via* hydride transfer.[96] Copyright 2021, American Chemical Society.

dependent, and even if Ni^{4+} is still present, the oxidation rate drops to zero as soon as the bias potential is no longer applied. Therefore, this pathway named as potential-dependent (PD) oxidation. Although using NiOOH as model to discuss the differences between the indirect and PD oxidation mechanisms, they believe that both mechanisms are equally applicable to other MOOH catalysts, except that the propensity for indirect and PD oxidation will vary depending on the type of MOOH. Once this is fully understood, the selection and tailoring of electrocatalyst materials to facilitate either the PD or indirect pathway may provide a way to control functional group selectivity. Choi's group[95] demonstrated that **DFF** and **FFCA** (containing only aldehyde groups) were oxidized *via* the indirect pathway and **HMFCA** (containing only alcohol groups) *via* the PD pathway. For **HMF**s containing both aldehydes and alcohols, which oxidation pathway dominates (*i.e.*, which group tends to be oxidized first) depends on the oxidation conditions. Under open-circuit conditions that allowed only indirect oxidation, the aldehyde group was preferentially oxidized, resulting in the generation of **HMFCA** over **DFF**. However, when 0.55 V *vs.* Ag/AgCl was applied, resulting in the dominance of PD oxidation and preferential oxidation of the alcohol group to form **DFF** (Fig. 9k). They also examined the effect of shifting the Ni(OH)$_2$/NiOOH peak position on **HMF** oxidation by compositional adjustment of NiOOH (Fig. 9l–n). The Ni(OH)$_2$/NiOOH potential directly affects the indirect oxidation rate of **HMF**, but it did not have much effect on the indirect oxidation of **FFCA**, since the oxidative adsorption of **FFCA** is the rate-determining step.[95]

Metal borides, nitrides, phosphides, sulfides, and selenides. Combining with non-metallic elements can further improve the performance of metal-based catalysts. Recently, much effort has been devoted to the construction of transition metal catalysts for **HMF** oxidation, such as borides,[84,97] nitrides,[98] phosphides,[99] chalcogenides,[100] due to their accessible regulation of electronic structure and high earth abundance. In addition to this, these catalysts can provide/enhance the catalytic active sites and expand the pH range of applicability.[83,84,100,101] This class of materials was shown to have the actual active substance as MOOH, with the high valence metal acting as the active site to promote the oxidation of the furan compounds, and a gradual increase in the high valence species with increasing applied voltage.[102–106] In addition, metal doping leads to a dramatic increase in electrochemical active surface area (ECSA), which permits the exposure of more active sites and effectively modulates the electronic properties of this

class of metal compounds, facilitating the rapid reconstruction of the surfaces as (oxy)hydroxides as the actual active sites.[107,108] By modulating the electronic structure of the catalyst, the d-band center of the active metal can be adjusted to an optimal position, thus balancing **HMF** adsorption and dehydrogenation. For example, NiS$_x$/Ni$_2$P,[109] CoO/CoCe,[110] Mo–Ni$_{0.85}$Se,[111] and MoO$_2$–FeP[112] catalysts exhibited superior **HMF** oxidation performance.

In summary, a wide variety of non-noble transition-metal oxides, hydroxides, and oxyhydroxides (including S, P, B, N, Se compounds) have been studied as electrocatalysts for **HMF** oxidation. There are some notable differences in their reactivity compared to noble metal catalysts. A major reason for this is that non-precious transition metal compounds typically produce **FDCA** as the main product, rather than stopping at a partial oxidation product. Based on the comprehensive overview of various catalysts, the following conclusions can be drawn. Firstly, **DFF** is suitable for generation under non-alkaline environment, while **HMFCA** is more suitable for generation under non-acidic conditions. Secondly, the noble metals in the catalysts for generating **FDCA** have smaller potentials but poorer selectivity, but non-precious metal catalysts suffer from the problem of instability in acidic environments. Then, the active site and reaction mechanism of **HMF** oxidation for generating **FDCA** can be summarized as follows: (1) medium potential *via* M^{2+}/M^{3+} indirect oxidation. (2) Coexistence of direct oxidation at low potential and indirect oxidation at medium potential. (3) There may also be high potential oxidation directly or indirectly *via* M^{3+}/M^{4+} (*e.g.* NiOOH/CoOOH).

3.3 Electrochemical oxidation of furfural (FF)

FF can be oxidatively converted to a variety of value-added chemicals such as **FA**, **MA** and **HFN**, which have a wide range of applications in products such as polyester resins, surface coatings, solvents, plastics, food additives and pharmaceuticals. Holewinski *et al.*[134] have investigated the oxidation reaction pathway of furfural on platinum catalyst in an acidic electrolyte. They found that the selectivity of the electrooxidation of furfural depended on the potential. The major products were **FA** and 5-hydroxyfuranic acid (**HFA**) below 1.2 V *vs.* RHE. At higher potentials, the selectivity shifts mainly to 5-hydroxyfuran-2-(5*H*)-furanone (**HFN**) with the appearance of maleic acid (**MA**) and **MA** is not easily oxidized further once formed (Fig. 10a). Wang *et al.*[59] had coupled anodic low-potential furfural oxidation with cathodic oxygen reduction reaction (ORR) to change electrocatalytic furfural oxidation and hydrogen production from an electrical energy input mode to an electrical energy output mode. Copper metal was employed as an electrocatalyst for low-potential furfural oxidation. An oxidation-electrical reduction method was used to pretreat the Cu foam electrode to increase the electrochemically active surface area to maximize the utilization of the Cu foam electrode (Fig. 10b). The reaction mechanism of this system is shown in Fig. 5b and belongs to the single-electron pathway. The effect of applied potential on the product distribution is shown in Fig. 10c. The **FA** concentration shows a volcano curve
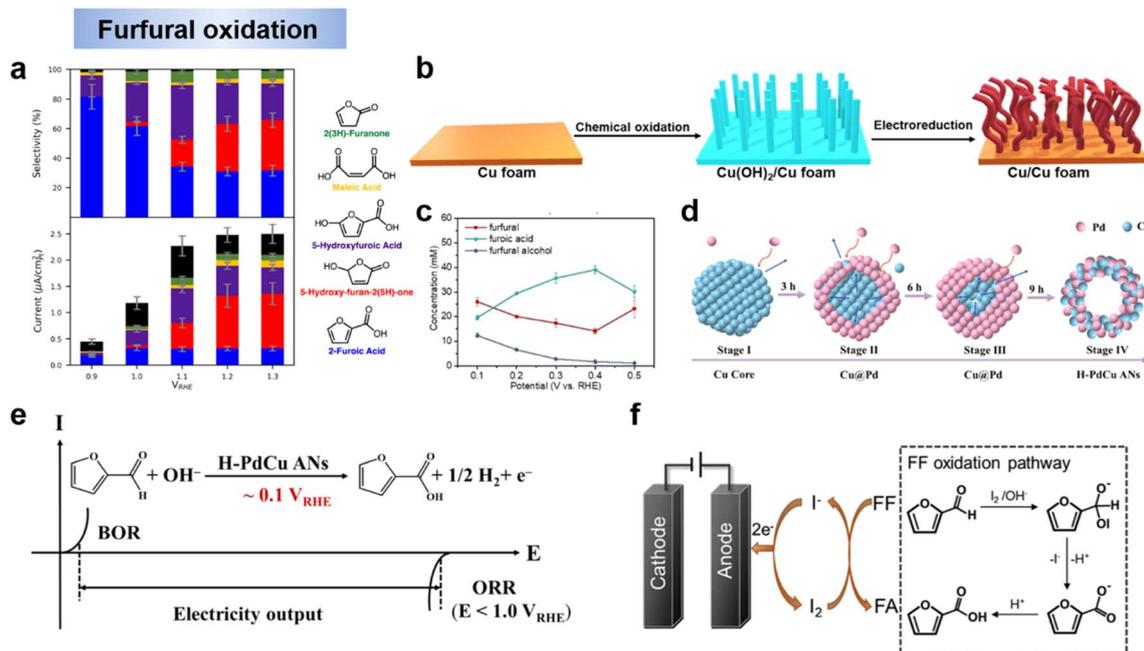
Fig. 10 (a) selectivity and partial currents toward major products of the electro-oxidation.[134] Copyright 2019, American Chemical Society. (b) Synthesis of the Cu electrode and (c) concentration of the organic compounds in the anode electrolyte as a function of applied potential for chronoamperometric tests over the Cu electrode.[59] Copyright 2021, Wiley-VCH. (d) Schematic diagram of the formation mechanism on H−PdCu and (e) the developed electricity output mode.[131] Copyright 2023, Elsevier. (f) Schematic diagram of iodide ion-mediated electrochemical oxidation of furfural.[135] Copyright 2022, Elsevier.

in the potential range of 0.1–0.5 V vs. RHE and peaks at 0.4 V vs. RHE. The decrease in performance at higher potentials may be related to the electrooxidation of the active metal Cu to inactive Cu₂O. When higher potentials were applied, the metal Cu showed electrochemical oxidation to Cu^{1+} (i.e., Cu_2O) and the anodic current density decreased dramatically. These results indicate that low applied potentials are favorable for maintaining the active metal characteristics of Cu electrodes. Not coincidentally, Zhang et al. showed experimentally and theoretically that H-PdCu ANs indeed accelerated the oxidation of furfural at an ultra-low potential (0.1 V vs. RHE) to generate H_2 via H* (aldehyde group release) recombination, realizing hydrogen production from electrical energy input to output (Fig. 10d and e).[131] In order to explain the mechanism of furfural oxidation on the catalyst surface, Li et al.[135] performed iodide-mediated anodic electrolysis of furfural in a flowing electrolysis. In this system, an "electrochemical–chemical" (E–C) process occurred (Fig. 10f). First, furfural is oxidized to furfuryl anion in the presence of active iodine and a base. At the same time, iodine is reduced to iodide ions and returned to the cyclic reaction while the furfuryl anion is oxidized to **FA**. Similar work on electrocatalytic oxidation of furfural with simultaneous hydrogen precipitation and coupled ORR on cathodic as discussed above were also reported by other researchers.[33,131,133] The above studies on the electrocatalytic oxidation of furfural showed that, the high potential was more favorable for the acquisition of **HFN** and **MA**, and the low potential tended to generate **FA**, and H_2 could be generated simultaneously with the oxidation of furfural by a suitable electrocatalytic electrode.

4   Selective electrochemical reduction of furan compounds

4.1   Pathway and mechanism for electrocatalytic reduction of furan compounds

Electrocatalytic reduction included hydrogenation and hydrogenolysis, as shown in Scheme 3a, where hydrogenation is an addition reaction directed at unsaturated bonds, whereas hydrogenolysis involves the substitution of an H atom for a group (in the presence of a bond break).[136] Recent studies on the reduction of **HMF** and **FF** have generally shown that in non-acidic media (i.e., near-neutral or alkaline media), hydrogenation is the dominant reaction, whereas hydrogenolysis is promoted only in acidic media.[25,137–141] Therefore, in this section, we will provide an overview of the pathway and mechanisms involved in the electrochemical reduction of **HMF** and furfural under different media conditions and discuss the factors that have an effect on the reaction selectivity.

4.1.1   Proton-coupled electron transfer (PCET). There are two common mechanisms for hydrogenation reactions on catalyst surfaces. The first is the Eley–Rideal mechanism, in which adsorbed substances (e.g., HMF_ads or FF_ads) react with external substances (e.g., protons) to form products (e.g., reducing intermediates), i.e., the transfer of a proton (H^+) from solution and an electron from the cathode, resulting in a net addition of H atoms to the organic material, also called the PCET mechanism (Scheme 3b).[138] Since the mechanism involves the transfer of protons in solution, better reaction kinetics are available only in solutions with high proton concentrations.
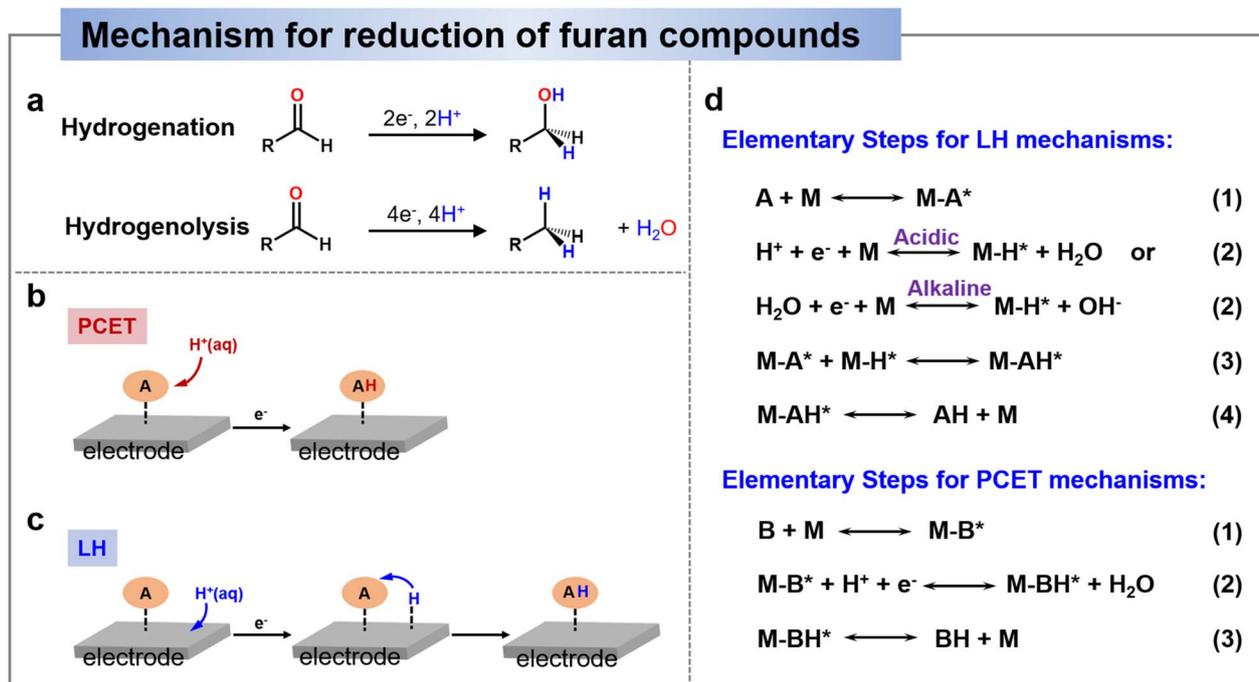
Scheme 3 (a) General schemes depicting the hydrogenation and hydrogenolysis reactions.[136] Copyright 2022, American Chemical Society. Schematic comparison of adding an H-atom to **HMF** by the PCET mechanism (b) and by the Langmuir–Hinshelwood (LH) mechanism (c). (d) Elementary steps for LH and PCET mechanisms.[142] Copyright 2022, Elsevier.

4.1.2 Langmuir–Hinshelwood (LH). The second mechanism is the Langmuir–Hinshelwood mechanism, where two adsorbed species (*e.g.*, HMF*/FF* and H*) react to form a product (Scheme 3c).[142] For example, in a non-acidic aqueous solution, adsorbed hydrogen atoms (H_{ads}) are formed on the surface of the electrode, and the H_{ads} are then transferred to HMFs (HMF_{ads}) that are also adsorbed on the electrode. Thus, the term hydrogen atom transfer (HAT) is used to describe the transfer of H_{adds} to the adsorbed organic material. The addition of H atoms is in the form of H_{ads} adsorbed on the surface of the active site, the coverage of H_{ads} on the catalyst surface is the key to the reaction. Since the electrocatalytic hydrogenation reaction mechanism is divided into two types (PCET and LH), the specific reaction mechanism is related to the proton concentration in solution, since the PCET reaction mechanism is kinetically competitive only when the proton concentration is high enough.[136] On the other hand, the reduction of furan compounds involves hydrogenation and hydrolysis, and although both hydrogenation and hydrolysis require the addition of H atoms, they may use different mechanisms for the addition of H atoms (PCET *vs.* LH) and/or involve different intermediates that are affected by pH in different ways.[138,142,143] Therefore, it is crucial to elucidate the mechanism of adding H atoms during hydrogenation and hydrogenolysis. Scheme 3d illustrates the reaction pathways of **HMF**/**FF** in different media, where A and B represent the reaction key intermediates and M represents the active site, respectively.[142]

4.1.3 Reduction pathways of 5-hydroxymethylfurfural (HMF) and furfural (FF). Choi *et al.*[138] showed for the first time that hydrogenation and hydrogenolysis of **HMF** involve the

formation of different intermediates through different mechanisms (LH and PCET), which may explain why low pH promotes hydrogenolysis rather than hydrogenation. All the reaction pathways discussed above for **BHMF**, **MF**, **MFA**, and **DMF** and their dependence on pH are summarized in Fig. 11a. **HMF** can form three intermediates (**HMF-Hc***, **HMF-Ho*** and **dehy HMF***). Energetically, **HMF-Ho*** is the least favorable, however, since **HMF-Ho*** is the only substance that can be formed *via* LH mechanism, the generation of **HMF-Ho*** and its corresponding product (**BHMF**) dominates at high pH. At low pH, the kinetics of PCET improve with the formation of thermodynamically more stable **HMF-Hc*** and **dehy-HMF***, which compete with the formation of **HMF-Ho**. **HMF-Hc*** can be converted to **BHMF** by PCET or LH mechanism, or to **MFA** by concerted hydride and proton transfer (CHPT) in acidic media. However, **MFA** production is thermodynamically more favorable. Thus, in acidic media where PCET is not kinetically limited, increased **HMF-Hc*** formation leads to increased **MFA** production. Similarly, enhanced **dehy HMF*** production in acidic media leads to increased **MF** production because the conversion of **dehy HMF*** to **MF** *via* CHPT is thermodynamically favorable, and furthermore, **MF** is the only possible product that can be produced from **dehy HMF***. Two intermediates (**MF-Hc***, **MF-Ho***) can be formed from **MF**. Energetically, **MF-Ho*** is less stable, however, **MF-Hc*** can only be formed by PCET, whereas **MF-Ho*** can be formed by either LH or PCET, and at high pH, where LH is dominant, **MF-Ho*** will be the main intermediate, leading to **MFA** generation. At low pH, PCET is kinetically competitive and thermally stable **MF-Hc*** is expected to be formed to a considerable extent, which can then be further reduced to **DMF** *via* the
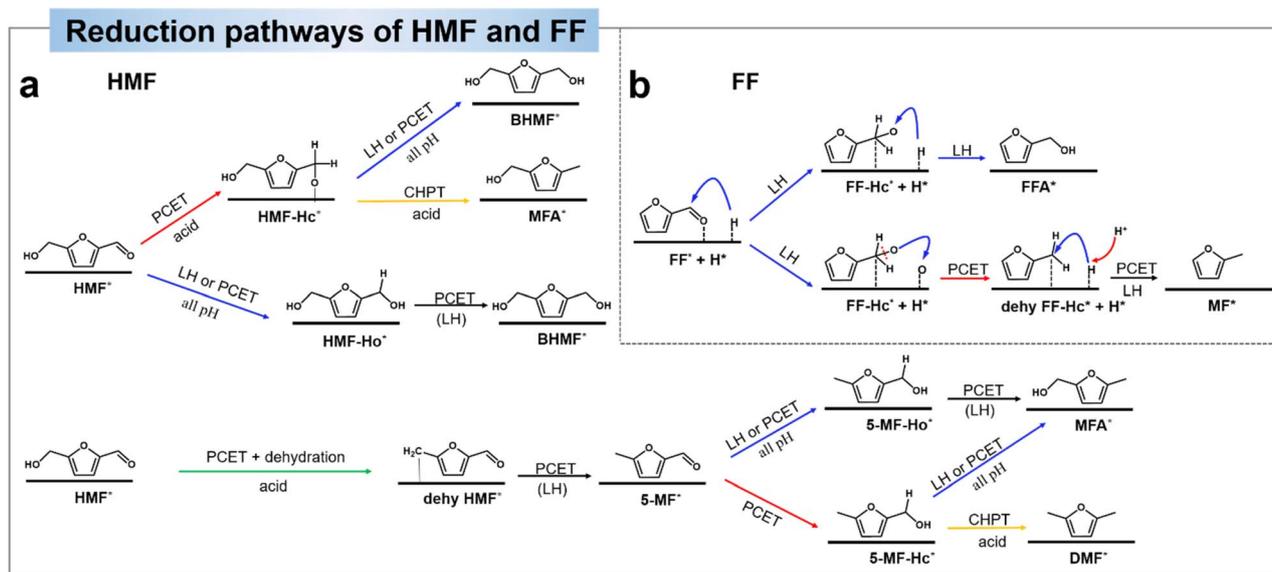
Fig. 11 (a) Proposed pathways of HMF to DHMF, MF, MFA, and DMF.[138] Copyright 2022, Wiley-VCN. (b) Proposed pathways of the electro-catalytic hydrogenation (ECH) of FF on the Cu electrode in acidic electrolytes.[142] Copyright 2022, Elsevier.

CHPT, which is also kinetically enhanced in acidic media. **MF-Hc*** can also be converted to **MFA** *via* PCET or LH, but the production of **MFA** is thermodynamically not as favorable as the production of **DMF**.

Similar to **HMF**, the reduction route of **FF** is simpler. Zou *et al.*[142] suggested that the hydrogenation step follows the LH mechanism and the hydrogenolysis step includes the LH–PCET mixing mechanism. By spectroscopic tracing of the behavior of the intermediates at the Cu electrode interface, the observed Cu–O_{ad} signals point to a direct C–O dissociation of the alkoxy intermediates during the **MF** generation process. Based on the experimental data, they analyzed that (1) **FA** and **MF** are generated in parallel. (2) The hydrogenolysis product (**MF**) has significant pH and potential effects in acid solution. (3) Deoxygenated reduction by direct C–O bonding in the hydrogenolysis pathway. The experimental results demonstrated that the hydrogenation and hydrogenolysis of **FF** were generated mainly through parallel reactions, which excluded all pathways for the dehydrogenation of **FFA** intermediates to **MF**, suggesting that **FFA** is not an intermediate for the generation of **MF**. The DFT results showed that the leaving mechanism of O intermediates through the PCET pathway was superior to that through the LH pathway, thus confirming the LH–PCET hybrid mechanism for the generation of **MF** in an acidic environment. Fig. 11b shows the electrochemical reduction route of **FF**.[142] The first hydrogenation step starts with the electro-chemically generated H_{ad} addition to the adsorbed carbonyl C thereby inducing the formation of **FF-Hc*** intermediates. The **FF-Hc*** intermediates can be competitive in that they can be hydrogenated to **FFA** by a second H_{ad} transfer (**FFA** route) or dissociated to dehy **FF-Hc*** and O_{ad} (**MF** route). In the **MF** route, dehy **FF-Hc*** is hydrogenated to **MF** by a second H_{ad} transfer, while O_{ad} is further hydrogenated to OH_{ad} and H_2O by PCET. In summary, **MF** formation is more favorable in acidic environments due to the fact that PCET is more favorable in environments with more H^+.

4.2 Catalysts design for electrocatalytic reduction of furan compounds

The selectivity and Faraday efficiency of **HMF** and **FF** electro-catalytic reduction depend mainly on the coverage of active H and organically adsorbed species on the catalyst surface and their rate of conversion, which can be controlled by modulating the cathode catalyst and experimental conditions.[144] The catalysts are described below according to the electrochemical reduction products of the furan compounds, and each representative catalyst and electrocatalytic reduction conditions are listed in Table 2.

4.2.1 Hydrogenation of furan compounds. According to the mechanism discussed above, hydrogenation of aldehyde groups generally occurs under non-acidic conditions. Hydrogenation of **HMF** to **BHMF** and **FF** to **FFA** has been demonstrated with various metals (*e.g.* Cu,[138,145–148] Ag,[138,145,149] Ni,[138,145,147] Co[145,147] Fe,[145,148] Zn,[150] Pd,[147] Ru,[147] Rh,[147] In,[138] Pb[148]). However, the selectivity and Faraday Efficiency (FE) of these hydrogenation products vary widely depending on the type of metal of the catalyst, the substrate concentration, and reduction potential, in addition to being affected by the electrolyte pH. Although hydrogenation of aldehyde groups is the main reduction reaction of **HMF** and **FF** in non-acidic media at high pH, the activity to produce **BHMF**/**FFA** varies considerably depending on the type of catalyst used.[145,151] Kyoung-Shin Choi[145] explored the selectivity of electrically reduced **HMF** and **FF** for various metals at pH 9.2. Combined experimental and computational results show that metals with high selectivity for generating **BHMF** (In, Cd, and Ag) bind very weakly to **HMF**, whereas metals that tend to hydrolysis to generate **MFA** (Cu, Ni, Co, and Fe) bind more strongly to **HMF**, elongating the C=O and C–O bonds on the HMF_{ads} (Fig. 12a and b). The elongation of the C=O bonds of aldehydes is more significant than that of alcohols, suggesting that the conversion of **HMF** to **MFA** is achieved mainly by cleavage of the aldehyde C=O bond, rather than by cleavage of

Review

Table 2 The summaries of electrocatalytic hydrogenation, hydrogenolysis and other reduction reactions of furan compounds

Substrate	Catalysts	Electrolyte	Concentration (mM)	Potential (V vs. RHE)	Conversion (%)	Product/Sel. (%)	FE (%)	Ref.
FF	15%-Cu/NC$_{900}$	1.0 M KOH (pH = 13.6)	30	−0.25	99	FFA, 100	95	152
FF	Cu	0.1 M Na$_2$CO$_3$–NaHCO$_3$	100	−0.57	71	FFA, 87	—	148
FF	Cu$_1$/PC	Acetate buffer (pH = 5)	40	−0.75	—	FFA, —	90	143
FF	Ag$_{60}$Pd$_{40}$	0.2 M potassium phosphate buffer (pH 6.9)	100	−0.5	18	FFA, —	96	158
FAL (FF)	MoS$_2$-DMA	0.05 M Na$_2$B$_4$O$_7$ solution (pH 9.18)	35	−0.25	—	FFA, >95	86.3	159
FF	Cu$_3$P/CFC	1 M KOH (pH = 14)	50	1.4 (cell voltage)	99	FA, 100	>95	160
FF	NP-Cu	0.2 M PBS	50	−1.5 V (vs. Ag/AgCl)	77	FFA, 96	95	161
HMF	Cu(OH)$_2$-ER/CF	0.1 M KOH	50	−0.15	98.5	BHMF, 100	92.3	137
HMF	15%-Cu/NC$_{900}$	1.0 M KOH (pH = 13.6)	30	−0.25	81	BHMF, 94	—	152
HMF	Ag$_{gd}$	0.5 M borate buffer (pH = 9.2)	20	−0.56	37	BHMF, 99	99	146
HMF	Ag/C	0.5 M sodium borate buffer (pH = 9.2)	20	−0.56	42	BHMF, 90	95	149
HMF	AgCu	0.5 M borate buffer (pH = 9.2)	20	−0.56	53	BHMF, 87	95	156
HMF	Ag/Cu foam	0.5 M sodium borate buffer (pH = 9.2)	20	−0.51	90	BHMF, >99	94	154
HMF	Ag/Cu foam	0.5 M sodium borate buffer (pH = 9.2)	50	−0.51	99	BHMF, 83	85	154
HMF	Ag/Cu foam	0.5 M sodium borate buffer (pH = 9.2)	100	−0.51	99	BHMF, 68	70	154
HMF	Ag/Cu GD	0.5 M borate buffer (pH = 9.2)	50	−0.51	99	BHMF, 87	85	157
HMF	Ru$_1$Cu	0.5 M PBS (pH = 7.0)	20	−0.3	87.3	DHMF, 97.5	85.6	25
HMF	Ru$_1$Cu	0.5 M PBS (pH = 7.0)	50	−0.5	92.4	DHMF, 97.0	89.5	25
HMF	Ru$_1$Cu	0.5 M PBS (pH = 7.0)	100	−0.5	97.1	DHMF, 89.7	88.0	25
HMF	MoS$_2$-DMA	0.5 M sodium borate buffer (pH = 9.2)	35	−0.25	30	DHMF, >99	75	159
HMF	OD-Ag (H-cell)	0.5 M sodium borate buffer (pH = 9.2)	20	−0.56	37	BHMF, 91.7	56.2	162
FF	Cu	0.5 M H$_2$SO$_4$	30	—	—	MF, 80	—	163
FF	Cu/Cu-400 nm	0.5 M H$_2$SO$_4$	100	−0.8 / −0.65	64	MF, —	73	164
FF	Cu$_1$/PC	Acetate buffer (pH 5)	40	−0.9	—	MF, —	60	143
FF	CuPd$_{0.021}$/C	0.1 M acetic solution (pH 2.9)	40	−0.58	—	MF, —	75	165
FF	Ni–Cu	0.5 M H$_2$SO$_4$ (pH 0.5)	40	10 mA cm^{-2}	—	MF, —	59	140
FF	Carbon paper	0.1 M KOH (pH 13)	100	−0.41	—	HDF, ~100	93	166
FF	Pd black	1 M H$_2$SO$_4$	0.1 M (membrane reactor)	200 mA cm^{-2}, 1 h	100	MTHF, 76	—	167
HMF	CuNi	0.2 M sulfate buffer (pH 2)	2 g L^{-1}	−0.46	—	DMF, 91.1	88	168
HMF	Pd SA/TiO$_2$	1 M PBS (pH 6.8)	20	−0.6	62.3	DMF, 90.3	~60	169
HMF	TiO$_2$	1 M PBS (pH 6.8)	20	−0.6	—	BHH, 70.2		169
HMF	CuO/Fe$_2$O$_3$/CF	0.1 M KOH (pH = 13)	10	10 mA cm^{-2}	72	MFA, ~28	84	170
HMF	Ni	0.5 M BBS (pH 9.2)	20	−0.4	40.4	MFA, 17.8	—	145
HMF	Pd/VN/CF	0.2 M HClO$_4$	10	20 mA, 45 min	>90	BHMTHF, >88	>86	98
HMF	Zn	0.2 M sulfate buffer (pH 2.0)	20	−0.89	—	HD, 72.4	81.6	171

the C–O bond after the aldehyde group is first hydrogenated to an alcohol, as shown in Fig. 12c. Once MFA is formed, the alcohol C–O bond is difficult to cleave, and therefore DMF is difficult to form under these conditions. Considerable amounts of Humins were produced when W and Ti were used as reduction catalysts for HMF. These metals bind the strongest to HMF, resulting in significant deformation of the furan ring as well as significant elongation of the C–O and C=O bonds (green shaded area in Fig. 12b). Too strong adsorption of HMF on the metal surface will

cause an increase in the coverage of HMF$_{ads}$ on the surface, which will easily generate dimerization products.

Unlike HMF, FF and FFA have only one alcohol or aldehyde group. Therefore, examining their propensity for hydrogenolysis provides a clearer picture of which bond is more susceptible to hydrogenolysis. When W, Fe, Co, Ni, Cu cathodes were used, the aldehyde group of FF underwent both hydrogenation and hydrolysis to give FFA and MF, while the hydrogenation product FFA was obtained with high selectivity
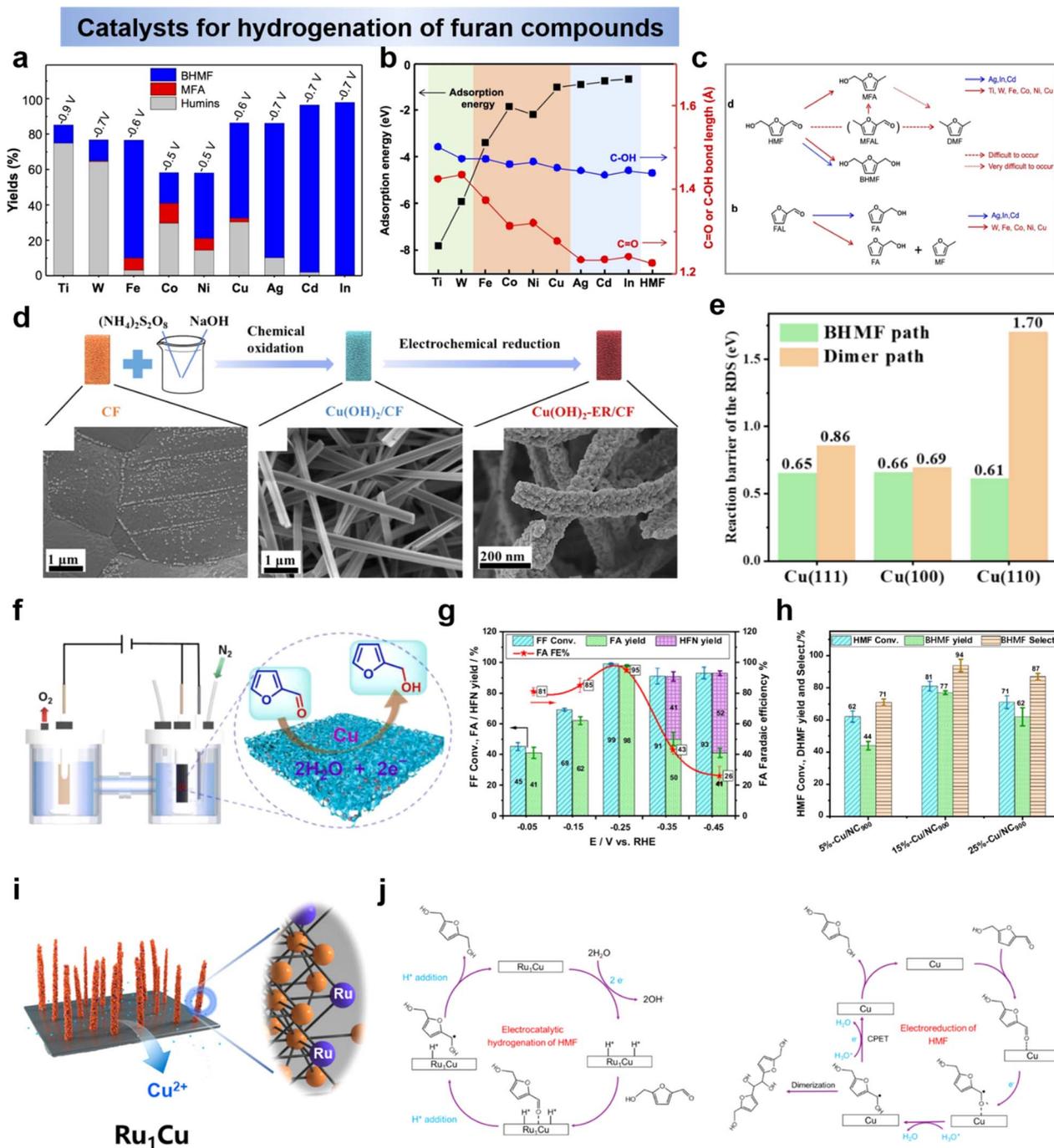
Fig. 12 (a) Yields of **BHMF**, **MFA** and humins by various metals and (b) adsorption energy of **HMF** (left axis) and bond lengths (right axis) of the C=O and the C−O of **HMF** and (c) electrochemical conversion pathways of **HMF**, FAL and **FA**.[145] Copyright 2021, Wiley-VCN. (d) SEM images for typical Cu(OH)$_2$-ER/CF and (e) comparison of the reaction barrier of the RDS for **BHMF** path and dimer path.[137] Copyright 2023, Elsevier. (f) Cu-catalyzed ECH of **FF** to **FA** and (g) **FF** conversion, **FA/HFN** yields and faradaic efficiency at various potentials and (h) ECH of **HMF** with Cu/NC$_{900}$ serial catalysts.[152] Copyright 2022, Elsevier. (i) Schematic illustration of synthetic route for Ru$_1$Cu SAA and (j) electrochemical reduction mechanism of **HMF** over Ru$_1$Cu and Cu.[25] Copyright 2022, Wiley-VCN.

when In, Cd, Ag were used as cathodes (Fig. 12c). On the other hand, when **FA** was reduced, no hydrogenolysis product was detected regardless of metal type. This again illustrates that C=O is more hydrogenolytic than C−O bond.[145]

Based on the mechanistic analysis of the hydrogenation of aldehydes to generate **BHMF**, it can be seen that the two main competing reactions have been identified: (i) hydro-dimerization leading to the formation of a diol, fostered at high substrate concentration, and (ii) hydrogen evolution

reaction (HER), promoted at high overpotential. Therefore, the catalyst with appropriate and moderate electrocatalytic activity is highly desirable to achieve efficient and selective conversion of **HMF** to **BHMF** or **FF** to **FFA**. For example, noble metals, represented by Pt, have a strong hydrogen-removal reaction (HER) capability during water cracking, thus leading to low Faraday efficiency.[153] In contrast, transition metals with poor catalytic properties for HER favor the subsequent hydrogenation step.[127,154] Cu-based electrodes have attracted the attention of researchers due to their better ability to catalyze **HMF** and relatively poor HER reactivity, providing a wide potential window and high Faraday efficiency for **BHMF**.[25,137,155] Recently, Wang's group[137] reconstructed the surface atomic arrangement of Cu foam by a two-step redox strategy (Fig. 12d), and demonstrated that the key factor controlling the **HMF** electrocatalytic hydrogenation reaction as well as the product selectivity is the crystallographic effect of Cu (Fig. 12e). Simultaneously, they experimentally confirmed that the hydrogenation reaction of **HMF** is primarily through the hydrogen atom transfer (HAT) pathway, which is a process requiring surface-adsorbed H_{ads} as the hydrogen source.[137] Liu et al.[152] reported highly efficient and selective electrocatalytic hydrogenation of **FF** to **FFA** with Cu electrocatalyst (Cu/NC_{900}) (Fig. 12f). Under optimal conditions, close to 100% selectivity and 95% Faraday efficiency for **FFA** and 99% **FF** conversion were obtained over the Cu electrocatalyst. The effect of potential on product distribution showed that low potentials ($-0.05 - -0.25$ V vs. RHE) mainly promoted the formation of **FFA**, whereas high potentials ($-0.35 - -0.45$ V vs. RHE) led to a competitive reaction and the formation of **HFN** (Fig. 12g). Inspired by the above results, the Cu/NC_{900} series catalysts were further applied in the electrocatalytic hydrogenation reaction of **HMF**, and 15%-Cu/NC_{900} exhibited the highest performance for the hydrogenation of **HMF** under optimal conditions, yielding **BHMF** in 77% yield and 94% selectivity (Fig. 12h). In addition, Ag has been shown to have good activity for the hydrogenation of furan compounds,[146] and combining two metals, Ag and Cu, in an electrocatalyst has been shown to be effective in promoting the hydrogenation of **HMF** and **FF**.[25,154–158] For **HMF** hydrogenation to **BHMF**, it can be carried out either by PCET or via surface-adsorbed H (H*) at the electrode by proton/water reduction (LH pathway). However, **HMF** hydrogenation often competes with the hydrogen-extraction reaction (HER), leading to a decrease in the FE of **BHMF**. In order to achieve a balance between FE and hydrogenation activity, Duan et al.[25] proposed a Ru_1Cu SAA catalyst that efficiently converts **HMF** to **DHMF** at lower potentials with enhanced activity and FE (Fig. 12i), where the FE of Ru_1Cu to 2,5-dihydroxymethylfuran was 85.6% with a yield of 0.47 mmol cm^{-2} h^{-1}, much higher than that at -0.3 V vs. RHE, the conversion of **BHMF** by Cu was 71.3% in a yield of 0.08 mmol cm^{-2} h^{-1}. This study also demonstrated that the doping of single-atom Ru altered the mechanism of **HMF** hydrogenation. Due to the higher H_2O activation activity of Ru, it can provide the required protons for hydrogenation in situ, independent of the proton concentration in the electrolyte. As a result, the

reaction on the Ru_1Cu cathode follows the Langmuir–Hinshelwood (LH) mechanism, while the reaction on the Cu cathode tends to follow the Proton-Coupled Electron Transfer (PCET) mechanism, as illustrated in Fig. 12j.

In summary, the electrocatalyst, electrocatalytic performance and electrochemical condition for hydrogenation of furan compounds are listed in Table 2.

4.2.2 Hydrogenolysis of furan compounds. Selective hydrogenolysis **FF** or **HMF** generates 2-methylfuran (**MF**) or 2,5-dimethylfuran (**DMF**), which are potential liquid transportation fuels. Cu has been found to be the electrode material for hydrogenolysis in acidic media because of its unique ability to generate hydrogenolysis products with high selectivity, and due to its high abundance in nature and moderate hydrogen overpotential. Many efforts have been made to design advanced Cu catalysts and optimize the reaction conditions for this reaction.[28,164,165,172] Nilges and Schröder[163] conducted a study on the influence of electrode type on the product distribution from the electrochemical reduction (ECR) of **FF**. They carried out experiments in an acidic water/acetonitrile electrolyte mixture (0.5 M H_2SO_4) using a constant current density of 10 mA cm^{-2}. As shown in Fig. 13a, their findings revealed distinct variations based on the electrode material. Specifically, Cu emerged as the most efficient electrode for producing 2-methylfuran (**MF**) through the ECR of **FF**. By optimizing the size of Cu particles and electrolysis parameters, biddinger and colleagues achieved a faradaic efficiency of 73% for the electroreduction of **FF** to **MF** on nanocrystalline Cu (400 nm) at an potential of -0.8 V versus RHE in a 0.5 M H_2SO_4 electrolyte solution (pH = 0.3).[164] This also demonstrates that Cu catalysts exhibit good activity for catalyzing the reduction of **FF** to **MF** under acidic conditions. However, there is intense competition from the hydrogen evolution reaction (HER) in acidic solution, leading to a decrease in faradaic efficiency (FE). Therefore, there is clearly significant room for improvement when using Cu as a catalyst for this reaction. Zhou et al.[143] reported excellent electrochemical hydrogenation performance of furfural in near-neutral acetic acid buffer (pH 5) using phosphorus-doped carbon-supported Cu single-atom catalysts (Cu_1/PC), as shown in Fig. 13b. Unexpectedly, this system exhibited an electrode potential-dependent product distribution. Comparative experiments suggested that the high activity and selectivity could be attributed to the presence of single copper atoms, which suppressed the hydrogen evolution reaction (HER), the phosphorus doping effect that enhanced furfural adsorption, thereby promoting its conversion to **MF**. The product selectivity could be conveniently controlled by changing the applied potential, resulting in high faradaic efficiencies for furfuryl alcohol and 2-methylfuran at -0.82 V vs. RHE and -9.0 V vs. RHE, respectively (Fig. 13c). Many efforts have been made to establish the relationship between adsorption geometry and product distribution in furfural reduction. However, detailed insights into how the catalyst surface structures influence the mechanism of furfural electrochemical hydrogenation (ECH) are still lacking. For an in-depth study of the electrochemical hydrogenation (ECH) mechanism of furfural, the strategy of Pd introduction into Cu catalysts improved the selectivity to **MF** (Fig. 13d).[165] The
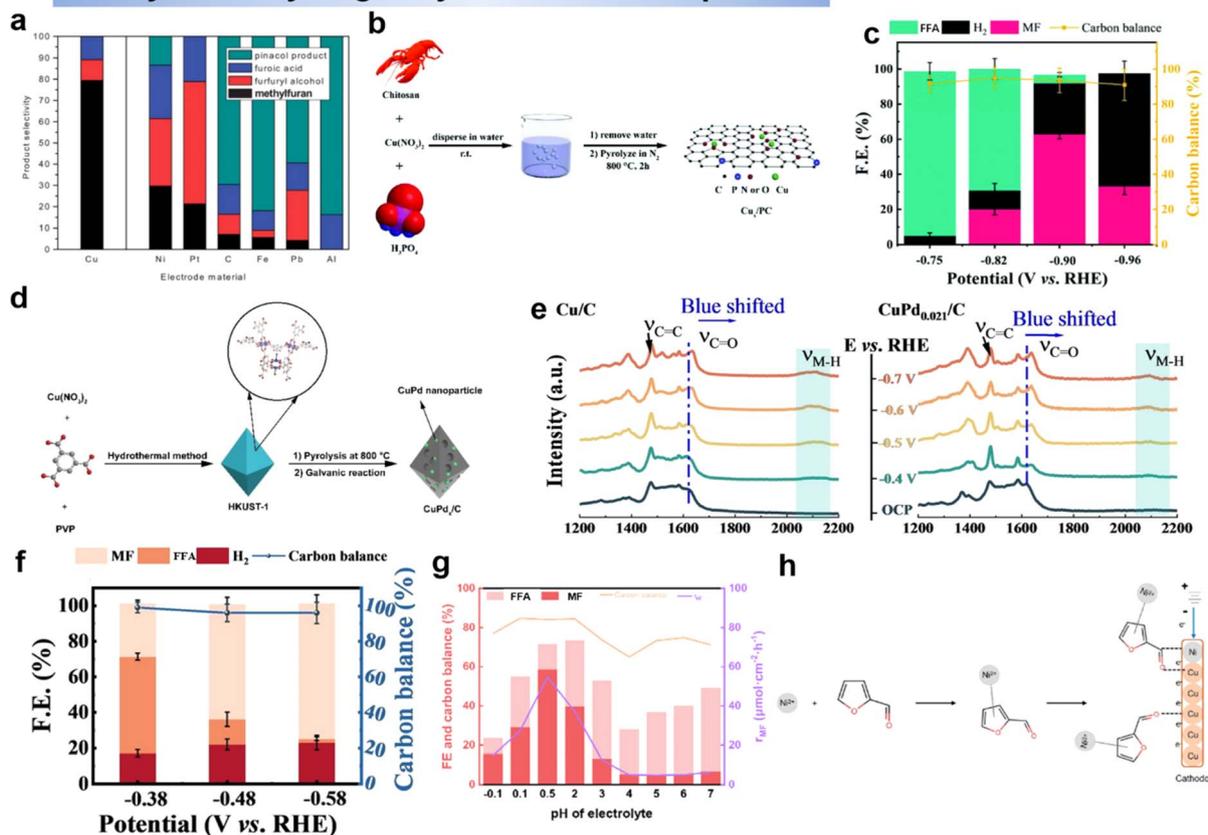
Fig. 13 (a) Product composition of the electrocatalytic reduction of furfural at different electrode materials.[163] Copyright 2013, Royal Society of Chemistry. Schematic illustration of the fabrication process for the Cu_x/PC catalysts (b) and Cu_1/PC (c) at different applied potentials.[143] Copyright 2021, Royal Society of Chemistry. (d) Schematic illustration of the method for the synthesis of $CuPd_x$/C catalyst and (e) potential dependent SERS spectra obtained *in situ* at Cu/C (left) and $CuPd_{0.021}$/C (right) and (f) FE and carbon balance data for the bulk electrolysis of furfural obtained with $CuPd_{0.021}$/C.[165] Copyright 2022, Wiley-VCN. (g) The FE, CB, r_p of **MF** varied with the increase in pH value and (h) speculation about the mechanistic roles of the Ni and Cu sites on the electrode.[140] Copyright 2023 Royal Society of Chemistry.

highest faradaic efficiency (FE) for **MF** and the corresponding average partial current density reached 75% and 4.5 mA cm^{-2} at -0.58 V *vs.* RHE in an aqueous acetic acid medium (pH 2.9) (Fig. 13f). *In situ* surface-enhanced Raman spectroscopy experiments demonstrated that the $CuPd_{0.021}$/C surface has a higher coverage of H_{ads}, which may contribute to the improvement of **MF** selectivity (Fig. 13e). Cui *et al.*[140] investigated the synthesis of **MF** by electrocatalytic reduction of **FF** using nickel–copper bimetallic as a catalyst. It was found that trace amounts of Ni mixed with Cu at the electrode significantly favored the formation of **MF** in the electrocatalytic reduction of **FF** for the synthesis of **MF** using nickel–copper bimetallic as a catalyst. And lower pH values were more favorable for **MF** generation (Fig. 13g). **FF** was adsorbed on both Ni and Cu sites of the electrode through the interaction with C and O atoms of the carbonyl group, which is hypothesized to be an important factor for **MF** formation (Fig. 13h). Overall, these studies provide important insights for designing efficient electrocatalysts and optimizing conditions. The catalysts reported for electrocatalytic hydrogenolysis summarized in Table 2.

4.2.3 Other reduction reactions. In addition to the hydrogenation and hydrogenolysis of the aldehyde and alcohol groups of furan compounds, there are a number of reduction reactions that are also of importance. The first is the dimerization reaction. **FF** and **HMF** can be electrocatalytically dimerized at the carbonyl position to generate C10–C12 biofuels.[173] The process involves the reaction of the carbonyl group of **HMF** or **FF** with an H$^+$/e$^-$ pair to generate a keto radical intermediate (C$^{\cdot-}$ OH), which reduces to form the corresponding alkoxy radical. The alkoxy radical can then be dimerized with another alkoxy radical *via* C–C coupling to produce a dimer product.[172] Researchers have explored the reductive dimerization of **FF** and have reported higher rates of hydrofurion (**HDF**) formation at pH = 13 than at pH = 7 and pH = 0. This is due to the fact that alkaline conditions markedly inhibit other competing reactions (*e.g.*, HER and hydrogenation), which facilitates the electrohydrogenation of furfural to **HDF**.[166] Wang *et al.*[169] elaborated that low *H coverage on TiO$_2$ favours the formation of bis(hydroxymethyl)hydrofuran (**BHH**) with a selectivity of 70.2%. Hydrogenation of the furan ring is the second type of valuable other reaction. Hydrogenation of the

C=C bond in the **HMF** furan ring can be achieved in acidic media. Li *et al.* reported the reduction of **HMF** to **BHMTHF** by using Pd nanoparticles anchored on vanadium nitride (Pd/VN) as a cathode in 0.2 M HClO$_4$, the selectivity and FE of **BHMTHF** were >88% and >86%, respectively.[98] In this reaction, **HMF** was first reduced to **BHMF**, followed by further reduction of **BHMF** to **BHMTHF** (**DHMTHF**). A membrane reactor for the electrochemically driven hydrogenation of furfural to 2-methyltetrahydrofuran (**MTHF**) reaction was reported by Curtis P. Berlinguette *et al.*[167] They showed how the membrane reactor can produce **MTHF** with >75% selectivity at 200 mA cm^{-2}, compared to the lower selectivity (<35%) and current density (50 mA cm^{-2}) of conventional ECH using a single cell.[167] Another remarkable reduction reaction observed in acidic media is the ring opening of furans. The reduction product, 2,5-hexanedione (**HD**) was produced by the reduction of **HMF** by reductive furan ring-opening and hydroxymethyl/aldehyde reduction to alkanes. Roylance and Choi reported the electrochemical reduction of **HMF** to **HD** on a Zn cathode at ambient temperature and atmospheric pressure in 0.2 M sulfate buffer (pH 2.0) with 81.6% FE and selectivity 72.4%.[171]

4.3 Factors affecting the electrocatalytic reduction of furan compounds

4.3.1 Electrolyte pH. The H$^+$ concentration of the electrolyte plays an important role in electrocatalytic reactions. The pH in the electrolyte affects the kinetics of electroreduction of organic matter at the electrode and the distribution of products by changing the reaction mechanism.[141] The origin of the pH-dependent selectivity of hydrogenation and hydrogenolysis was first explained by Choi *et al.*[138] Aldehyde hydrogenation plays a dominant role and the main product is **BHMF** at pH 7–9. However, both aldehyde hydrogenolysis and alcohol hydrogenolysis are promoted with decreasing pH, which increases the yield of 2,5-dimethylfuran (**DMF**) as shown in Fig. 14a. In general, hydrogenolysis (combining hydrogenation and deoxygenation) is more challenging than hydrogenation (which does not involve the cleavage of carbon–oxygen bonds). Therefore, determining the factors and conditions that promote hydrogenolysis is important for the reductive value addition of biomass-derived oxygenated compounds. In acidic media, the alcohol group of **HMF** undergoes hydrogenolysis to form **5-MF**, a key intermediate in the formation of **DMF**. Once **BHMF** and **MFA** are formed first, further hydrogenolysis of their alcohol groups is difficult. The conversion of **HMF** to **MF** and **5-MF** to **DMF** requires PCET, a process that is possible only when the concentration of protons in the solution is sufficiently high and kinetically feasible.

To explain the phenomenon that aldehyde selective hydrogenolysis occurs in strongly acidic electrolytes while aldehyde hydrogenation mainly occurs under alkaline electrolytic conditions, Zou *et al.*[142] systematically explored the effect of electrolyte pH on the selective reduction of furfural. As shown in Fig. 14b, the selectivity of **MF** decreased from 40.1% to 1.4% and **FFA** increased from 45.2% to 98.1% after 30 min of current electrolysis at pH ranging from 2 to 8, and no dimerization

products were observed.[142] This indicates that the selectivity of **FFA** increases significantly with pH increase, and it is quite difficult to make **MF** by hydrogenolysis of **FFA** under electrolytic conditions. Therefore, the hydrogenation and hydrogenolysis products during **FF** electrolysis were mainly formed by parallel reactions in which **FFA** was not an intermediate in the generation of **MF**, as shown in Fig. 14c.

Extrapolating from the reaction kinetics, it was found that acidic conditions (low pH) are more favorable for C–O/C=O breaking hydrogenolysis, whereas neutral and weakly alkaline conditions (high pH) are more favorable for hydrogenation. The formation of **MF** appears to be a hybrid LH-PCET process, and since PCET is affected by the proton donor and the potential, it is difficult for O$_{ad}$ to transfer through H$_{ad}$ to generate H$_2$O when there is a shortage of H$^+$, and thus it is difficult to generate **MF** in neutral or alkaline media.[142] In acidic electrolytes, the rate of hydrofuran generation is not affected by pH, and the formation of hydrofuran is more favorable at pH = 13 because alkaline conditions inhibit other competing reactions and facilitate the dimerization of furfural hydrogenation to hydrofuran (Fig. 14d).[166] Overall, the selectivity of the reduction products of **HMF** and **FF** was related to the pH of the electrolyte, especially for the hydrogenolysis of aldehyde and alcohol moieties. Acidic conditions were more suitable for hydrogenolysis, whereas neutral and alkaline conditions were more suitable for hydrogenation, and different pH led to differences in the mechanism of electroreduction of **HMF** and **FF**, with the PCET process being more suitable for acidic conditions.

4.3.2 Operating potential. The selectivity of reduction products is closely tied to the applied potential. Optimal potentials correspond to the coverage of H$_{ads}$ and reactants on the electrode surface during electrocatalytic reduction.[163] Positive potentials result in lower efficiency due to reduced interaction between H$_{ads}$ and reactants. More negative potentials enhance availability for HER or electrocatalytic reduction, as seen in experiments with benzaldehyde and furfural on Cu electrodes.[146] **FF** electrochemical reduction to THFA and **FFA** is favorable, while reduction to **MF** is slightly unfavorable. Since **FF**'s reduction potential is much smaller than HER, **FF** reduction to **MTHF** is unfavorable, as shown in Fig. 14e.[167] Under acidic conditions, **MF** selectivity is potential-dependent, with increased Faraday efficiency at higher overpotentials. Conversely, under alkaline-based conditions, **FFA** selectivity remains largely unchanged, indicating that only hydrogenolysis is potential-controlled, while hydrogenation is not.[142] Choi's team investigated **HMF** electrochemical reduction at pH = 9.2, categorizing reduction potential into three regions as shown in Fig. 14f.[146] The first region (-0.26 V $\geq E \geq -0.36$ V *vs.* RHE) involves a competing reaction before HER initiation, suggesting **HMF** formation does not involve surface adsorbed hydrogen atoms (H$_{ads}$). At this point, the electrode surface is expected to be covered only by **HMF** or its reduction intermediates, prompting the formation of C–C bonds between **HMF** molecules and/or their reduction intermediates to generate the dimer **BHH**. The second potential region ($-0.36 \geq E \geq -0.86$ V *vs.* RHE) sees increased **BHMF** formation and selectivity with weakened C–C coupling as H$_{ads}$ coverage rises. The third region
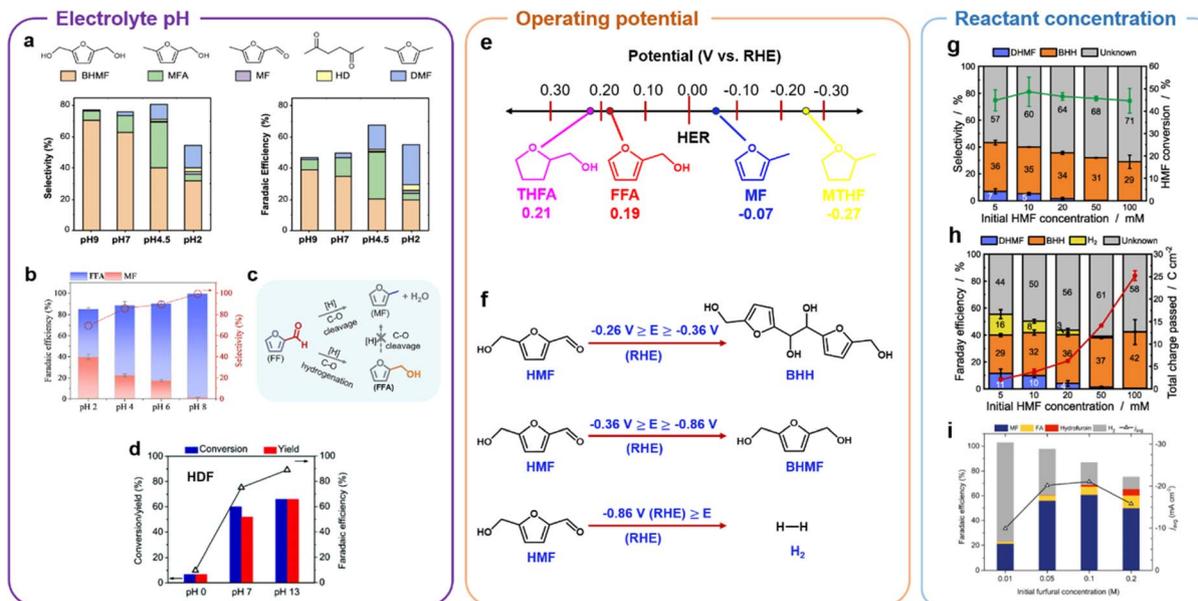
Fig. 14 (a) Selectivity (left) and FE (right) for products produced by a Cu foam electrode.[138] Copyright 2022, Wiley-VCN. (b) FE of corresponding product and the selectivity after electrolysis and (c) reaction pathway for **FF** on the Cu electrode.[142] Copyright 2022, Elsevier. (d) Furfural conversion, hydrofuroin yield, and FE for partial electrolysis conducted at pH 7 and 13.[166] copyright 2020, Royal Society of Chemistry. (e) Potentials of THFA, **FA**, **MF**, **MTHF**, and the hydrogen evolution reaction (HER).[167] Copyright 2023, Royal Society of Chemistry. (f) Potential dependence reaction pathways for HMFRR.[146] Copyright 2016, American Chemical Society. (g) **HMF** conversion (line) and product selectivity and (h) total charge passed and FE of products and H_2.[174] Copyright 2021, Wiley-VCN. (i) Preparative electrolysis of furfural with various initial furfural concentrations.[172] Copyright 2017, American Chemical Society.

($E \leq -1.6$ V *vs.* RHE) features competition between H_2 precipitation and **BHMF** generation, reducing **BHMF** Faraday efficiency. Additionally, **BHMF** conversion rate is higher in this region due to increased current density.[146]

4.3.3 Reactant concentration. Reactant concentration is also a factor that affects the performance of electrochemical processes. Elevated concentrations enhance the coverage of adsorbed reactants on the electrode surface, increasing the electrocatalytic reduction rate while suppressing the HER rate. However, excessively high substrate concentrations can lead to undesirable side reactions, including dimerization and polymerization.[164] Therefore, it is necessary to choose a suitable substrate concentration to modulate the coverage of reactants and H_{ads}.[149,162] Kloth *et al.* reported studied electro-dimerization reactions with varying **HMF** concentrations (5–100 mM) in a carbonate buffer (pH 9.2). They observed an increase in the FE of **BHH** with increasing **HMF** concentration but decreased selectivity due to **HMF** depletion from non-electrochemical side reactions. Higher initial **HMF** concentrations led to reduced selectivity and FE of **BHMF**, as well as inhibition of HER was observed (Fig. 14g and h).[174] Furfural also showed the same effect of substrate concentration. The effect of initial **FF** concentration was examined in the range of 0.01–0.2 M in an electrolyte at pH 0.5. Fig. 14i shows that the competition between **FF** reduction and HER is highly dependent on the **FF** concentration, with the FE of HER decreasing from 80.0% to 9.9% over the range of concentrations evaluated. Increasing the volumetric furfural concentration usually increase the rate of **FF** suction hydrogenation to form **FA** and **MF**, while HER rates

declined due to heightened competition for available H_{ads}.[172] The rate of hydrofuran (**HDF**) formation without H_{ads} steadily increased with increasing **FF** concentrations.

5 Paired electrolysis of furan compounds

In electrochemistry, oxidative and reductive half-reactions are usually paired with each other, such as the formation of H_2 and O_2 from the electrolysis of water at the cathode and anode. However, hydrogen and oxygen precipitation reactions (HERs and OERs) are less efficient due to high activation barriers.[175] Paired electrolysis is important by converting organics into valuable chemicals, especially for the conversion of alternative OERs under slow kinetic conditions. Combining ideal half-reactions into an efficient catalyst for paired electrolysis maximizes energy efficiency to 200% of theoretical maximum electron efficiency. This approach reduces production costs in the chemical and pharmaceutical fields, but faces challenges such as half-reaction matching, current density mismatch, chemical incompatibility and crossover issues.[149] Currently there are several types of paired electrolysis as follows.

5.1 Paired electro-oxidation with HER

Molecular hydrogen (H_2) is a promising energy carrier due to its high energy density and environmentally friendly properties. Electrolytic water decomposition, with hydrogen precipitation reaction (HER) on the cathode and oxygen precipitation reaction (OER) on the anode, is a cost-effective and carbon-neutral

hydrogen production method. However, the slow OER process limits water electrolysis efficiency, necessitating higher voltages (>1.23 V) for H_2 production (Fig. 15a).[176] To reduce costs, efficient anode reactions, such as biomass electrooxidation, have gained attention. **HMF** and **FF**, as biomass platform molecules, are oxidized to produce high-value products, like **FDCA**. Layered bimetallic hydroxides (LDHs) serve as a typical anode in the electrooxidation of furan compounds with HER.[54] Zeng et al.[117] developed a bifunctional catalyst, Rh-SA/NiFe NMLDH, showing high activity (1.48 V at 100 mA cm^{-2}) and durability for **HMFOR** and HER. In 2021, Wang et al.[43] reported a bipolar hydrogen production system using Cu as the anode and Pt as the cathode, achieving **HMF** oxidation to **HMFCA** at a low potential of 0.1 V vs. REH, releasing H_2 at both electrodes, as shown in Fig. 15b. This system requires only 0.27 V for a current density of 100 mA cm^{-2}, significantly lower than conventional **HMF** electrooxidation coupled hydrogen (1.6 to 1.7 V).[43]

5.2 Paired electro-oxidation with CO$_2$RR

Electrolysis of CO_2 for the production of high value-added chemicals (HVCs) is a sustainable strategy to address energy and climate issues. To improve CO_2RR economics and electrolysis efficiency, the search for a kinetically favorable anodic reaction to replace OER offers promise for sustainable production with high yields, selectivity, reaction rates, and energy consumption. Han et al.[177] used PdO$_x$/ZIF-8 as the cathode and PdO as the anode to establish a CO_2RR-**HMFOR** paired electrolysis system that requires only 1.06 V under strongly acidic conditions of starting cell voltage, which significantly reduces the energy consumption compared to the conventional CO_2RR-OER system (1.77 V) (Fig. 15c). As shown in Fig. 15d, at a high current density of 103.5 mA cm^{-2}, the CO_2RR Faraday efficiency reached 97.0% and the HMFOR organic acid yield was 84.3%, including maleic acid (20.0%) and formic acid (64.3%).[177] This paired electrolysis system excelled in terms of FE and current density. However, challenges
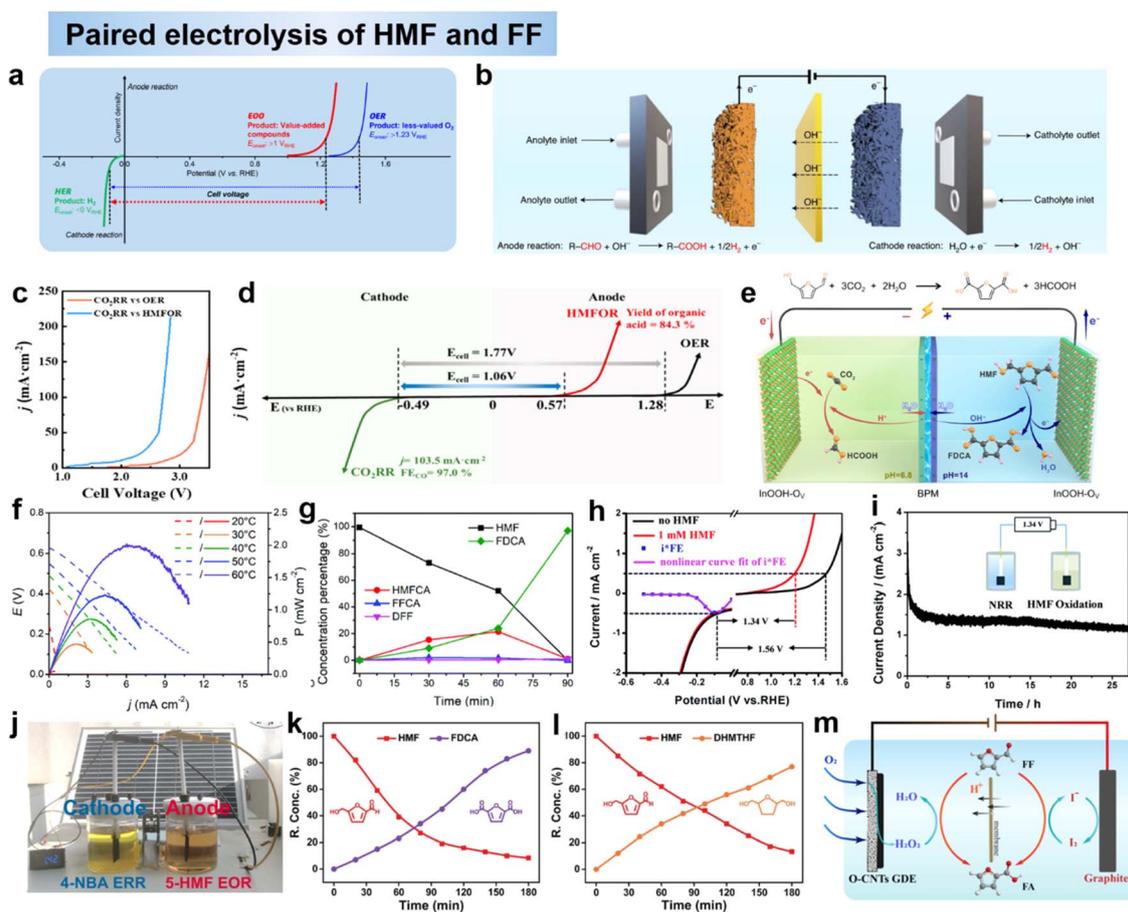

Fig. 15 (a) Schematic representation showing the potential ranges of the OER, EOO, and HER.[176] Copyright 2022, Wiley-VCN. (b) Schematic of the two-electrode electrolyser employing low-potential aldehyde oxidation coupling with HER.[43] Copyright 2021, Springer Nature. (c) LSV curves of CO$_2$RR with OER or HMFOR and (d) the comparison between a traditional single reaction and paired electrolysis system.[177] Copyright 2022, American Chemical Society. (e) Integrated electrolysis cell coupling CO$_2$RR with HMFOR.[178] Copyright 2023, Springer Nature. (f) polarization and power curves of **HMF**-fuel cells and (g) percentage of chemical versus time plot.[179] Copyright 2020, Royal Society of Chemistry. (h) LSV polarization curves for NRR coupled with OER and **HMF** oxidation, and (i) the stability test towards NRR coupled with **HMF** oxidation.[69] Copyright 2019, Royal Society of Chemistry. (j) Demonstration of pairing 4-NBA ERR (left) and **5-HMF** EOR (right) in H-type cell by using a solar-driven system.[99] Copyright 2022, Springer Nature. (k) Relative concentration of **HMF** and **FDCA** and (l) **HMF** and **DHMTHF**.[180] Copyright 2019, Wiley-VCN. (m) Schematic diagram of linear paired electrolysis of **FF** to **FA**.[135] Copyright 2023, Elsevier.

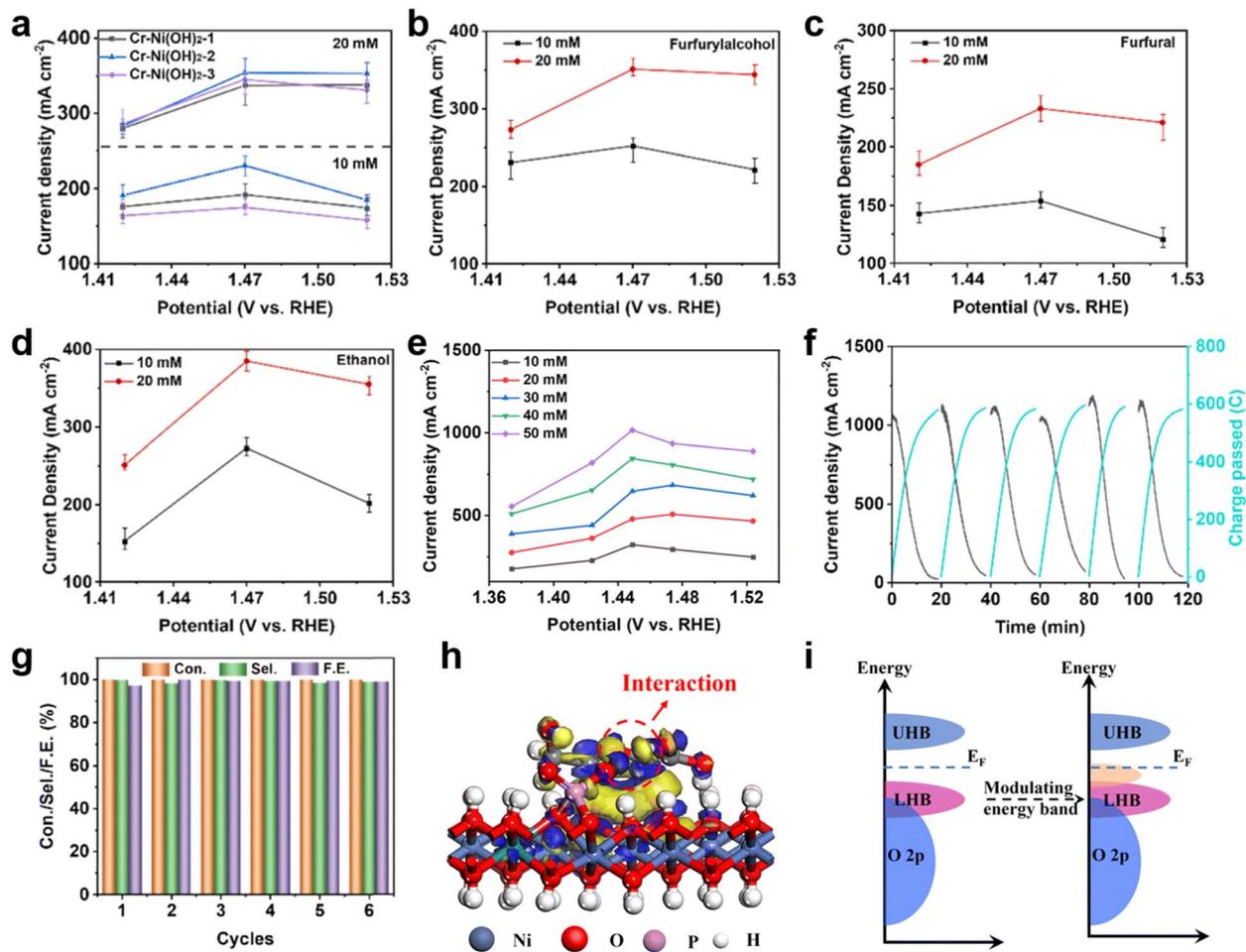## High current density electrocatalysis of furan compounds

Fig. 16 (a) Current densities of Cr−Ni(OH)$_2$/NF at HMF concentrations of 10 and 20 mM and (b)−(d) the electrocatalytic performance of Cr−Ni(OH)$_2$/NF for furfuralcohol, furfural and ethanol oxidation.[183] Copyright 2023, Elsevier. (e) The actual current densities of PO$_4$/Ru-Ni(OH)$_2$/NF obtained by segmented chronoamperometry for the HMFOR and (f) current density and charge−time plots for six cycles of electrolysis experiments on PO$_4$/Ru-Ni(OH)$_2$/NF and (g) HMF conversion, FDCA selectivity and faradaic efficiency obtained for six cycles, (h) charge densities of PO$_4$/Ni(OH)$_2$ when HMF is adsorbed on it, and (i) schematic of the transition of the electronic structure via modulating the energy band.[184] Copyright 2024, Royal Society of Chemistry.

persist in improving productivity due to different pH requirements for the two electrodes and the competition of OER and HER with HMFOR and CO$_2$RR. Addressing these challenges, Ye et al.[178] reported that indium-rich oxygen oxide (InOOH-Ov) is a bifunctional catalyst for CO$_2$ reduction and HMF oxidation, with FEs exceeding 90.0% at both optimized potentials. This catalyst provides a viable pathway for the simultaneous production of valuable chemicals at two electrodes by integrating CO$_2$ reduction and HMF oxidation in an electrochemical cell to form 2,5-furandicarboxylic acid in high yields (both around 90.0%) (Fig. 15e).

5.3 Paired electro-oxidation with ORR

Fuel cell technology involves two important chemical reactions, including the fuel oxidation reaction at the anode and the ORR reaction at the cathode. Theoretically, the use of high-performance bifunctional catalysts plays a key role in reducing

the reaction energy barrier and improving the reaction efficiency. To this end, Zhang et al.[179] designed a direct HMF fuel cell combining ORR and organic synthesis using PtNiS$_x$ as a catalyst. The results showed that the close interaction and interfacial effect between Pt and NiS$_x$ nanoparticles gave the catalyst excellent ORR and HMFOR activities (Fig. 15f). The discharge efficiency of the HMF-containing fuel cell was 2.12 mW cm^{-2} and the current density was 6.8 mA cm^{-2} at 60 °C. In addition, the FE of valuable FDCA at the anode was close to 98% (Fig. 15g).

5.4 Paired electro-oxidation with NRR

Ammonia (NH$_3$) is not only an important source for industrial utilization but also an important renewable energy carrier. Electrocatalytic nitrogen reduction reaction for the synthesis of NH$_3$ (NRR) is a sustainable and economically viable process under environmental conditions. Conventional electrocatalytic
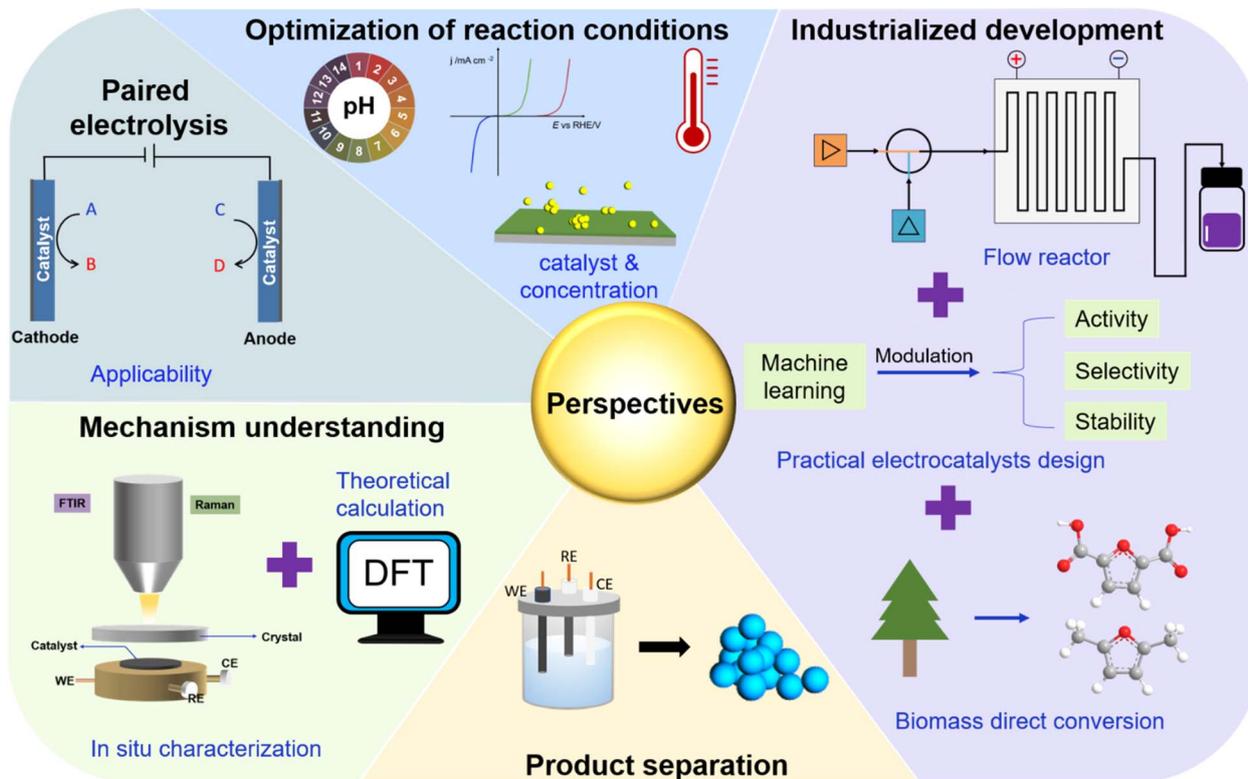
Fig. 17 Schematic illustration showing the future perspectives of electrocatalytic conversion of furan compounds.

synthesis of NH_3 in alkaline media can be divided into cathodic NRR and anodic OER, and the replacement of OER by oxidation reactions with thermodynamically favorable biomass such as furfural and 5-hydroxymethylfurfural (**HMF**) throughout the hydrolysis process has been developed as a new strategy. Xu *et al.*[69] used Ru(III)-PEI@MWCNT as a bifunctional catalyst for NRR and HMFOR. After 27 h of stable electrolysis at a current density of 0.50 mA cm^{-2}, the cell voltage was only 1.34 V, which was 220 mV lower than the oxygen precipitation potential, and the Faraday efficiency of the **FDCA** was maintained at 94%, indicating the excellent performance of NRR-coupled **HMF** oxidation (Fig. 15h and i). Oschatz's team reported the synthesis of nitrogen boron co-doped porous carbon with a unique pore structure, high thermal atom doping and high oxidation potential.[45] The created B–N motifs combine a large number of unpaired electrons and frustrated Lewis pairs, allowing the electronic structure of the B–N motifs to be combined with the electronic structure. They performed well in both electrochemical oxidation of **HMF** and NRR in the absence of metal additives. The yield of NH_3 was stable at 21.3 μg h^{-1} mg^{-1}, with a FE of 15.2%. The conversion of **FDCA** was 71% with a yield of 57%.

5.5 Paired electro-oxidation with organic reaction

In recent years, in order to improve the energy conversion efficiency, research has focused on coupling electrocatalytic oxidation reactions with small molecule reduction reactions (*e.g.*, HER, CO$_2$RR, NRR, *etc.*). In addition to coupling the small

molecule reduction reaction, matching the rates of organic oxidation and organic hydrogenation at the same time can realize the simultaneous output of high value-added products at both electrodes, improving the catalytic efficiency and eco-efficiency. In recent years, these electrocatalytic oxidation reactions have been combined with electrocatalytic small-molecule reduction reactions (HER, CO$_2$RR, NRR, *etc.*) to improve the energy conversion efficiency. In addition to coupling with small molecule. For instance, Sun *et al.* constructed a paired electrolytic system for electrocatalytic oxidation of **HMF** to **FDCA** and hydrogenation of p-NP to p-AP, with an excellent conversions and efficiencies.[105] Renewable energy driven electrolysis is an effective way to fully utilize energy. Therefore, Yang *et al.*[99] reported solar cell-powered paired electrolysis using solar cell drive at 1.420 V for 4-NBA reduction and HMFOR (Fig. 15j). Successful paired electrolysis of 4-NBA and **HMF** by constructing FeP–MoP heterojunction electrodes achieved lower voltage reaction than water decomposition, suggesting that the paired electrolysis system is more efficient.

Additionally, Pang *et al.* reported a paired electrolytic system for the electrocatalytic hydrogenation of HMFOR and 4-nitrophenol to synthesize 4-aminophenol.[53] The paired electrocatalytic system exhibited excellent reaction performance with excellent yields and Faraday efficiencies. In addition to pairing **HMF** with other organic substrates for electroreduction, pair electrolysis of **HMF** as both anodic and cathodic substrates to generate high value-added products has been reported. Li *et al.*[180] successfully prepared three-dimensional vanadium

nitride (VN) and Pd/VN hollow nanorods for the electrocatalytic oxidation and hydrogenation reaction of **HMF** to generate **FDCA** and **DHMTHF** with excellent conversion and selectivity (Fig. 15k and l). Different types of pair electrolysis systems such as parallel pair electrolysis, convergent pair electrolysis, divergent pair electrolysis and linear pair electrolysis were proposed by Ibanez et al.[181] Almost all of what we mentioned earlier are divergent paired electrolysis, which mainly involves electrode passivation, inconsistent products, and poor compatibility of anodic and cathodic reactions.[162] Li reported a redox-mediated linear paired electrolysis system that combines a hydrogen peroxide-mediated cathodic process and an I_2-mediated anodic process for the simultaneous conversion of **FF** to **FA** (Fig. 15m).[135] His linear paired electrolysis has the same substrate at both electrodes and yields the same product at both the anode and cathode, and avoids undesirable water cleavage reactions and furfural reduction side reactions by altering the electrolysis reaction paths, improving the energy reduction and electronic efficiency.

6   Industrial scale development of electrocatalytic conversion of biomass-derived furan compounds

The key to the industrial application of electrocatalytic conversion of furan compounds is the development of high current density catalysts. Up to now, researchers have optimised the electrode design by coupling different metal sites with different activities towards hydroxyl and aldehyde groups on the furan ring, which can achieve the conversion of furan compounds at lower potentials. Taking the oxidation reaction of **HMF** as an example, although the optimised various catalysts have high conversion and Faraday efficiency, the current density during electrolysis is too low (less than 100 mA cm^{-2}) to meet the requirements of industrial production.[38,182] The main reason that currently prevents the industrialisation of electrocatalytic HMFOR is that the electrooxidation reaction competes with OER at high potentials, resulting in a current density of HMFOR that does not gradually increase with increasing voltage. The occurrence of OER at high potential leads to an increase in current density, but the reaction efficiency of HMFOR decreases dramatically. More critically, no clear relationship has been established between catalyst performance and electrolysis efficiency, and there is a lack of a unified theoretical basis on how to design catalysts to achieve high current density, which seriously hinders the improvement of catalytic performance and the research and development of HMFOR. For this reason, Mu et al. proposed segmented i–t measurements within the voltage window to replace the LSV curve to extract the effective current density and obtain the maximum conversion efficiency.[183] By comparing the actual current densities, it was found that a lower onset overpotential does not imply that higher current densities can be achieved within the voltage window, and it was confirmed that the proton-coupled electron transfer (PCET) process is the key to influence the anodic peak current. The anodic peak current density achievable within the voltage window is actually a better indicator of catalyst performance than the onset overpotential due to electrolysis efficiency. Based on this, they designed electrode materials capable of achieving current densities above 200 mA cm^{-2} for **HMF** conversion. As shown in Fig. 16a, Cr–Ni (OH)$_2$/NF with a Cr doping rate of 1.42% showed a current density of up to 230 mA cm^{-2} at an **HMF** concentration of 10 mM, and when the **HMF** concentration was increased to 20 mM, the current density could reach more than 360 mA cm^{-2}, which showed an extremely high **HMF** oxidation activity. The electrocatalytic performance of Cr–Ni(OH)$_2$/NF-2 on furfuryl alcohol, furfural and ethanol was also tested (Fig. 16b–d), and the results showed that the modified catalytic material could achieve efficient conversion of substrates, demonstrating the versatility of Cr–Ni(OH)$_2$/NF for electrocatalysis of biomass molecules. This work yielded HMFOR current densities greater than 200 mA cm^{-2}, but still insufficient to reach industrialisation. Therefore, Mu et al. propose a proton transfer-mediated strategy to overcome the energy barrier of the dehydrogenation process of **HMF**.[184] They synthesised PO$_4$ and Ru modified Ni(OH)$_2$ (PO$_4$/Ru–Ni(OH)$_2$/NF), which exhibited excellent electrocatalytic performance at 1.45 V vs. RHE potential for HMFOR, and the initial current densities were able to reach more than 1000 mA cm^{-2} during all six cycles with high selectivity for **FDCA** (98%) and a faradaic efficiency of 97% (Fig. 16e–g). DFT calculations revealed that PO$_4$ on the Ni(OH)$_2$ surface interacts with the O–H bonds of the adsorbed **HMF** molecules, elongating the O–H bonds and lowering the free energy of bond dissociation, which is an indication that phosphate interactions accelerate the oxidation of **HMF** by making it easier for hydrogen to detach from the **HMF** molecules (the red circle in Fig. 16h). In addition, the high valence metal Ru extracts electrons from the d-band and forms a partial filling near the Fermi energy level (Fig. 16i), increasing the conductivity of the Ni(OH)$_2$ surface. This work provides a good example for the electrooxidation reaction of industrial grade alcohols and aldehydes.

7   Conclusions and perspectives

In summary, we have outlined recent advances in electrocatalytic hydrogenation, hydrolysis and oxidative dehydrogenation processes for biomass-derived furan compounds (**HMF** and **FF**). In recent years, progress has been made in electrocatalytic mechanisms, electrode material development, and factors affecting the reaction (e.g., electrolyte pH, reaction potential, substrate concentration). Despite the progress, unclear aspects remain, including site identification and the mechanism of action of complex multisite catalysts. Factors affecting hydrogenation and hydrolysis are not fully understood, and interactions between aldehyde and alcohol groups in **HMF** pose challenges. The gap between current research and industrial applications creates an urgent need to accelerate the development of electrocatalytic conversion processes for biomass platform molecules. In this process, five key factors (shown in Fig. 17) require special attention to bridge the knowledge gap and translate research results into practical applications. This outlook will help to deepen the

understanding of electrochemical mechanisms and pave the way for large-scale applications and conversion of various C–O/C=O-containing organics.

7.1 Understanding of reaction mechanism

Despite advances in the design of electrode materials for the electrocatalytic conversion of furan compounds, uncertainties in identifying active sites and understanding the reaction mechanism remain, leading to increased challenges. Different catalysts exhibit HMFOR capabilities, but the identification of the actual active sites and species, especially multivalent and multi-metal sites, is controversial. In particular, the electrocatalytic reduction reaction mechanism of furan analogs derived from biomass has been little studied. In order to comprehensively understand the reaction mechanism of the electrocatalytic system of furan compounds, the model of "*in situ* characterization and experimental validation with theoretical calculation" is a feasible strategy for the design of descriptors and the identification of active sites. This provides the basis for a deeper understanding of the electrocatalytic mechanism and for exploring more effective design of electrode materials and activity modulation strategies.

7.2 Optimization of reaction conditions

Many reactions are carried out only under alkaline or acidic conditions, *e.g.*, electrocatalytic oxidation of **HMF** to synthesize **FDCA** is suitable for alkaline conditions, while hydrogenolysis of **HMF** is suitable for acidic conditions. In contrast, it is of great importance to perform electrocatalytic reactions under neutral conditions, which reduces the corrosiveness to equipment and is more suitable for industrial production. In addition, in the reduction of furan compounds, the choice of reaction medium is crucial because it can be used not only as a solvent but also as a hydrogen source. Therefore, there is an urgent need to develop renewable reaction media with good solubility to improve the efficiency and sustainability of the electrocatalytic reduction process. In addition, increasing the concentration of reactants is necessary for industrial production. Currently, the reaction substrate concentration is usually low (<100 mM) due to substrate instability and limited solubility, so it is necessary to develop catalysts with better performance to promote the increase of reactant concentration. At the same time, achieving higher catalytic efficiencies will reduce the number of catalysts used, contributing to more sustainable and economical industrial processes.

7.3 Paired electrolysis

Although pairwise electrolysis of furan compounds improves the energy efficiency and kinetics of the anodic reaction, the reaction coupled with **HMF** reduction still requires in-depth investigation. And the practical applicability of paired electrolysis still needs to be carefully evaluated. In a two-electrode system, it is impractical to independently control the reaction voltages at the cathode or anode, which may affect the adaptability and versatility of pairwise electrolysis. Therefore, further research and development is needed to address these

challenges and to optimize the operating parameters of paired electrolysis for wider industrial and commercial viability. Determining the appropriate paired electrolysis reaction is critical and process costs need to be evaluated to improve productivity. A promising future direction is the coupling of reactors with renewable energy cells, such as solar cells, to reduce power costs and minimize losses. This innovative coupling strategy not only improves energy efficiency but also contributes to a more sustainable and environmentally friendly electrochemical process.

7.4 Product separation

Currently, product separation is mainly performed by poorly soluble and thermodynamic methods, such as extraction and precipitation, leading to higher production costs. In the synthesis of **FDCA** by electrocatalytic oxidation of **HMF**, the most efficient separation method is to precipitate **FDCA** by acidifying the electrolyte because **FDCA** is highly soluble in alkaline solutions. However, this method increases the cost and generates salt waste. Therefore, there is an urgent need to develop cost-effective separation methods suitable for industrial production in electrocatalysis. Membrane separation technology is a potential solution that may provide an efficient and economically viable separation process, thereby reducing the cost and environmental impact of conventional methods.

7.5 Industrialization development

Current research is focused on the laboratory scale, while challenges such as high current density operation, competing reactions at low potentials and high current densities need to be addressed to achieve industrial scale. Successful industrialization involves several key aspects: first, highly active and selective catalysts, such as alloy-type, single-atom and synergistic catalysts, need to be developed to improve performance. Additionally, exploring methods like molecular modification, such as Cl-modified Cu catalysts to promote the hydrogenolysis of **HMF**, is essential.[185] Second, given the stability of the electrocatalysts, the active sites and competing reactions of the substrate electrolysis must be accurately identified and separated. Then, the fabrication of large-area electrodes and a device design suitable for industrialization need to be considered. Due to the high concentration of substrate for industrial production, the small area electrode cannot meet the demand for high concentration substrate conversion. It is necessary to increase the area of the electrode to provide active sites for more substrate molecules while ensuring the activity and stability of the catalyst. At the same time, large-area electrodes need to be matched with suitable reactors. Flow reactor effectively control substrate concentration, flow rate, prevent competing reactions, and provide sufficient interfaces to facilitate transfer. Membrane reactors, on the other hand, can improve selectivity and Faraday efficiency, but in terms of practicality, the corrosion resistance of the material, the pH of the electrolyte, the suitability of the septum, and the robustness of the catalyst-carrier bond need to be considered. Finally, direct conversion of lignocellulose to oxidation or reduction products is an economically viable

industrial direction, and simplification of the process and improved feedstock utilization will enhance the economic viability of industrialization.

Author contributions

All of the authors contributed to the manuscript preparation. P. Z. and Y. C. conceived the outline of the manuscript. P. Z. wrote the original draft of the manuscript. M. S. and Z. S. searched the literature. X. L. and Y. C. discussed and helped revise the manuscript.

Conflicts of interest

The authors declare no conflict of interest.

Acknowledgements

Notes and references

1 Q. Hou, X. Qi, M. Zhen, H. Qian, Y. Nie, C. Bai, S. Zhang, X. Bai and M. Ju, *Green Chem.*, 2021, **23**, 119–231.

2 Y. C. Feng, S. S. Long, X. Tang, Y. Sun, R. Luque, X. H. Zeng and L. Lin, *Chem. Soc. Rev.*, 2021, **50**, 6042–6093.

3 L. Guo, X. Zhang, L. Gan, L. Pan, C. Shi, Z. F. Huang, X. Zhang and J. J. Zou, *Adv. Sci.*, 2023, **10**, e2205540.

4 S. Wang, A. Cheng, F. Liu, J. Zhang, T. Xia, X. Zeng, W. Fan and Y. Zhang, *Ind. Chem. Mater.*, 2023, **1**, 188–206.

5 W. G. Zhao, F. Wang, K. Y. Zhao, X. X. Liu, X. T. Zhu, L. Yan, Y. Yin, Q. Xu and D. L. Yin, *Carbon Resour. Convers.*, 2023, **6**, 116–131.

6 W. P. Deng, Y. C. Feng, J. Fu, H. W. Guo, Y. Guo, B. X. Han, Z. C. Jiang, L. Z. Kong, C. Z. Li, H. C. Liu, P. T. T. Nguyen, P. N. Ren, F. Wang, S. Wang, Y. Q. Wang, Y. Wang, S. S. Wong, K. Yan, N. Yan, X. F. Yang, Y. B. Zhang, Z. R. Zhang, X. H. Zeng and H. Zhou, *Green Energy Environ.*, 2023, **8**, 10–114.

7 M. Besson, P. Gallezot and C. Pinel, *Chem. Rev.*, 2013, **114**, 1827–1870.

8 Q. Jin, L. Yang, N. Poe and H. Huang, *Trends Food Sci. Technol.*, 2018, **74**, 119–131.

9 P. Sudarsanam, R. Zhong, S. Van den Bosch, S. M. Coman, V. I. Parvulescu and B. F. Sels, *Chem. Soc. Rev.*, 2018, **47**, 8349–8402.

10 V. G. Yadav, G. D. Yadav, S. C. J. C. t. Patankar and e. policy, *Clean Technol. Environ.*, 2020, **22**, 1757–1774.

11 D. Carpenter, T. L. Westover, S. Czernik and W. Jablonski, *Green Chem.*, 2014, **16**, 384–406.

12 J. J. Bozell and G. R. Petersen, *Green Chem.*, 2010, **12**, 539–554.

13 Y. Kwon, K. J. P. Schouten, J. C. van der Waal, E. de Jong and M. T. M. Koper, *ACS Catal.*, 2016, **6**, 6704–6717.

14 E. Hayashi, Y. Yamaguchi, K. Kamata, N. Tsunoda, Y. Kumagai, F. Oba and M. Hara, *J. Am. Chem. Soc.*, 2019, **141**, 890–900.

15 S. Chu, Y. Cui and N. Liu, *Nat. Mater.*, 2016, **16**, 16–22.

16 Y. Shao and V. M. Zavala, *Comput. Chem. Eng.*, 2019, **127**, 31–40.

17 M. Yang, Z. Yuan, R. Peng, S. Wang and Y. Zou, *Energy Environ. Mater.*, 2022, **5**, 1117–1138.

18 S. A. Akhade, N. Singh, O. Y. Gutierrez, J. Lopez-Ruiz, H. Wang, J. D. Holladay, Y. Liu, A. Karkamkar, R. S. Weber, A. B. Padmaperuma, M. S. Lee, G. A. Whyatt, M. Elliott, J. E. Holladay, J. L. Male, J. A. Lercher, R. Rousseau and V. A. Glezakou, *Chem. Rev.*, 2020, **120**, 11370–11419.

19 Z. Sun, S. Wang, X. Wang and Z. J. F. Jiang, *Fuel*, 2016, **164**, 262–266.

20 G. Lv, H. Wang, Y. Yang, T. Deng, C. Chen, Y. Zhu and X. J. A. C. Hou, *ACS Catal.*, 2015, **5**, 5636–5646.

21 C. Y. Zhang, X. Chang, L. Zhu, Q. G. Xing, S. P. You, W. Qu, R. X. Su and Z. M. He, *Int. J. Biol. Macromol.*, 2019, **128**, 132–139.

22 T. Muñoz, L. Y. Rache, H. A. Rojas, G. P. Romanelli, J. J. Martinez and R. Luque, *Biochem. Eng. J.*, 2020, **154**, 107421.

23 Z. H. Zhang, S. Y. Yao, C. X. Wang, M. M. Liu, F. Zhang, X. B. Hu, H. Chen, X. Gou, K. Q. Chen, Y. M. Zhu, X. Y. Lu, P. K. Ouyang and J. Fu, *J. Catal.*, 2019, **373**, 314–321.

24 W. P. Han, M. X. Tang, J. L. Li, X. K. Li, J. W. Wang, L. G. Zhou, Y. Yang, Y. Q. Wang and H. Ge, *Appl. Catal., B*, 2020, **268**, 118748.

25 K. Ji, M. Xu, S. M. Xu, Y. Wang, R. Ge, X. Hu, X. Sun and H. Duan, *Angew. Chem., Int. Ed.*, 2022, **61**, e202209849.

26 H. Y. Wang, C. H. Zhu, D. Li, Q. Y. Liu, J. Tan, C. G. Wang, C. L. Cai and L. L. Ma, *Renew. Sust. Energ. Rev.*, 2019, **103**, 227–247.

27 L. Hu, J. Xu, S. Zhou, A. He, X. Tang, L. Lin, J. Xu and Y. J. A. C. Zhao, *ACS Catal.*, 2018, **8**, 2959–2980.

28 A. S. May and E. J. Biddinger, *ACS Catal.*, 2020, **10**, 3212–3221.

29 A. Jaswal, P. P. Singh and T. J. G. C. Mondal, *Green Chem.*, 2022, **24**, 510–551.

30 P. J. C. S. R. Gallezot, *Chem. Soc. Rev.*, 2012, **41**, 1538–1558.

31 M. Besson, P. Gallezot and C. J. C. r. Pinel, *Chem. Rev.*, 2014, **114**, 1827–1870.

32 C. Wang, H. Xu, R. Daniel, A. Ghafourian, J. M. Herreros, S. Shuai and X. J. F. Ma, *Fuel*, 2013, **103**, 200–211.

33 D. Ouyang, D. Gao, J. Hong, Z. Jiang and X. J. J. o. E. C. Zhao, *J. Energy Chem.*, 2023, **79**, 135–147.

34 B. Xia, G. Wang, S. Cui, J. Guo, H. Xu, Z. Liu and S.-Q. Zang, *Chin. Chem. Lett.*, 2023, **34**, 107810.

35 H. Luo, J. Barrio, N. Sunny, A. Li, L. Steier, N. Shah, I. E. L. Stephens and M.-M. Titirici, *Adv. Energy Mater.*, 2021, **11**, 2101180.

36 C. Chen, L. Wang, B. Zhu, Z. Zhou, S. I. El-Hout, J. Yang and J. Zhang, *J. Energy Chem.*, 2021, **54**, 528–554.

37 X. Jiang, W. Li, Y. Liu, L. Zhao, Z. Chen, L. Zhang, Y. Zhang and S. Yun, *SusMat*, 2023, **3**, 21–43.

38 Y. Lu, T. Liu, Y.-C. Huang, L. Zhou, Y. Li, W. Chen, L. Yang, B. Zhou, Y. Wu, Z. Kong, Z. Huang, Y. Li, C.-L. Dong, S. Wang and Y. Zou, *ACS Catal.*, 2022, **12**, 4242–4251.

39 M. T. Bender, Y. C. Lam, S. Hammes-Schiffer and K. S. Choi, *J. Am. Chem. Soc.*, 2020, **142**, 21538–21547.

40 Y. Lu, T. Liu, C. L. Dong, C. Yang, L. Zhou, Y. C. Huang, Y. Li, B. Zhou, Y. Zou and S. Wang, *Adv. Mater.*, 2021, **34**, e2107185.

41 Y. Yang and T. Mu, *Green Chem.*, 2021, **23**, 4228–4254.

42 Y. J. Song, Z. H. Li, K. Fan, Z. Ren, W. F. Xie, Y. S. Yang, M. F. Shao and M. Wei, *Appl. Catal., B*, 2021, **299**, 120669.

43 T. H. Wang, L. Tao, X. R. Zhu, C. Chen, W. Chen, S. Q. Du, Y. Y. Zhou, B. Zhou, D. D. Wang, C. Xie, P. Long, W. Li, Y. Y. Wang, R. Chen, Y. Q. Zou, X. Z. Fu, Y. F. Li, X. F. Duan and S. Y. Wang, *Nat. Catal.*, 2022, **5**, 66–73.

44 T. Cao, M. Wu, V. V. Ordomsky, X. Xin, H. Wang, P. Metivier and M. Pera-Titus, *ChemSusChem*, 2017, **10**, 4851–4854.

45 Q. Qin, T. Heil, J. Schmidt, M. Schmallegger, G. Gescheidt, M. Antonietti and M. Oschatz, *ACS Appl. Energy Mater.*, 2019, **2**, 8359–8365.

46 W. Chen, C. Xie, Y. Wang, Y. Zou, C.-L. Dong, Y.-C. Huang, Z. Xiao, Z. Wei, S. Du, C. Chen, B. Zhou, J. Ma and S. Wang, *Chem*, 2020, **6**, 2974–2993.

47 B. J. Taitt, D.-H. Nam and K.-S. Choi, *ACS Catal.*, 2018, **9**, 660–670.

48 R. Bababrik, D. Santhanaraj, D. E. Resasco and B. Wang, *J. Appl. Electrochem.*, 2020, **51**, 19–26.

49 W. Chen, L. Xu, X. Zhu, Y. C. Huang, W. Zhou, D. Wang, Y. Zhou, S. Du, Q. Li, C. Xie, L. Tao, C. L. Dong, J. Liu, Y. Wang, R. Chen, H. Su, C. Chen, Y. Zou, Y. Li, Q. Liu and S. Wang, *Angew. Chem., Int. Ed.*, 2021, **60**, 7297–7307.

50 N. Heidary and N. Kornienko, *Chem. Sci.*, 2020, **11**, 1798–1806.

51 R. Ge, Y. Wang, Z. Li, M. Xu, S. M. Xu, H. Zhou, K. Ji, F. Chen, J. Zhou and H. Duan, *Angew. Chem., Int. Ed.*, 2022, **61**, e202200211.

52 T. H. H. Le, T. G. Vo and C. Y. Chiang, *J. Catal.*, 2021, **404**, 560–569.

53 X. Pang, H. Bai, H. Zhao, W. Fan and W. Shi, *ACS Catal.*, 2022, **12**, 1545–1557.

54 M. Zhang, Y. Liu, B. Liu, Z. Chen, H. Xu and K. Yan, *ACS Catal.*, 2020, **10**, 5179–5189.

55 N. Zhang, Y. Zou, L. Tao, W. Chen, L. Zhou, Z. Liu, B. Zhou, G. Huang, H. Lin and S. Wang, *Angew. Chem., Int. Ed.*, 2019, **58**, 15895–15903.

56 F. J. Holzhäuser, T. Janke, F. Öztas, C. Broicher and R. Palkovits, *Adv. Sustainable Syst.*, 2020, **4**, 1900151.

57 J. C. Hasse, N. Agrawal, M. J. Janik and A. Holewinski, *J. Phys. Chem. C*, 2022, **126**, 7054–7065.

58 S. Kar, Q. Q. Zhou, Y. Ben-David and D. Milstein, *J. Am. Chem. Soc.*, 2022, **144**, 1288–1295.

59 T. H. Wang, Z. F. Huang, T. Y. Liu, L. Tao, J. Tian, K. Z. Gu, X. X. Wei, P. Zhou, L. Gan, S. Q. Du, Y. Q. Zou, R. Chen, Y. F. Li, X. Z. Fu and S. Y. Wang, *Angew. Chem., Int. Ed.*, 2022, **61**, e202115636.

60 T. Wang, L. Tao, X. Zhu, C. Chen, W. Chen, S. Du, Y. Zhou, B. Zhou, D. Wang, C. Xie, P. Long, W. Li, Y. Wang, R. Chen, Y. Zou, X.-Z. Fu, Y. Li, X. Duan and S. Wang, *Nat. Catal.*, 2022, **5**, 66–73.

61 X. Lu, K. H. Wu, B. Zhang, J. Chen, F. Li, B. J. Su, P. Yan, J. M. Chen and W. Qi, *Angew. Chem., Int. Ed.*, 2021, **60**, 14528–14535.

62 Y. Lu, T. Liu, C. L. Dong, Y. C. Huang, Y. Li, J. Chen, Y. Zou and S. Wang, *Adv. Mater.*, 2021, **33**, 2007056.

63 S. Choi, M. Balamurugan, K. G. Lee, K. H. Cho, S. Park, H. Seo and K. T. Nam, *J. Phys. Chem. Lett.*, 2020, **11**, 2941–2948.

64 H. Zhou, Z. H. Li, S. M. Xu, L. L. Lu, M. Xu, K. Y. Ji, R. X. Ge, Y. F. Yan, L. N. Ma, X. G. Kong, L. R. Zheng and H. H. Duan, *Angew. Chem., Int. Ed.*, 2021, **60**, 8976–8982.

65 Y. Du, H. Sheng, D. Astruc and M. Zhu, *Chem. Rev.*, 2020, **120**, 526–622.

66 V. P. Kashparova, E. N. Papina, I. I. Kashparov, I. Y. Zhukova, I. B. Ilchibaeva and E. S. Kagan, *Russ. J. Gen. Chem.*, 2017, **87**, 2733–2735.

67 S. R. Kubota and K. S. Choi, *ChemSusChem*, 2018, **11**, 2138–2145.

68 R. Latsuzbaia, R. Bisselink, A. Anastasopol, H. van der Meer, R. van Heck, M. S. Yagüe, M. Zijlstra, M. Roelands, M. Crockatt, E. Goetheer and E. Giling, *J. Appl. Electrochem.*, 2018, **48**, 611–626.

69 G. R. Xu, M. Batmunkh, S. Donne, H. N. Jin, J. X. Jiang, Y. Chen and T. Y. Ma, *J. Mater. Chem. A*, 2019, **7**, 25433–25440.

70 K. R. Vuyyuru and P. Strasser, *Catal. Today*, 2012, **195**, 144–154.

71 K. L. Zhou, Z. Wang, C. B. Han, X. Ke, C. Wang, Y. Jin, Q. Zhang, J. Liu, H. Wang and H. Yan, *Nat. Commun.*, 2021, **12**, 3783.

72 J. Zheng, W. C. Sheng, Z. B. Zhuang, B. J. Xu and Y. S. Yan, *Sci. Adv.*, 2016, **2**, e1501602.

73 D. J. Chadderdon, L. Xin, J. Qi, Y. Qiu, P. Krishna, K. L. More and W. Li, *Green Chem.*, 2014, **16**, 3778–3786.

74 M. Park, M. Gu and B. S. Kim, *ACS Nano*, 2020, **14**, 6812–6822.

75 Y. Kwon, S. C. S. Lai, P. Rodriguez and M. T. M. Koper, *J. Am. Chem. Soc.*, 2011, **133**, 6914–6917.

76 Y. Xie, L. Sun, X. Pan, Z. Zhou and G. Zhao, *Appl. Catal., B*, 2023, **338**, 123068.

77 X. Lu, K.-H. Wu, B. Zhang, J. Chen, F. Li, B.-J. Su, P. Yan, J.-M. Chen and W. Qi, *Angew. Chem., Int. Ed.*, 2021, **60**, 14528–14535.

78 L. Zheng, Y. Zhao, P. Xu, Z. Lv, X. Shi and H. Zheng, *J. Mater. Chem. A*, 2022, **10**, 10181–10191.

79 D. Chen, Y. Ding, X. Cao, L. Wang, H. Lee, G. Lin, W. Li, G. Ding and L. Sun, *Angew. Chem., Int. Ed.*, 2023, **62**, e202309478.

80 I. Yamada, A. Takamatsu, K. Asai, H. Ohzuku, T. Shirakawa, T. Uchimura, S. Kawaguchi, H. Tsukasaki, S. Mori, K. Wada, H. Ikeno and S. Yagi, *ACS Appl. Energy Mater.*, 2018, **1**, 3711–3721.

81 Y. C. Yang, D. X. Xu, B. L. Zhang, Z. M. Xue and T. C. Mu, *Chem. Eng. J.*, 2022, **433**, 133842.

82 Y. X. Lu, C. L. Dong, Y. C. Huang, Y. Q. Zou, Y. B. Liu, Y. Y. Li, N. N. Zhang, W. Chen, L. Zhou, H. Z. Lin and S. Y. Wang, *Sci. China: Chem.*, 2020, **63**, 980–986.

83 X. Deng, X. Kang, M. Li, K. Xiang, C. Wang, Z. Guo, J. Zhang, X.-Z. Fu and J.-L. Luo, *J. Mater. Chem. A*, 2020, **8**, 1138–1146.

84 S. Barwe, J. Weidner, S. Cychy, D. M. Morales, S. Dieckhofer, D. Hiltrop, J. Masa, M. Muhler and W. Schuhmann, *Angew. Chem., Int. Ed.*, 2018, **57**, 11460–11464.

85 X. Deng, M. Li, Y. Fan, L. Wang, X.-Z. Fu and J.-L. Luo, *Appl. Catal., B*, 2020, **278**, 119339.

86 R. Zhang, S. Jiang, Y. Rao, S. Chen, Q. Yue and Y. Kang, *Green Chem.*, 2021, **23**, 2525–2530.

87 Z. Y. Zhou, Y. N. Xie, L. Z. Sun, Z. M. Wang, W. K. Wang, L. Z. Jiang, X. Tao, L. N. Li, X. H. Li and G. H. Zhao, *Appl. Catal., B*, 2022, **305**, 121072.

88 E. López-Fernández, J. Gil-Rostra, J. P. Espinós, A. R. González-Elipe, A. de Lucas Consuegra and F. Yubero, *ACS Catal.*, 2020, **10**, 6159–6170.

89 B. Zhou, Y. Li, Y. Zou, W. Chen, W. Zhou, M. Song, Y. Wu, Y. Lu, J. Liu, Y. Wang and S. Wang, *Angew. Chem., Int. Ed.*, 2021, **60**, 22908–22914.

90 X. Deng, G. Y. Xu, Y. J. Zhang, L. Wang, J. Zhang, J. F. Li, X. Z. Fu and J. L. Luo, *Angew. Chem., Int. Ed.*, 2021, **60**, 20535–20542.

91 B. Liu, S. Xu, M. Zhang, X. Li, D. Decarolis, Y. Liu, Y. Wang, E. K. Gibson, C. R. A. Catlow and K. Yan, *Green Chem.*, 2021, **23**, 4034–4043.

92 Y.-F. Qi, K.-Y. Wang, Y. Sun, J. Wang and C. Wang, *ACS Sustainable Chem. Eng.*, 2021, **10**, 645–654.

93 Y. Xie, Z. Zhou, N. Yang and G. Zhao, *Adv. Funct. Mater.*, 2021, **31**, 2102886.

94 H. C. Xu, G. R. Xin, W. X. Hu, Z. X. Zhang, C. L. Si, J. G. Chen, L. F. Lu, Y. T. Peng and X. Y. Li, *Appl. Catal., B*, 2023, **339**, 123157.

95 M. T. Bender and K. S. Choi, *ChemSusChem*, 2022, **15**, e202200675.

96 M. T. Bender, R. E. Warburton, S. Hammes-Schiffer and K.-S. Choi, *ACS Catal.*, 2021, **11**, 15110–15124.

97 X. J. Song, X. H. Liu, H. F. Wang, Y. Guo and Y. Q. Wang, *Ind. Eng. Chem. Res.*, 2020, **59**, 17348–17356.

98 S. Q. Li, X. Sun, Z. H. Yao, X. Zhong, Y. Y. Coo, Y. L. Liang, Z. Z. Wei, S. W. Deng, G. L. Zhuang, X. N. Li and J. G. Wang, *Adv. Funct. Mater.*, 2019, **29**, 1904780.

99 G. Yang, Y. Jiao, H. Yan, Y. Xie, C. Tian, A. Wu, Y. Wang and H. Fu, *Nat. Commun.*, 2022, **13**, 3125.

100 L. F. Gao, Z. B. Liu, J. L. Ma, L. J. Zhong, Z. Q. Song, J. A. Xu, S. Y. Gan, D. X. Han and L. Niu, *Appl. Catal., B*, 2020, **261**, 118235.

101 Y. Zhao, B. Jin, A. Vasileff, Y. Jiao and S.-Z. Qiao, *J. Mater. Chem. A*, 2019, **7**, 8117–8121.

102 N. Jiang, B. You, R. Boonstra, I. M. Terrero Rodriguez and Y. Sun, *ACS Energy Lett.*, 2016, **1**, 386–390.

103 B. You, X. Liu, N. Jiang and Y. Sun, *J. Am. Chem. Soc.*, 2016, **138**, 13639–13646.

104 B. You, N. Jiang, X. Liu and Y. Sun, *Angew. Chem., Int. Ed.*, 2016, **55**, 9913–9917.

105 P. Zhang, X. Sheng, X. Chen, Z. Fang, J. Jiang, M. Wang, F. Li, L. Fan, Y. Ren, B. Zhang, B. J. J. Timmer, M. S. G. Ahlquist and L. Sun, *Angew. Chem., Int. Ed.*, 2019, **58**, 9155–9159.

106 B. Zhou, C.-L. Dong, Y.-C. Huang, N. Zhang, Y. Wu, Y. Lu, X. Yue, Z. Xiao, Y. Zou and S. Wang, *J. Energy Chem.*, 2021, **61**, 179–185.

107 Y. Sun, J. Wang, Y. Qi, W. Li and C. Wang, *Adv. Sci.*, 2022, **9**, 2200957.

108 R. P. Luo, Y. Y. Li, L. X. Xing, R. Y. Zhong, Z. Y. Qian, G. P. Yin, Y. C. Wang and L. Du, *Appl. Catal., B*, 2022, **311**, 121357.

109 B. Zhang, H. Fu and T. Mu, *Green Chem.*, 2022, **24**, 877–884.

110 X. Huang, J. Song, M. Hua, Z. Xie, S. Liu, T. Wu, G. Yang and B. Han, *Green Chem.*, 2020, **22**, 843–849.

111 C. Yang, C. Wang, L. Zhou, W. Duan, Y. Song, F. Zhang, Y. Zhen, J. Zhang, W. Bao, Y. Lu, D. Wang and F. Fu, *Chem. Eng. J.*, 2021, **422**, 130125.

112 G. Yang, Y. Jiao, H. Yan, Y. Xie, A. Wu, X. Dong, D. Guo, C. Tian and H. Fu, *Adv. Mater.*, 2020, **32**, 2000455.

113 Y. Zhou, T. J. A. Slater, X. Luo and Y. Shen, *Appl. Catal., B*, 2023, **324**, 122218.

114 H. M. Li, X. Y. Huang, Y. Lv, J. L. Zhang and W. Li, *Int. J. Hydrogen Energy*, 2023, **48**, 38279–38295.

115 A. R. Poerwoprajitno, L. Gloag, J. Watt, S. Cychy, S. Cheong, P. V. Kumar, T. M. Benedetti, C. Deng, K. H. Wu, C. E. Marjo, D. L. Huber, M. Muhler, J. J. Gooding, W. Schuhmann, D. W. Wang and R. D. Tilley, *Angew. Chem., Int. Ed.*, 2020, **59**, 15487–15491.

116 B. You, X. Liu, X. Liu and Y. Sun, *ACS Catal.*, 2017, **7**, 4564–4570.

117 L. Zeng, Y. Chen, M. Sun, Q. Huang, K. Sun, J. Ma, J. Li, H. Tan, M. Li, Y. Pan, Y. Liu, M. Luo, B. Huang and S. Guo, *J. Am. Chem. Soc.*, 2023, **145**, 17577–17587.

118 W.-J. Liu, L. Dang, Z. Xu, H.-Q. Yu, S. Jin and G. W. Huber, *ACS Catal.*, 2018, **8**, 5533–5541.

119 L. Wang, J. H. Cao, C. J. Lei, Q. Z. Dai, B. Yang, Z. J. Li, X. W. Zhang, C. Yuan, L. C. Lei and Y. Hou, *ACS Appl. Mater. Interfaces*, 2019, **11**, 27743–27750.

120 Y. Zhang, Z. Xue, X. Zhao, B. Zhang and T. Mu, *Green Chem.*, 2022, **24**, 1721–1731.

121 Z. F. Zhao, T. Y. Guo, X. Y. Luo, X. T. Qin, L. X. Zheng, L. Yu, Z. Q. Lv, D. Ma and H. J. Zheng, *Catal. Sci. Technol.*, 2022, **12**, 3817–3825.

122 Y. Song, W. Xie, Y. Song, H. Li, S. Li, S. Jiang, J. Y. Lee and M. Shao, *Appl. Catal., B*, 2022, **312**, 121400.

123 M. Li, L. Chen, S. Ye, G. Fan, L. Yang, X. Zhang and F. Li, *J. Mater. Chem. A*, 2019, **7**, 13695–13704.

124 S. Liang, L. Pan, T. Thomas, B. Zhu, C. Chen, J. Zhang, H. Shen, J. Liu and M. Yang, *Chem. Eng. J.*, 2021, **415**, 128864.

125 B. Zhang, Z. Li, Y. Zhou, Z. Yang, Z. Xue and T. Mu, *Small*, 2023, **19**, 2306663.

126 B. Zhang, Z. Yang, C. Yan, Z. Xue and T. Mu, *Small*, 2023, **19**, 2207236.

127 S. R. Kubota and K.-S. Choi, *ACS Sustainable Chem. Eng.*, 2018, **6**, 9596–9600.

128 H. Wu, J. Song, H. Liu, Z. Xie, C. Xie, Y. Hu, X. Huang, M. Hua and B. Han, *Chem. Sci.*, 2019, **10**, 4692–4698.

129 A. M. Román, N. Agrawal, J. C. Hasse, M. J. Janik, J. W. Medlin and A. Holewinski, *J. Catal.*, 2020, **391**, 327–335.

130 X. X. Li, L. C. Cong, H. B. Lin, F. B. Liu, F. Y. Han and N. Lin, *Sci. China: Chem.*, 2022, **65**, 2576–2587.

131 X. Zhang, T.-Y. Liu, Y. Zhou, L. Zhang, X.-C. Zhou, J.-J. Feng and A.-J. Wang, *Appl. Catal., B*, 2023, **328**, 122530.

132 B. Liu, Z. Zheng, Y. Liu, M. Zhang, Y. Wang, Y. Wan and K. J. J. o. E. C. Yan, *J. Energy Chem.*, 2023, **78**, 412–421.

133 T. Begildayeva, J. Theerthagiri, S. J. Lee, A. Min, G. A. Kim, S. Manickam, M. Y. J. E. Choi and E. Materials, *Energy Environ. Mater.*, 2022, e12563.

134 A. M. Román, J. C. Hasse, J. W. Medlin and A. Holewinski, *ACS Catal.*, 2019, **9**, 10305–10316.

135 X. Li, L. Cong, H. Lin, F. Liu, X. Fu, H.-C. Xu and N. J. G. E. Lin, *Green Energy Environ.*, 2022, **9**, 104–113.

136 M. T. Bender, X. Yuan, M. K. Goetz and K.-S. Choi, *ACS Catal.*, 2022, **12**, 12349–12368.

137 M. X. Li, T. X. Zheng, D. F. Lu, S. W. Dai, X. Chen, X. C. Pan, D. B. Dong, R. G. Weng, G. Xu and F. A. Wang, *J. Energy Chem.*, 2023, **84**, 101–111.

138 X. Yuan, K. Lee, M. T. Bender, J. R. Schmidt and K.-S. Choi, *Chemsuschem*, 2022, **15**, e202200952.

139 A. Aboukhater, M. Abu Haija, F. Banat, I. Othman, M. A. Sabri and B. Govindan, *Catalysts*, 2023, **13**, 260.

140 Y. M. Cui, Z. Wang and S. G. Li, *Catal. Sci. Technol.*, 2023, **13**, 1846–1854.

141 I. K. M. Yu, F. L. Deng, X. Chen, G. H. Cheng, Y. Liu, W. Zhang and J. A. Lercher, *Nat. Commun.*, 2022, **13**, 7154.

142 L. Zhou, Y. Y. Li, Y. X. Lu, S. Y. Wang and Y. Q. Zou, *Chin. J. Catal.*, 2022, **43**, 3142–3153.

143 P. Zhou, Y. Chen, P. Luan, X. Zhang, Z. Yuan, S.-X. Guo, Q. Gu, B. Johannessen, M. Mollah, A. L. Chaffee, D. R. Turner and J. Zhang, *Green Chem.*, 2021, **23**, 3028–3038.

144 S. Chen, R. Wojcieszak, F. Dumeignil, E. Marceau and S. Royer, *Chem. Rev.*, 2018, **118**, 11023–11117.

145 D. K. Lee, S. R. Kubota, A. N. Janes, M. T. Bender, J. Woo, J. R. Schmidt and K.-S. Choi, *Chemsuschem*, 2021, **14**, 4563–4572.

146 J. J. Roylance, T. W. Kim and K.-S. Choi, *ACS Catal.*, 2016, **6**, 1840–1847.

147 J. A. Lopez-Ruiz, E. Andrews, S. A. Akhade, M.-S. Lee, K. Koh, U. Sanyal, S. F. Yuk, A. J. Karkamkar, M. A. Derewinski, J. Holladay, V.-A. Glezakou, R. Rousseau, O. Y. Gutiérrez and J. D. Holladay, *ACS Catal.*, 2019, **9**, 9964–9972.

148 L. C. Liu, H. H. Liu, W. M. Huang, Y. P. He, W. L. Zhang, C. N. Wang and H. B. Lin, *J. Electroanal. Chem.*, 2017, **804**, 248–253.

149 X. H. Chadderdon, D. J. Chadderdon, T. Pfennig, B. H. Shanks and W. Li, *Green Chem.*, 2019, **21**, 6210–6219.

150 M. S. Dhawan, G. D. Yadav and S. C. Barton, *Sustainable Energy Fuels*, 2021, **5**, 2972–2984.

151 Y. Kwon, E. d. Jong, S. Raoufmoghaddam and M. T. M. Koper, *ChemSusChem*, 2013, **6**, 1659–1667.

152 W. Xu, C. Yu, J. Chen and Z. Liu, *Appl. Catal., B*, 2022, **305**, 121062.

153 B. H. Wu and N. F. Zheng, *Nano Today*, 2013, **8**, 168–197.

154 G. S. de Luna, P. H. Ho, A. Lolli, F. Ospitali, S. Albonetti, G. Fornasari and P. Benito, *Chemelectrochem*, 2020, **7**, 1238–1247.

155 X. Yue, W. X. Zhao, S. Y. Wang and Y. Q. Zou, *Chin. J. Struct. Chem.*, 2022, **41**, 2205063–2205069.

156 L. Zhang, F. Zhang, F. C. Michel, Jr. and A. C. Co, *Chemelectrochem*, 2019, **6**, 4739–4749.

157 G. Sanghez de Luna, P. H. Ho, A. Sacco, S. Hernández, J.-J. Velasco-Vélez, F. Ospitali, A. Paglianti, S. Albonetti, G. Fornasari and P. Benito, *ACS Appl. Mater. Interfaces*, 2021, **13**, 23675–23688.

158 J. T. Brosnahan, Z. Zhang, Z. Yin and S. Zhang, *Nanoscale*, 2021, **13**, 2312–2316.

159 J. W. Tan, W. B. A. Zhang, Y. J. Shu, H. Y. Lu, Y. Tang and Q. S. Gao, *Sci. Bull.*, 2021, **66**, 1003–1012.

160 X. Zhang, M. Han, G. Liu, G. Wang, Y. Zhang, H. Zhang and H. Zhao, *Appl. Catal., B*, 2019, **244**, 899–908.

161 Z. Yang, X. Chou, H. Kan, Z. Xiao and Y. Ding, *ACS Sustainable Chem. Eng.*, 2022, **10**, 7418–7425.

162 H. Liu, T.-H. Lee, Y. Chen, E. W. Cochran and W. Li, *Green Chem.*, 2021, **23**, 5056–5063.

163 P. Nilges and U. Schröder, *Energy Environ. Sci.*, 2013, **6**, 2925–2931.

164 S. Jung, A. N. Karaiskakis and E. J. Biddinger, *Catal. Today*, 2019, **323**, 26–34.

165 P. Zhou, L. Li, V. S. S. Mosali, Y. Chen, P. Luan, Q. Gu, D. R. Turner, L. Huang and J. Zhang, *Angew. Chem., Int. Ed.*, 2022, **61**, e202117809.

166 X. Shang, Y. Yang and Y. Sun, *Green Chem.*, 2020, **22**, 5395–5401.

167 M. D. Stankovic, J. F. Sperryn, R. S. Delima, C. C. Rupnow, M. B. Rooney, M. Stolar and C. P. Berlinguette, *Energy Environ. Sci.*, 2023, **16**, 3453–3461.

168 Y.-R. Zhang, B.-X. Wang, L. Qin, Q. Li and Y.-M. Fan, *Green Chem.*, 2019, **21**, 1108–1113.

169 Y. Wu, Y. Jiang, W. Chen, X. Yue, C. L. Dong, M. Qiu, T. T. T. Nga, M. Yang, Z. Xia, C. Xie, L. Xu, R. Wang, S. Wang and Y. Zou, *Adv. Mater.*, 2023, **36**, 2307799.

170 P. Hauke, T. Merzdorf, M. Klingenhof and P. Strasser, *Nat. Commun.*, 2023, **14**, 4708.

171 J. J. Roylance and K.-S. Choi, *Green Chem.*, 2016, **18**, 2956–2960.

172 X. H. Chadderdon, D. J. Chadderdon, J. E. Matthiesen, Y. Qiu, J. M. Carraher, J.-P. Tessonnier and W. Li, *J. Am. Chem. Soc.*, 2017, **139**, 14120–14128.

173 J. Anibal and B. J. Xu, *ACS Catal.*, 2020, **10**, 11643–11653.

174 R. Kloth, D. V. Vasilyev, K. J. J. Mayrhofer and I. Katsounaros, *Chemsuschem*, 2021, **14**, 5245–5253.

175 R. S. Sherbo, R. S. Delima, V. A. Chiykowski, B. P. MacLeod and C. P. Berlinguette, *Nat. Catal.*, 2018, **1**, 501–507.

176 G. B. Chen, X. D. Li and X. L. Feng, *Angew. Chem., Int. Ed.*, 2022, **61**, e202209014.

177 J. Bi, Q. Zhu, W. Guo, P. Li, S. Jia, J. Liu, J. Ma, J. Zhang, Z. Liu and B. Han, *ACS Sustainable Chem. Eng.*, 2022, **10**, 8043–8050.

178 F. Ye, S. Zhang, Q. Cheng, Y. Long, D. Liu, R. Paul, Y. Fang, Y. Su, L. Qu, L. Dai and C. Hu, *Nat. Commun.*, 2023, **14**, 2040.

179 J. L. Wang, X. Zhang, G. Z. Wang, Y. X. Zhang and H. M. Zhang, *Chem. Commun.*, 2020, **56**, 13611–13614.

180 S. Li, X. Sun, Z. Yao, X. Zhong, Y. Coo, Y. Liang, Z. Wei, S. Deng, G. Zhuang, X. Li and J. Wang, *Adv. Funct. Mater.*, 2019, **29**, 1904780.

181 J. G. Ibanez, B. A. Frontana-Uribe and R. Vasquez-Medrano, *J. Mex. Chem. Soc.*, 2016, **60**, 247–260.

182 J. Woo, B. C. Moon, U. Lee, H.-S. Oh, K. H. Chae, Y. Jun, B. K. Min and D. K. J. A. C. Lee, *ACS Catal.*, 2022, **12**, 4078–4091.

183 Z. Yang, B. Zhang, C. Yan, Z. Xue and T. Mu, *Appl. Catal., B*, 2023, **330**, 122590.

184 Z. Yang, S. Wang, C. Wei, L. Chen, Z. Xue and T. Mu, *Energy Environ. Sci.*, 2024, **17**, 1603–1611.

185 X. Yuan, K. Lee, J. R. Schmidt and K.-S. Choi, *J. Am. Chem. Soc.*, 2023, **145**, 20473–20484.